EFFECT OF NON-LINEAR SOIL STRUCTURE INTERACTION ON THE SEISMIC RESPONSE OF CRITICAL INFRASTRUCTURE FACILITIES

by

Dhrubajyoti Datta

A Dissertation

Submitted to the Faculty of Purdue University

In Partial Fulfillment of the Requirements for the degree of

Doctor of Philosophy

Lyles School of Civil Engineering

West Lafayette, Indiana

May 2020

THE PURDUE UNIVERSITY GRADUATE SCHOOL
STATEMENT OF COMMITTEE APPROVAL

Dr. Amit H Varma, Chair

Department of Civil Engineering

Dr. Rodrigo Salgado

Department of Civil Engineering

Dr. Monica Prezzi

Department of Civil Engineering

Dr. Robert Nowack

Department of Earth, Atmospheric and Planetary Sciences

Approved by:

Dr. Dulcy M. Abraham

Head of the Graduate Program

For my mom and dad who have always inspired me to be better than I was yesterday

ACKNOWLEDGMENTS

I would like to express my sincere gratitude to my advisor, Prof. Amit Varma who has always inspired me to think out-of-the-box and provided valuable inputs in organizing and directing my PhD research in the right direction. Prof. Varma has always believed in my capabilities and has always given me the liberty to innovate and incorporate new ideas to this field of study.

I would also like to thank the members of my doctoral committee, Prof. Rodrigo Salgado, Prof. Monica Prezzi and Prof. Robert Nowack, who have provided me with insightful suggestions and allowed me to widen the scope of my research. Their comments encouraged me to look at the soil structure interaction problem from the perspective of geotechnical engineering and seismology.

I would also like to thank my mentor at Idaho National Laboratory, Justin Coleman where I interned for two summers and who was highly supportive of my research and introduced me to MASTODON. Additionally, I would like to thank Dr Swetha Veeraraghavan and Dr. Chandrakanth Bolisetti for assisting me with SSI simulations in MASTODON. I would especially like to thank Robert Spears who was instrumental in providing practical inputs and troubleshooting issues pertaining to my finite element simulations. Ashwani Goel of Dassault Systemes, West Lafayette provided counsel on the use of soil models in ABAQUS.

Finally, I would like to thank my parents, family members, and friends who have constantly inspired me to be the best in what I do and supported me through difficult phases.

TABLE OF CONTENTS

LIST OF TABLES

LIST OF FIGURES

LIST OF ABBREVIATIONS

SSI	Soil Structure Interaction
LSSI	Linear Soil Structure Interaction
NLSSI	Non-linear Soil Structure Interaction
NPP	Nuclear Power Plant
RB BM	Reactor Building Basemat
TB BM	Turbine Building Basemat
RCT	Resonant Column Test
PBT	Piezoelectric Bender element Test
LSRA	Linear Site Response Analysis
NLSRA	Non-Linear Site Response Analysis

ABSTRACT

Soil structure interaction plays a crucial role in the behavior, analysis and design of heavy infrastructure of high importance such as power plants, processing facilities, hospitals, precision engineering facilities, hydraulic power infrastructure, etc. The change in frequency content of the ground motion as seismic waves propagate through the subsoil might result in the reduction or amplification of the response acceleration of seismically excited structures. SSI has a significant influence on the calculated in-structure response spectra (ISRS), and the calculated seismic design demand forces. The fundamental hypothesis is that nonlinearities at the soil-structure interface have the potential to influence the peak acceleration demands due to energy dissipation. The sources of the non-linearity include (i) non-linear structural behavior, (ii) non-linear soil behavior and (iii) geometric non-linearities across the interface such as gapping and sliding. The dissertation aims to establish a non-linear SSI analysis methodology in time domain to understand the response of structural basemat with respect to the free-field motion when subjected seismic excitation. The contribution of each source of nonlinearity on the basemat response is examined through an array of sensitivity studies. The numerical studies are carried out on the Fukushima Daichii nuclear power plant in Japan with ground motion history from the Tohoku earthquake.

1. INTRODUCTION

Resilience of built infrastructure to extreme events such as earthquakes, landslides, etc is a significant challenge to the human endeavor. Our understanding of seismic events and their influence on structural systems and their functionality is in its adolescence in spite of decades of research, education, standardization and policy making. For example, the Fukushima event in Japan, arguably one of the most advanced countries in seismic resilience, has highlighted the need for sustained research on the impact of soil-structure interaction on the seismic response and resilience of built infrastructure including power plants, hospitals, industrial processing plants, and other important structures. The dissertation will contribute and further our understanding of the nonlinearity and complexities in soil-structure interaction, and its impact on the structural response. On the basis of numerical and experimental results, small-scale benchmark models are formulated with constitutive relationships to develop the contact formulation for the soil-structure interface. This is then incorporated in commercial finite element softwares for simulating non-linear response of mega-scale structural systems under static and dynamic loading conditions. A significant number of boundary-value problems in soil dynamics and structural mechanics involve interaction of soil with structural elements, including the effects of loading on shallow or deep foundations, penetration problems, retaining wall-soil interaction, soil reinforcement and liquefaction underneath and around structures and buried pipelines. Current analysis and design methodologies rely on linear soil-structure interaction (SSI) analyses that simplify the material properties of the soil and the structural details besides ignoring the interface behavior altogether. Recent seismological and structural response data recorded at the Fukushima Daiichi sites indicate that the acceleration records measured at the basemat are lower than the free field ground motions recorded at the sites. The reasons for this attenuation are unclear, but may be attributed to

nonlinearities associated with the behavior of the foundation soil, structure and their interface. For a majority of problems, SSI involves stresses that are so severe that soil particles may crush and change as a material during the loading process. In addition, shear strain localization along the soil structure interface occurs, which differs from localization within a soil mass because of the effects of interface roughness and particle crushing. The dissertation aims to investigate the fundamental effects of such interface behavior using non-linear constitutive models, implemented through a combination of direct shear type experiments and detailed finite element simulations.

1.1 Research Motivation and Objective

Soil structure interaction effects are important because there are energy dissipation mechanisms in the soil, the structure, and at the soil-structure interface that can reduce the effects of design basis earthquakes on the facility and, more importantly, its services and components (equipment, hardware of various types), which are crucial for the facility to remain functional after the seismic event. The reduction of peak acceleration demands due to energy dissipation can be attributed to non-linear soil behavior, geometric non-linearities at the interface or due to structural nonlinearities. The key motivation of the dissertation is to understand the effects of each source of non-linearity which contributes to the reduction of the foundation response as observed for the Fukushima Daichii NPP, shown in Table 1.1. The non-linear soil structure interaction analysis is carried out in stages by individually introducing sliding, gapping and material nonlinearity into the system and varying the scale of analysis. The material model is verified by comparing numerical analysis results for a series of cyclic direct shear tests [1] and applied to full scale NLSSI analysis of the Fukushima Daichii NPP. An array of sensitivity studies is also performed to analyze the change in acceleration attenuation when the sources of nonlinearity are altered. The ideal contact parameters and boundary conditions for a full-scale analysis are also determined.

Table 1.1: Reduction in acceleration of the basemat at Fukushima Daichii Unit 1 and 6 for the Tohoku earthquake [2]

Location	Point Id	Location Vertically	Max acceleration (Gal)		
			NS	EW	UD
Unit 1	1-R2	-1.23 m	460	447	258
Unit 6	P3	1m	290	431	163
Free Field (South Points by Unit 1)	GS1	-2 m	463	600	326
Free Field (North Points by Unit 6)	GN1	-2 m	570	699	239

In regions of high seismicity, base slab uplift is a common phenomenon arising from strong ground motions due to overturning moments [3]. Linear elastic analysis is often ineffective and overestimates the uplift parameters when a portion of the base slab is in contact with the soil; due to significant stress localization at the toe and considerable impact forces developed when the structure resettles itself. Early SSI studies used equivalent translational and rotational spring stiffness depending on site soil conditions, based on elastic half-space theory to simulate sliding, gapping and rocking effects [4]. The structure's modal response was calculated using a linear lumped mass model with non-linear softening at the base using assumptive base moment-rotation curves. It did not consider damping in the soil strata, which has a significant impact on the attenuation of peak acceleration/displacement response of the structure. In the early 80's, with growing popularity of FEA, the focus shifted from spring-dashpot systems to defining joint interface elements for addressing separation and sliding in dynamic SSI problems, such that transmission of tensile forces across the interface could be controlled. Dynamic properties pertaining to sliding were governed by the Mohr-Coulomb failure criterion which varied the cohesion and friction angle between soil (modeled as an elasto-plastic material) and structure. Numerical simulations revealed that translation was the dominant component when sliding and rocking of the structure took place. Furthermore, the amplification of amplitude in the structure was compensated by its decrease in the surrounding soil strata and vice-versa during sliding [5, 6].

Current industry practice in the built environment and nuclear sector, focuses on linear and equivalent linear frequency domain analysis methods for site response and SSI analysis. This is based on the assumption that the seismic demand has a linear correlation with the ground motion intensity and does not account for non-linear interface effects. The dissertation focuses on developing fundamental knowledge, based on the combination of experimental and numerical results, to evaluate effects of nonlinearities at the soil-structure interface on the seismic response of mega-scale structural systems. The evaluation is carried out by performing verification studies on small scale finite element models to ensure that the non-linear hysteretic soil behavior is correctly implemented by the material model. The results are then benchmarked by comparison with experimental data. In the final stage, the material and interaction model parameters are scaled up to simulate the structural response of a full-scale nuclear power plant subjected to seismic loads, with an account of non-linear material and interface effects.

1.2 Research Methodology

The research objectives are focused on building a robust framework for non-linear soil structure interaction analyses that is independent of site conditions, soil type or ground motion content; which are intended to be achieved through the following tasks:

1.2.1 Comparative analysis of contact models

An appropriate contact model is developed for the soil-structure interface through a series of parametric studies. The geometric non-linearities associated with the interface; primarily sticking and slipping are investigated using both kinematic and inertial interaction methods. A series of simulations are performed on a symmetric structure resting on a soil domain with non-reflecting boundaries by applying quasi-static and cyclic loading in MASTODON [7], an open-source FEA

application developed by the Idaho National Laboratory. The tangential and normal behavior of the interface are simulated using a simple Coulomb friction formulation. The shear stresses and strains are obtained at the interface and compared to the theoretical values. A thin-layer-element based interface formulation is also developed using a phenomenological soil model I-SOIL in MASTODON, which takes material damping into account. Upon establishing the appropriate contact formulation for the interface, a full-scale soil-structure interaction analysis is performed. The response at the interface is compared using algorithms like Lagrange Multiplier, Penalty and Kinematic contact methods in ABAQUS and MOOSE

1.2.2 Identification of structural response due to geometric nonlinearities, excluding material nonlinearities

An exploratory study is conducted to compare numerical SSI analysis results with measured ground motions to evaluate sources of geometric nonlinearity contributing to the observed reduction in peak spectral acceleration between the soil and the structure. To achieve this goal, a series of full-scale linear SSI and nonlinear SSI (NLSSI) analyses is performed on the Fukushima Daichii nuclear power plant using the site soil profile and ground motion data measured near Unit 6 of the power plant. Exploratory studies are performed to assess the boundary conditions of the surrounding basemat soil and the large soil domain. The individual soil layers are constrained to move in pure shear and the base of the large soil domain is modelled as a non-reflecting boundary. The focus of the analyses is on evaluation of two specific localized nonlinear effects at the interface; gapping and sliding. A full scale finite element model of the NPP-soil assembly is developed in ABAQUS and benchmarked against the free field data [2] obtained from the site. The geometric interfacial non-linearities are then introduced into the linear SSI model in ABAQUS [8] and the acceleration response of the structure is tracked through comparison of response

spectra. In order to assess the physical nature of the structural response, sensitivity studies are performed by varying parameters associated with the sliding and gapping formulations at the interface.

1.2.3 Non-linear soil-structure analysis of cyclic shear tests considering material and geometric nonlinearities

The focus is on modeling a set of direct shear-type tests for a concrete foundation sliding on Ticino sand confined in a concrete chamber under continuous confining pressure. The foundation is subjected to cyclic displacement-controlled load packets of gradually increasing amplitudes. The non-linear soil domain is accurately modelled using a multilinear inelastic hysteretic model in ABAQUS. The force-displacement response from the analytical SSI models are compared with the experimental data. Behavior of the interface is modelled through a non-linear soil model in addition to established contact algorithms from Sec 1.2.1; and a comparison is made between the two approaches. The key objective of this step was to effectively calibrate the soil material model such that it can be used in the full scale NLSSI analysis of the Fukushima NPP.

1.2.4 Full scale Non-linear Soil-Structure Interaction analysis of the Fukushima NPP

The non-linear material model is calibrated for the local soil strata properties and shear wave velocity data at the Fukushima NPP Unit 6. Element tests are performed on the basemat-soil interface to calibrate the reference pressure and pressure dependency parameters for the large scale simulations. The material and geometric nonlinearities are introduced step-by-step to assess the impact of each source of nonlinearity on the basemat response. The full scale NLSSI models of the NPP are analyzed by comparing the response spectra at the basemat and the free field ground motion obtained from site response analyses.

1.3 Research Organization

The flow of the dissertation is organized into following chapters:

- Chapter 2 does an exhaustive literature review of the different aspects of the soil-structure interaction analysis procedures. A brief review of the direct and substructure method of analysis is discussed and a qualitative analysis of time and frequency domain analysis procedures is discussed. The procedures involved in site response analysis discussed in some detail, as it is a precursor to SSI analysis. The numerical models used for simulating geometric and material nonlinearities at the soil structure interface are discussed along with the test data needed for calibration of the numerical models.
- Chapter 3 focuses on the comparative analyses of contact algorithms for NLSSI analyses. These include the penalty, kinematic, augmented Lagrange and the thin layer element formulation. Two-element finite element models are used for simulating contact at the soil-structure interface when subjected to pseudo-static and cyclic loading conditions. They are benchmarked on the basis of simple shear tests based on the Coulomb failure criterion. A sensitivity study is performed on the basis of pressure dependency criterion, friction model, pressure overclosure relationship, etc. by comparing the interfacial shear stress-strain response. The comparison is carried out in MASTODON, an open source FEA program developed by the Idaho National Lab on its existing MOOSE framework and ABAQUS. This is followed by verification/validation studies of large scale isotropic and symmetric direct shear test models in ABAQUS and MASTODON.
- Chapter 4 identifies the structural response of large scale infrastructure facilities, primarily focused on nuclear power plants subjected to strong ground motion and how it is impacted by geometric non-linearities at the interface. A detailed description of the Fukushima

Daichii Reactor 6 building, including the reactor and turbine building, the soil domain and the ground motion content is presented. The modeling of individual components in ABAQUS including the meshing details, load conditions, ground motion content and linear elastic material models is discussed. Comparative studies are performed on the implementation of constraint conditions to simulate non-reflecting boundaries. The appropriate interaction parameters are adopted for simulating contact in the normal and tangential direction. Finally, the nonlinear SSI results are compared on the basis of their acceleration response spectra. A sensitivity study is also performed to compare the basemat and in-structure response spectra by varying the friction coefficients (sliding effect) and the normal pressure overclosure relationships (gapping effects).

- Chapter 5 is focused on calibration and verification of the non-linear material model used in this dissertation. A series of direct shear type tests on shallow foundations resting on dense Ticino sand was performed at the European Laboratory of Structural Analysis in ISPRA, Italy. Detailed analytical models are formulated to verify the behavior of the non-linear hysteretic soil model within the experimental stress-strange range while taking pressure dependency into account. Finally, the full scale numerical results are compared with the force-displacement and moment rotation response from the experiments.
- Chapter 6 utilizes the hysteretic soil material model for full scale NLSSI analysis of the Fukushima Unit 6. The results are then compared with the LSSI results. A sensitivity study is also performed on the variation in structural response due to changes in material nonlinearity and contact formulation.
- Chapter 7 gives a summary of the NLSSI analysis procedure described in this dissertation. It draws some key conclusions from the different stages of analysis and identifies the key

source of nonlinearity responsible for attenuation of acceleration response at the basemat. Some of the drawbacks and limitations are also discussed.

2. LITERATURE REVIEW

The response of structures and its underlying soil deposits to earthquakes is irregular due to variations in the three dimensional stress-strain fields and the anisotropy in the soil material properties. The key design philosophy is based on the conjecture that structures should be constructed on stiff soil or rigid ground. However, due to variations in the mechanical properties of soils and wave propagation effects, the potential failure mechanisms are different to pinpoint. This makes it difficult to assess the structural response without nonlinear dynamics analysis procedures. The nuclear industry is dominated by reactor and turbine buildings, which tend to be stocky with a large plan area and impose heavy loads on the soil. Over the course of this dissertation, it will be observed that large imposed loads are responsible for changing the foundation stiffness, in addition to altering the morphology of the surrounding soil mass. In case of seismic events dominated by wave propagation effects, the soil is subjected to low levels of strain [9]. Higher level of strains are normally observed in cases pertaining to slope stability and retaining structures. However, the strain levels can be highly unpredictable when the soil mass is subjected to dynamic loads. This type of behavior is governed by the dynamic soil properties which are used to effectively model the behavior of cyclically loaded soils.

Once we are able to effectively model the dynamic properties of the soil domain, the next phase is the prediction of the ground motion at the surface. This is referred to site response analysis. The site response analysis is used to model the propagation of waves from the bedrock to the top of the soil surface. This is affected by the properties of the individual soil layers as well as the boundaries that exist between them. The energy transmission between the fault rupture source and the site is extremely complex and is often described through empirical relationships from

previously recorded ground motion characteristics. A brief review of site response analysis strategies will be discussed in the subsequent sections.

The next stage deals with the modelling of the local soil properties surrounding the foundation. The localization of stresses surrounding the foundation basemat causes a change in the frequency content and damping characteristics of the dynamic structural response. These are often cited as inertial interaction effects. The presence of the structure modifies the free field motion due to material and geometric nonlinearities, often referred to as kinematic interaction effects [10]. A series of interaction and element-based contact algorithms were developed on the FEA and DEM numerical frameworks to simulate kinematic interaction effects, which is reviewed in Sec 3.

2.1 Measurement of dynamic soil properties from field tests and experiments

The measurement of dynamic soil properties and characterization of the soil morphological parameters under varied strain ranges is key to performing an accurate soil structure interaction analyses. It should be noted that a series of tests in the field as well as in the laboratory need to be performed in ordered to effectively model the soil behavior in the vicinity of the foundation and away from the foundation. The soil has 'dynamic' properties because it continually changes with the change in hydrostatic pressure, dilation properties, pore water pressure, shear wave velocity, confinement, etc. The testing methodology of dynamic soil parameters take the initial stress state, expected response to cyclic loading, Poisson ratio, stiffness characteristics, density and damping characteristics into consideration. The stiffness and damping properties are especially critical to the evaluation of the nonlinear hysteretic behavior exhibited by soils when subjected to cyclic shear loading. A soil sample doesn't necessarily behave in the same way for a particular strain range and the variation is even more pronounced for different soil types. The strains are normalized in order to effectively model the variation of shear strength with the number of loading

cycles, often classified as low strain and high strain tests. Low strain experiments are intended to arrest the onset of non-linear behavior and are performed under small loading cycles typically in the range of 0.01%-0.001%. They are performed to measure the low-strain shear moduli [9].The Seismic Reflection Test is a common low strain test which is useful for determining wave propagation velocities and thickness of individual soil layers for large-scale and deep soil strata, by measuring reflection of waves from soil layer interfaces [11]. The delineation of stratigraphic layers is performed using the Seismic Refraction Test by measuring the first arrival times of the p- and s-waves from an impulse source to the receiver. For oil and natural gas exploration, the Suspension Logging tests are efficient in measurement of wave propagation velocities at higher frequencies [12] and is particularly effective for soft soil deposits of small thicknesses. In addition to p- and s-wave arrival times, Rayleigh waves are effective for determining free field shear wave velocities by measuring the points vibrating in phase for a steady-state vibration. On the other hand, high strain tests such as the Standard Penetration Test (SPT), Cone Penetrometer Test (CPT) and Dilatometer Tests [13] are useful for measuring the friction ratios; which varies with the cohesion in the soil. The penetration resistance can be used in empirical relationships to obtain the relative density and shear modulus of the sand.

Laboratory tests are performed under more controlled conditions, where the soil specimens are subjected to stable initial stresses and uniform changes in the stresses and strains. It should be noted that the accuracy of laboratory experiments depends on its capability to mimic the loading conditions, initial stress state and confinement characteristics of the problem at hand. Some popular low-strain element tests for determination of dynamic soil properties would be the Resonant Column Test (RCT), the Piezoelectric Bender Element tests (PBT) and the Ultrasonic Pulse Test (UPT). The RCT is the most common low strain test for measuring the dynamic

deformation characteristics (the shear wave velocity and damping ratio) of soils. A cylindrical solid or hollow specimen is subjected to harmonic torsional excitation or axial loading with varying frequency and the acceleration amplitude response is obtained. The lowest frequency at which the voltage output of the accelerometer is maximized is the fundamental frequency or first mode resonance. The frequency response function can be obtained by shutting of the electromagnetic loading system while the specimen oscillates at the resonant frequency. The process can be repeated by varying the excitation amplitude and increasing the confining stresses. The shear wave velocity of soil sample from the resonant column test can be obtained as:

$$\frac{\sum I}{I_0} = \frac{\omega_n . l}{V_s} \tan \frac{\omega_n . l}{V_s} \tag{2.1}$$

where, $\sum I$: sum of moment of inertia of soil and membrane

I_0 : mass moment of inertia of rigid mass placed on top of sample

l : length or height of specimen

V_s : shear wave velocity of the specimen

ω_n : undamped natural circular frequency

The shear modulus can be obtained from the shear wave velocity as $G = \rho . V_s^2$, where ρ is the density of the soil mass.

RCT tests have also been used for coarse soil specimens and rocks for obtaining low strain shear modulus at nuclear plant sites [14]. The UPT is effective for obtaining shear wave velocities of soft materials, by measuring the distortion in the dimensions of the piezoelectric receivers and voltage differences. PBT is performed by placing two bender elements on opposite sides of a soil specimen, where a voltage pulse applied by the transmitter produces an s-wave. The pulse is distorted when it reaches the receiver element. The time period between the two pulses divided by the distance between the ends of the two bender elements gives the shear wave velocity of the

sample. The bender elements are assembled using two piezoelectric materials such that when their faces are subjected to a voltage, one of them expands while the other contracts [9]. Bender elements are effective for large scale model tests which attempt to imitate the boundary conditions of a real problem and study the impact of multiple soil parameters. This is due to the fact that the soil is undisturbed over the course of the test. Full scale prototype or model tests are effective in modeling the behavior of soil due to cyclic shaking. However, this behavior depends on the stress levels, with lower stresses resulting in dilative behavior while higher stresses might result in contractive behavior. Another issue with performing model tests is the scaling of the stresses with the increased gravitational forces [15].The tests performed under normal gravitational conditions (1-g tests) are generally performed with shaking tables and geotechnical laminar box [16], and those under scaled gravitational fields are performed in centrifuge facilities.

Fig 2.1: (i) Geotechnical laminar box facility at SEESL, SUNY Buffalo and (ii) fully assembled bender element [16]

Similitude and boundary effects are key considerations while performing model tests. Sidewalls or adsorbent wall linings are often used to reflect energy [17], while some correction factors are also used to rectify the inconsistencies of the cohesive stresses between the model and original prototype [18]. Experimental techniques undertaken to verify the analytical accuracy of uplift, gapping and sliding behavior are primarily supported by centrifuge test data. The comparisons of centrifuge test results with linear SSI simulations indicate that discrepancies occur due to local nonlinear transformations in the soil over the reduced ground contact area [19]. Recorded values from embedded earth pressure gauges indicate that initial stresses were released and permanent deformations remained in the ground. In the experiments, local increase in ground contact area (defined as contact area divided by foundation area) occurred due to rotational deformation, which wasn't captured in the linear soil model. A nonlinear interface and soil model needs to be implemented to improve the accuracy of the analysis [19] and its comparison with experimental data.

Fig 2.2: The NEES Centrifuge Facility at UC Davis supporting 2D seismic simulations in the vertical and horizontal direction

Centrifuge tests with a radius of rotation (r), rotates a 1/N scale model of the original prototype at a rotational velocity of $\sqrt{\frac{N}{r}}$ to generate an acceleration field which is N times the acceleration due to gravity (g). The variation in gravitational field with radius causes higher accelerations to be induced at the top of the model as compared to its base, and also curves the horizontal plane [20]. Since, pore water pressure dissipation occurs much faster in the model test than on the site, highly viscous fluid such as glycerin is used. Centrifuge models give useful information pertaining to the energy dissipation mechanisms, moment-rotation response from overturning effects and non-linear load deformation characteristics for shallow foundations [21].

The volumetric changes in soil are generally observed for loadings of high strain amplitude. For drained loading, the volumetric strain changes whereas for undrained loading the pore water pressure changes. Since soil behavior is governed by effective stresses at high strains, the measurement of volumetric changes and pore water drainage needs to monitored [9]. The cyclic triaxial test is a commonly used laboratory test for the measurement of the dynamic shear modulii. It involves pneumatic application of radial stresses to a cylindrical specimen with the simultaneous application of axial loads. Normally the radial stresses are held constant while the axial stresses are cycled at 1 Hz frequencies. The deviator stresses (difference between axial and radial stresses) are obtained under isotropically or anisotropically consolidated conditions. Stress-strain curves generated by these tests are used to obtain the damping characteristics and the secant shear modulus of the specimen. The cyclic direct simple shear test is much more effective in emulating the deformation of a soil sample to vertically propagating shear waves. Its lateral boundaries are restrained against expansion and the shear stresses are applied to the top and bottom of the specimen. This sometimes results in the buildup of moments due to non-uniform complimentary shear stresses, which can be arrested my modifying the diameter-height ratio. Last but not the least,

cyclic torsional shear tests are more advantageous than the cyclic simple shear test, owing to the fact that it allows the application of isotropic initial stress condition. The cyclic shear can be imposed on any horizontal plane by continuous rotation of the principal axes.

The shear strength of soil can be influenced by cyclic loading. The amplitude and frequency of the applied loading plays a crucial role in determining the nature of experiments. The measurement of dynamic stresses and strains are often anticipated better in laboratory experiments than field tests, since the pore water pressure, volumetric changes and boundary conditions can be monitored more effectively. However, field tests are more effective in deciphering the macro-mechanical properties of undisturbed soil deposits. In the next section, we will be specifically reviewing experiments which focus on the soil-structure interface behavior.

2.2 Experimental studies on the behavior of the soil-structure interface

Dynamic SSI testing to measure the behavior at interfaces between structural and particulate media gained momentum in the mid-1980s. The earliest experiments focused on the frictional resistance between dry sand and metals or concrete when subjected to monotonic or cyclic loading. The influence of the surface roughness of steel, 50 percent mean diameter (D_{50}), uniformity coefficient of sand etc. on the friction properties were investigated through direct shear tests [22]. It was observed that the normalized roughness of the sand-steel interface and the roundness of sand particles could be correlated to the friction coefficient. This was useful for establishing relationships between skin friction and displacement for steel piles embedded in sand. Different boundary conditions also have a significant impact on the friction angle of sand-steel interfaces. This was demonstrated through a series of plain strain and parallel guided direct shear experiments on quartz and sand [23].The results confirmed a dependence of the interfacial shear zone thickness on boundary conditions and the friction angle. The friction angle was bound between the internal

friction angle of sand and quartz, and was insensitive to the vertical stresses. However, contrasting results were observed for another set of 3-D interface tests when tested under 2D and 3D constant normal stress and normal stiffness boundary conditions. The ratio of shear stress to normal stress was observed to decrease with the increase in normal stress. Shear stress vs lateral displacement curve varied for the interface of steel with dense and loose sand, and prominent peak shear stresses were identified for the dense samples. The mobilized shear stresses were also observed to increase with the loading cycles. The roughness and hardness index of metallic surfaces has a significant effect on the friction angle of the sand [24]. The experimental data pointed to the fact that the peak friction angle decreases with the surface hardness and increases with the surface roughness. Shearing failure occurred in the vicinity of the interface even though the sand particles stuck to the metallic surface. Monotonic and cyclic shear interface tests on different sand samples and aluminum plates [25] under constant normal stiffness (ratio of increase in normal stress to vertical displacement) also led to similar observations. The interfacial shear stresses were associated with dilatant behavior for rough surfaces and contractive behavior for smooth surfaces and the mobilization of shear stresses resulted from the initiation of normal stresses.

Desai [26] developed the Cyclic Multi-Degree of Freedom (CYMDOF) device, which was capable of performing fatigue load- and displacement-controlled tests. It focused on performing sensitivity studies of the soil-concrete interface with reference to normal stresses, relative density of sand, displacement amplitude and number of loading cycles to assess stick-slip behavior across large interfaces. The experimental trends point to the mobilization of shear stresses accompanied by growth in the interfacial stiffness with the increase in normal stresses. Also, there was an increase in peak shear stresses with the number of cycles which occurred even more rapidly for high density sands. Stress path effects during debonding/rebonding could not be deciphered. The

displacement controlled tests were used to parameterize the modified Ramberg-Osgood model for modeling the constitutive behavior of the interface which can be classified as non-linear elastic. Static behavior of the interface was described with a Mohr-Coulomb stress envelop with an account of tension softening and hardening effects (depends on dilatancy or contractive behavior of the soil domain).

However, small scale interface tests with image-based particle tracking capabilities and local interface stress-strain data might be a better path to understand fundamental nonlinear SSI behavior.

Image-based analysis methods can be used in laboratory investigations to understand the underlying mechanisms in soil-structure interaction problems. In the past decade, image correlation techniques, such as particle image velocimetry (PIV) and digital image correlation (DIC), have gained traction. In the DIC technique, a transparent observation window located exactly at one of the symmetry planes of the prototype structural element enables the observer to study the response of soil during loading of plates, probes and foundations [27, 28, 29]. After image processing, the displacement and strain fields within the soil domain are obtained throughout the loading process. The unique capabilities of a DIC calibration chamber allow direct observation of soil-foundation response under monotonic or cyclic loading, enabling a methodical assessment of the mechanisms that play a significant role in the response at the interfaces. This would not be possible using other, conventional testing techniques. Charged coupled camera devices are also effective in recording particle movement at the interface. The critical relative roughness (ratio of the surface roughness of the hard continuum medium to the diameter of sand particles) results in strain localization which causes a shear band formation leading to large inter-particle relative displacement [30].Similar cyclic and static shear tests were performed to

investigate the behavior of gravel (mean diameter varying from 7-10 mm)-steel plate interfaces using cutting-edge photographic technology. Particle tracking of interfacial shear displacement revealed that the tangential stiffness reduces with the increase in shear displacement and the shear stresses increased linearly with the imposed normal stress. The normal behavior of the interface is affected by the rotation, rearrangement and relative displacement of individual particles leading to reduction in voids.

A number of constitutive material models and interaction algorithms were devised for efficiently modelling the non-linear soil surrounding the interface when subjected to monotonous and cyclic loading. The numerical models took into consideration several crucial factors pertaining to soil behavior such as the (i) variation in normal stress, (ii) confinement pressure, (iii) pressure dependency, (iv) mean particle diameter, (v) pore water pressure, (vi) shear modulus, (vii) number of loading cycles, (viii) internal friction angle and (ix) critical shear strains. Some parameters pertaining to the interface which were analyzed included (i) roughness of the interface to assess friction parameters, (ii) shape characteristics of the soil particles, (iii) boundary conditions, (iv) shear band thickness, (iv) normalized interfacial shear stresses and (v) pressure overclosure relationships. The above–mentioned parameters were incorporated in some multiphysics-based and empirical models to effectively emulate the stress-strain response of the soil-structure interface when subjected to dynamic loads.

2.3 Numerical material models for assessment of soil dynamic behavior

The mechanical behavior of granular media is unpredictable and complex when subjected to cyclic and seismic loading. Studies have indicated that the stress-strain relationship is predominantly non-linear hysteretic with the strain range varying within 0.001% to 0.01%. The motivation is to model the essential aspects of cyclic behavior of soil with utmost accuracy while taking into

consideration the factors mentioned in the previous section. The soil models can be broadly classified as equivalent linear models, nonlinear cyclic models and constitutive models which are mostly empirical in nature. The first two models primarily focus on the hysteretic behavior of the soil and the parameters governing the shape of the hysteresis loop, whereas constitutive models focus on multiple factors such as plasticity effects, tension softening hardening, pore water pressure effects, etc. which require a significant amount of test data to calibrate and are limited to the soil type under consideration. However, there are certain traditional plasticity-based constitutive models which possesses a wider range of applicability. Some key soil material models will be discussed in the subsequent sections, which are commonly applied for site response and soil structure interaction analysis.

2.3.1 Equivalent linear and cyclic non-linear models

The cyclic shear stress-strain response of soils during earthquakes varies with the frequency and amplitude. A prime assumption for modelling the response was the cycling of the shear stress between a positive and negative value which are of equal magnitude and thereby forms a loop, referred to as complete stress reversal [31]. The shape of this hysteresis loop is characterized by two main parameters (i) the slope of the line at any point of the loop is described as the tangent shear modulus (G_{tan}) which continuously varies during the loading; and (ii) the slope of the line joining the end points of the loop referred to as the secant shear modulus (G_{sec}) which is the mean response over one complete cycle and is representative of the stiffness of the soil

$$G_{sec} = \frac{\tau_i}{\gamma_i} \tag{2.2}$$

where τ_i and γ_i are the shear stress and shear strain amplitude.

(iii) the area covered under the hysteresis loop which is a measure of the energy dissipation and is referred to as the damping ratio (ξ), given by [31, 32]

$$\xi = \frac{W_D}{4\pi.W_S} = \frac{A_{loop}}{2\pi.G_{sec}{\gamma_i}^2} \tag{2.3}$$

where W_D is the strain energy dissipated by the soil, W_S is the maximum strain energy and A_{loop} is the area under the hysteresis loop. It is also important to note that the value of the G_{sec} and γ_i will vary for the same soil at different pressures. Hence, these equivalent linear material parameters need to be defined for a particular reference strain (γ_{ref}). The highest value of the shear modulus is obtained when the shear strain tends to zero, also referred to as the initial or maximum shear modulus (G_{max}).

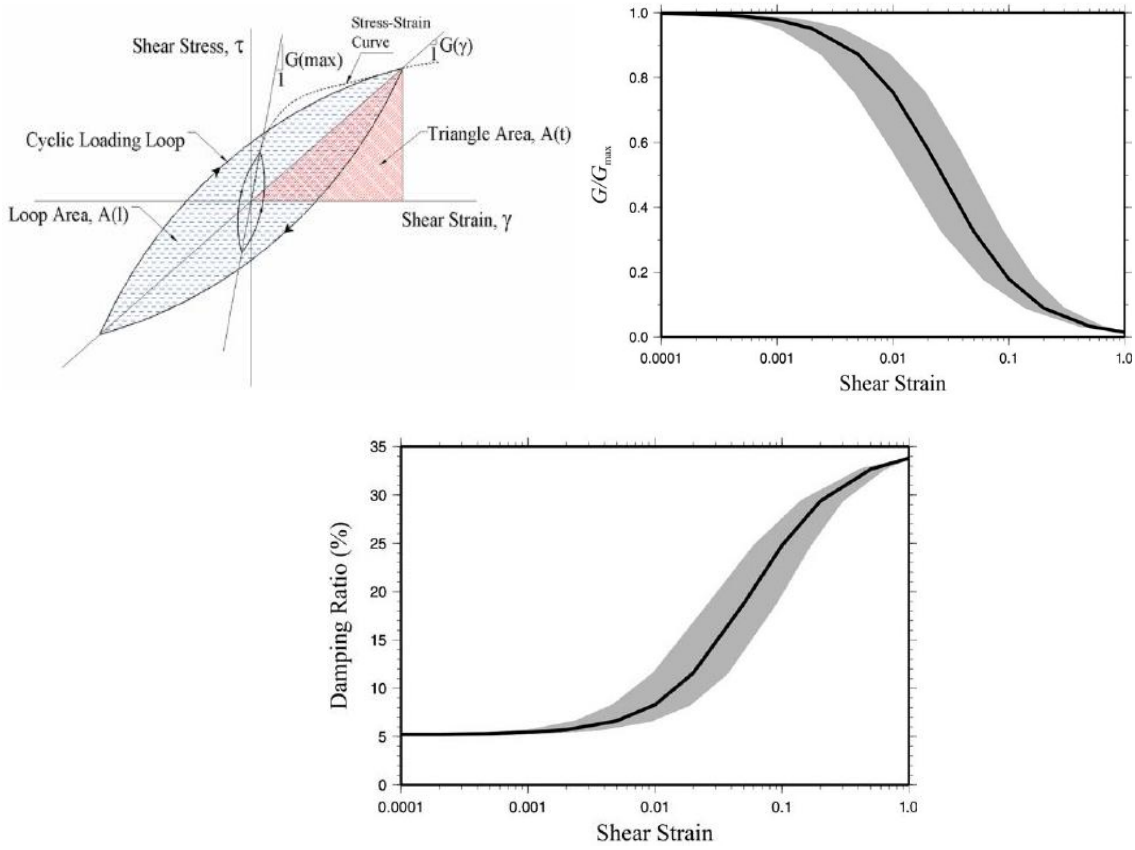

Fig 2.3: The (a) shear stress vs. shear strain backbone curve obtained from the (b) modulus reduction curve and (c) the damping ratio vs. shear strain curve [33]

The non-linear behavior is most accurately represented by nonlinear cyclic models which portray the actual stress-strain path when the soil is subjected to cyclic loads. These models are capable of predicting the shear strength of the soil taking pore water pressure effects into account and are sensitive to the changes in effective stress state during undrained loading cycles. When a soil sample is subjected to cyclic loading, its shear modulus goes on decreasing while it simultaneously dissipates more energy. The variation of the $\frac{G}{G_{max}}$ ratio and the damping coefficient with increasing shear strain are referred to as the modulus reduction curve and the damping curve respectively. When the shear modulus is multiplied with the shear strain and represented as a stress-strain curve it is defined as the backbone curve. For a single reference strain or confining pressure, a combination of the secant shear modulus and the damping ratio depicts the equivalent linear hysteretic behavior of the soil. These parameters also depend on the effective principal stress and given the simplicity of its experimental calibration from RCT and MTST data, it is widely used for seismic site response and SSI analyses. The shape of the backbone curve can be approximated as a hyperbolic function $\tau = f(\gamma)$, which is closely bound to the initial low strain stiffness (G_{max}) and high strain shear strength (τ_{max}). This hyperbolic function can be expressed as

$$f(\gamma) = \frac{G_{max}\gamma}{1+\frac{G_{max}}{\tau_{max}}|\gamma|} \tag{2.4}$$

The nature of the backbone curve can also be obtained from analytical approximations of some popular non-linear models such as the Ramberg-Osgood model [34]. The 3-D yielding behavior of materials have often been defined successfully under the tenets of plasticity theory which define material failure in terms of a yield surface, a hardening law and a flow rule. However, soil hysteresis behavior cannot often be generalized with a single flow rule or hardening law. Masing's hypothesis is often used to extrapolate the stress strain curve from the initial loading phase to the

unloading/reloading phase [35]. It states that 1-D symmetrical closed hysteresis loops are of the same pattern as the initial stabilized loading curve multiplied by a factor of two. The unloading and reloading behavior starting from a point of reversal (γ_r, τ_r) can be obtained as [34]

$$\frac{\tau-\tau_r}{2} = f(\frac{\gamma-\gamma_r}{2}) \tag{2.5}$$

The adoption of Masing's rule leads to two corollaries. Firstly, the greater the peak shear strain the lower the secant modulus, which means that the effective shear wave velocity ($V_S = \sqrt{\frac{G}{\rho}}$) decreases with the increase in shear strain. Secondly, the dissipation of energy at each hysteresis cycle is directly proportional to the area of the loop. It is also recommended that if the unloading/reloading curve exceeds the maximum strain in the previous cycle and crosses the backbone curve, it follows the backbone curve until the stress reversal in the next cycle. Additionally, if the unloading/reloading curve intersects the un-/reloading curve of the previous cycle it follows the stress-strain curve of the previous cycle [35]. The Masing rules have since been modified to account for modulus degradation due to pore water pressure effects [36] and strength/stiffness reduction for consecutive cycles using a reduction factor modification method [37]. The yielding behavior of materials which follow Masing's hypothesis was modeled through a combination of elastic-perfectly plastic slip elements arranged either in series-parallel or parallel-series [38]. The model was formulated on the assumption that the material properties are distributed over a large number of elements which dictate the form of the hysteresis behavior. The model can be thought of as a combination of slip planes or Coulomb friction elements which depict the distributed yield components of the system. The Iwan-type [38] model has been adopted in the hysteretic material model used in this study for dynamic non-linear SSI analyses. The advantages of using these non-linear cyclic models is that the shear strain can be non-zero when the shear stresses tend to zero, which allows the user to depict permanent strains. Other models focused on the determination of

volumetric strain due to shearing loads, are able to model the stiffness degradation under undrained load cycles or hardening when pore water pressure is generated [39, 40].

2.3.2 Constitutive modelling of soils and the soil-structure interface

Advanced constitutive models allow for accurate representation of the soil behavior or the interface by accounting for (i) initial stress conditions, (ii) stiffness factors: includes variation in stress paths, strain levels, consolidation ration, soil permeability and density, (iii) irreversible deformations and permanent strains depending on loading conditions, (iv) soil strength influenced by strain rates, undrained behavior and directional dependence or anisotropy, (v) drainage condition primarily influenced by the pore water pressure, and (vi) dilatancy, contraction and compaction parameters [41]. These models are bound by the fundamental tenets of plasticity theory which can be listed as (a) the yield surface: provides the envelop of critical stress upto which elastic behavior is noticed (b) the hardening law: describing the variation in the yield surface with the onset of plasticity and (c) flow rule: which provides the relationship between incremental plastic strain with stress increment, The most common and fundamental plasticity model would be the Mohr-Coulomb model which is elastic-perfectly plastic in nature, with the stress-strain behavior being described by the elastic modulus (E) and Poissons ratio (ν) in the elastic range. The failure criterion is defined by the cohesion and the friction angle and has a hexagonal failure envelope which has been verified through triaxial tests [42]. The hexagonal contour was modified to a simpler conical envelope [43]. This model successfully captured the effective stress path under drained conditions, however varies significantly for undrained soils.

Undrained soils are often observed to undergo some irreversible straining before the maximum is reached. Normally consolidated clays have been modeled as a strain hardening material using triaxial test data known as the Cam-Clay model [44]. The model was extended to

account for three-dimensional stress state [45] and multi-nested loci were applied to the yield surface [46]. The modified Cam-clay model is based on the assumption that the mean effective stress has a logarithmic correlation with the void ratio. This model is mostly suitable for modeling deformation rather than failure mainly for normally consolidated clays. Further modifications were introduced in developing bounding envelope models which enables smooth transition from elastic to plastic behavior [47]. The plastic shear strain of soft soils is modeled using a friction hardening formulation, while a cap hardening formulation is used to model the volumetric strain during compression [48]. This model, popularly known as the PLAXIS Hardening Model; draws a clear distinction between the compression and shear hardening which are responsible for introducing irreversible plastic strains due to deviatoric loading and isotropic compressive forces. The behavior of soils under cyclic loading was observed to significantly vary with the behavior of the soil-structure interface. The experimental results discussed in the previous section, led researchers to address the interfacial shear stress-strain behavior in terms of constitutive relationships which were executed through numerical models on a FEA or DEM framework. These models could be broadly classified into element-type, non-linear elastic and elasto-plastic categories.

In the early 60s, a two dimensional joint element was proposed to model the shear stress-strain behavior of the interface [49] which was developed into a 3D solid element for application in finite element analysis [50]. The relative motion between adjacent elements was expressed in terms of uncoupled degrees of freedom [51] and the deformation modes were deciphered using the virtual work principle [52]. However, the stick-slip behavior observed from cyclic shear experiments couldn't be modeled efficiently. Furthermore, there were issues with correlating the normal and shear stiffnesses. The thin-layer element model [53] intended to address the shortcomings of its precursors. Translational degrees of freedom were considered at interface

nodes and sliding was depicted through relative motions between surrounding soil elements and independent degrees of freedom. The Stress/strain relationship was correlated by a constitutive matrix (the shear stiffness found from direct shear tests and normal stiffness from participation of thin layer elements and adjoining solid elements) and was applied to displacement controlled finite element procedures. It was also observed that the zero thickness interface element [49] did not produce the desired normal stress vs lateral displacement trends. A number of numerical examples in both two and three dimensions were solved to validate the model. The thin layer model was further modified to account for dynamic SSI effects. The Disturbed State Concept [54] modeled the dynamic response of the granular media by referencing its current state to an intact (or initial) state considering induced anisotropy, micro-cracking or softening behavior. The fully disturbed state is characterized by the materials incapacity to carry further shear stress or the deformation at constant shear without change in volume, averaged over a planar projected area.

With the introduction of critical state soil mechanics, a number of non-linear models were developed. This is based on the assumption that when the critical state at large shearing is attained, shear deformation continues without dilatancy and change of stress ratio. The critical void ratio is inversely affected by confining pressure and the behavior of soil at any state depends on the distance between the current and critical state. This led to the development of hyperbolic relationships between the interfacial shear stress and the lateral tangential displacement. The modified Ramberg-Osgood model was also used to describe the cyclic behavior of the sand-steel interface from the CYMDOF experiments [26]. An elasto-plastic model with a non-associative flow rule was used to simulate the stick-slip behavior of sand-steel interfaces for low strains [55]. It was able to successfully model the shear band and deformation in the vicinity of the interface. This model was further modified to incorporate the non-linear rate dependent shear strains [56].

A hierarchy of models have been reviewed in the last two sections. The models vary widely in complexity and applicability, and the user should assess the problem carefully in order to justify the material model. It is important to note that no single constitutive relationship can be efficiently used to model all soil types. Soil is such a complex material, that the same specimen may show a wide variation in its response when the physical parameters are changed.

2.4 Review of site response analysis procedures

The investigation of earthquakes over the past decades have shown that the local site conditions can significantly affect the ground shaking characteristics during an earthquake. During the Mexico City earthquake of 1981, a significant amplification of the ground motion was observed at sites situated more than 300 kms from the epicenter. These amplifications were attributed to the local unconsolidated lacustrine deposits which had changed the intensity and frequency of the ground motion. The Northridge (1994), Kobe (1995), Gujarat (2001) and Nepal (2015) earthquakes amongst others point to the fact that the local geomorphological conditions and topographical features influence the propagation of seismic waves through layered soil deposits.

Site response analysis refers to the evaluation of the free-field response of a soil deposit when subjected to ground motions, in the absence of the structure. This is essential for predicting the dynamic stresses and strains on the soil surface resulting from the soil stratigraphy or nonlinearity and assessment of liquefaction hazards. It also helps in formulating design response spectra for sites which are especially useful for evaluating the slope stability and assessing the possibility of bearing-type failures due to dynamic loads. The fault rupture mechanism at the earthquake source plays an important role in determining the transmission of the ground motion to the surrounding soil or bedrock. However, modelling of fault mechanisms is very complex and empirical correlations have been formulated to predict the nature of energy dissipation and site response

based on the attributes of previous quakes. The mechanism of wave propagation is affected by the interface between different soil layers, where they undergo refraction and reflection depending on the shear wave velocity. It is safe to presume that the shear wave velocity of the top soil and the layers close to the surface are lower than those of the underlying layers, which cause the inclined waves to be reflected more towards the vertical direction. For 1D site response analysis, the boundaries between soil layers are assumed to be parallel to each other and extend infinitely in the horizontal plane. The response of the soil domain due to ground shaking is dominated by horizontally polarized and vertically propagating SH waves [9]. The quantification of local site effects for ground response analysis requires us to define the ground motion components based on its source of origin. The motion at the free surface or top soil is defined as the free field motion, while the motion at top of the bedrock or base of the soil deposit is referred to as the bedrock motion. The ground motion at a location where the bedrock is exposed at the soil surface is called the rock outcrop motion, and in the absence of the soil domain is referred to as the bedrock outcrop motion. The ground motion in the interior of the soil domain is referred to as the 'within' motion, which can be applied at the base of soil strata assuming that the bedrock is rigid.

One dimensional site response analysis is an effective tool for assessing and quantifying the effects of the local geology and geomorphology on propagation of seismic shear waves through the soil deposits. It can be broadly classified into linear, equivalent linear or nonlinear approach in the time or frequency domain. The linear approach involves the usage of transfer functions which relies on the principal of superposition, to evaluate the response parameters such as shear stresses and strains, free field acceleration, displacement, etc. in terms of the input bedrock acceleration. This approach involves the conversion of the input motion (at bedrock) into a Fourier series typically using Fast Fourier Transforms, which is then multiplied with the transfer function to

obtain the free field motion as a Fourier series, which can be converted to time domain using inverse FFT [9]. The transfer functions can be modified to account for damping, rigidity of the bedrock and elastic properties of layered soil strata. Since, the shear modulus and damping ratios are constant for the linear method, the mobilized shear stresses remain inconsistent with the changes in the strain levels. The linear approach was modified to provide rational estimate of the ground response by accounting for the soil nonlinearity. It is possible to model the nonlinear hysteretic behavior of soil using equivalent linear properties like the secant shear modulus and the equivalent damping ratio for a specific shear strain (see Sec 2.3), which was modelled using a linear spring and dashpot [57]. The shear modulus and damping ratios are obtained from laboratory experiments which use simple harmonic loading where the strain levels are characterized by peak shear amplitudes. However, actual ground motions display harmonic as well as transient (common in seismic acceleration histories) behavior, where the peak acceleration may be portrayed by a few spikes in the record. Since the harmonic loading represents a more drastic loading scenario as compared with the transient loading, the material properties are empirically calculated at two-thirds of the maximum effective shear strain [57]. With the evolution of hysteretic soil models [31], the equivalent linear soil properties were used to perform 1D site response analysis in the frequency domain using numerical tools like SHAKE [58] and SHAKE 91 [59] and was also implemented as a 2D finite element solution [60]. The equivalent linear approach can also be used to formulate transfer functions to derive ground motions at any depth of the soil domain from the free field motion. This process is called deconvolution and is primarily used to obtain ground motions at the interfaces between soil layers. Deconvolution process is iterative and there are some difficulties associated with obtaining strain compatible soil parameters when strain levels are high [61]. The initial step is to define the stiffness and damping parameters of individual layer followed

by a wave propagation analysis. Finally, the material properties are updated based on the maximum strain in each layer multiplied with the effective shear strain to maximum shear strain ratio [59], expressed in terms of the earthquake magnitude (M) as:

$$R_\gamma = \frac{M-1}{10} \tag{2.6}$$

The equivalent linear analysis method can lead to anomalous resonance or amplifications resulting from the coincidence of a random strong motion frequency with the natural frequency of the soil deposit. In reality, the stiffness of the soil deposit changes with the confining stresses and reference pressure during the course of an earthquake and wouldn't result in such amplifications. The pressure dependence of the equivalent linear soil parameters was adopted in the equivalent linear approach to account for the change in damping ratio of the soil with the frequency of the ground motion for frequency domain site response analysis [62]. The usage of effective shear strains tends to over-soften or overdamp the predicted free field response for peak shear strains larger than the residual shear strain and vice versa for low values of peak shear strain. However, effective stresses are quite effective in modeling the inception, distribution and eventual dissemination of pore water pressure when modelled using nonlinear time domain methods.

The well-founded stress-strain constitutive model is the core of nonlinear site response analysis. The parameters needed for formulating such a model would require significant test data both from the field and laboratory. While the equivalent linear method is an approximation of the seismic ground response, the nonlinear approach evaluates the site response through direct integration of the equations of motion in small intervals in the time domain, which allows us to incorporate any advanced constitutive model. The multi-degree of freedom lumped parameter model was developed to perform time domain site response analysis for multi-layered soil deposits [9]. Each layer is represented as a lumped mass with a linear spring and a dashpot for viscous

damping. The mass matrix is formed by combining half the mass from two consecutive layers at their interface and the stiffness matrix is updated at each time step to simulate the soil nonlinearity. Multilinear models were developed to perform time domain analysis [63] which were further extended to a rheological model based on an Iwan-type formulation. Several other cyclic stress-strain models like the hyperbolic (MKZ) model [64], the modified hyperbolic model, the Hardin-Drnevich-Cundall-Pyke (HDCP) model and the Ramberg-Osgood model were incorporated in nonlinear time domain programs such as DESRA-2 [65], DYNA1D [66], TESS1 [40], DYNAFLOW [67] and DEEPSOIL [68]. The DYNA1D model was centered on a soil plasticity model that depicts the undrained and drained behavior, anisotropy and path dependent stress-strain properties with isotropic kinematic hardening. The simultaneous propagation of compressive and shear waves was expressed through a multidirectional model that captured the gradual softening of soils due to evolution of pore water pressure [69]. One dimensional site response analysis was also performed on open source platforms like OpenSEES [70] using pressure dependent and pressure independent constitutive model parameters which represented the generation and dissipation of pore water pressure. The hyperbolic model was improved to account for modulus degradation and pore water pressure effects in D-MOD [71]. The modified Kondner Zelasko (MKZ) model defined the stress strain relationship for loading and unloading as [36]:

$$\tau = \frac{\gamma . G_0}{1+\beta\left(\frac{\gamma}{\gamma_r}\right)^2} \tag{2.7}$$

$$\tau = \frac{2.G_0.\left(\frac{\gamma-\gamma_{rev}}{2}\right)}{1+\beta\left(\frac{\gamma-\gamma_{rev}}{2.\gamma_r}\right)^s} + \gamma_{rev} \tag{2.8}$$

where, γ is the shear strain, γ_r is the reference shear strain, G_0 is the maximum shear modulus, β is a dimensionless factor and s is a dimensionless exponent. The model was further modified to include pressure dependency parameters and viscous damping formulation was incorporated for

low-strain damping [72]. The rate effect of strain rate dependence was also investigated and resulted in a difference of 20% and 10% for high and low amplitude ground motions respectively. The dynamic response of soil vary when simulated using the techniques discussed above, due to the inherent differences in their numerical formulation. However, based on the site and ground motion content one method can be more beneficial over the other. For example, the equivalent linear method is effective for modelling ground motions and where the frequency content is limited within a 20 Hz bound. In such cases, the bedrock motion can be expressed accurately with fewer Fourier terms which improves the accuracy in obtaining the free field motion through transfer function. Frequency domain methods are widely used due to their simplicity and low computational requirements. However, with the increase in computational capacity over the past decades, nonlinear time domain methods are more efficient in capturing the soil material nonlinearity over varying pressures and non-linear site conditions.

2.5 Review of soil structure interaction procedures

Soil structure interaction is a multidisciplinary field which resides in the intersection between structural mechanics, geotechnical engineering, soil dynamics and earthquake engineering, geophysics and computational sciences. It considers the combined response of the foundation, structure, the nonlinear soil strata surrounding the foundation and the underlying soil domain when subjected to a free-field motion. SSI is a combination of inertial and kinematic effects experienced by a rigid structure resting on a flexible soil mass. FEMA P-750 [73] made a broad classification of the SSI effects under the above mentioned categories. The inertia developed in the structure subjected to seismic forces causes transverse base shear, twisting and overturning moments to develop at the foundation which is transmitted to the flexible soil by means of rotations and displacements. The rotations and displacements result in dissipation of energy at the interface due

to hysteretic soil damping and radiation damping. These effects are classified under inertial interaction effects as they are linked to the structural inertia. Inertial interaction results in lengthening of the time period while simultaneously changing the damping characteristics of the soil. The stresses in foundations, piles and retaining structure cannot be determined without defining the displacement fields along the soil-structure interface. Site response data from multiple earthquakes have indicated that the foundation input motion is always different from the free-field motion. This can be attributed to wave scattering, base slab averaging and embedment effects [10], which are a result of the differential displacements and rotations caused by the kinematic effects of the stiff foundation resting on soft soil. Base slab averaging refers to the balancing of the spatial ground motion within the foundation footprint and results in a reduction in translation and enhanced overturning moments. SSI can be referred to as a coupled contact problem where the inertial and kinematic interaction effects are a function of each other [74]. The ductility of a structure has a direct correlation with the strength reduction of the interface which reduces with the time period. The elongation of the time period due to SSI can be beneficial to the structure and has been expressed through empirical relationships using conservation of energy principles for rigid foundations on stiff soil [75]. However, an increase in ductility demands was observed for rigid foundations on soft soils when the natural period of the structure exceeded the dominant period of the ground motion by 20% [76], which highlights the detrimental side of SSI. Investigation on structural collapse of bridge piers during the Kobe earthquake of 1995 [77] prove that sites with soft alluvial deposits tend to amplify the structural response by elongating the natural time period of the pier and intensifying the free field ground motion, which has further substantiated the negative effects of SSI.

SSI is not often considered in the design of regular structures, even though it has been extensively used for analysis of seismic demands of nuclear related safety facilities. Efforts to characterize and model soil-structure interaction for performance-based seismic design was initiated by NIST, which aimed to develop a set of guidelines for implementing SSI in seismic response analysis where the input ground motions at the foundation basemat is an accurate representation of the local site conditions and material nonlinearities. The pragmatic application of SSI was driven by the FEMA 440 [78] which provided some guidelines by adopting a nonlinear static pushover approach to SSI, which was later adopted in ASCE 41-06 [79]. However, there is still a dearth of well-defined provisions for inclusion of SSI in design codes globally, due to a lack of consensus in the numerical analysis procedures and its level of complexity, as well as a large variation in site characteristics.

The initial phases of SSI analyses relied on the modeling of the soil-structure system as a set of masses connected through a system of springs and dashpots [80], or a rigid structure resting on a viscoelastic medium over rigid bedrock. The application of harmonic excitation to two identical cylindrical masses resting on an elastic half-space revealed that the displacement history of the disturbed mass is modified by the second mass by means of small perturbations, when it approached its resonant frequencies [81]. A matrix formulation was developed for the dynamic perturbations induced on a secondary foundation by a harmonically-excited circular foundation [82]. Majority of the SSI studies in recent time, was driven by the nuclear industry, which is generally composed of a turbine building in the vicinity of a reactor assembly, which possess the tendencies of a harmonically-excited foundation system as described above. Furthermore, NPPs are composed of several frequency-rated sensitive equipment which could be affected by the slightest perturbation. The seismic response of adjacent nuclear reactor buildings [83] was studied

by modeling the NPP superstructure as a spring-mass system exposed to vertically propagating shear waves along orthogonal directions. Earthquake ground motions are highly random in nature, and depending on the local site conditions, poses serious challenges in developing a single methodology for assessing the response of various types of structures. The effects of SSI was thought to be beneficial based on the assumption that SSI increases the flexibility of the structure, thereby elongating its natural period. Since the effective damping ratio was thought to increase, the base shear demands were reduced when considering SSI defects. This led to the neglect of SSI effects for all practical design purposes. Forensic investigations from several earthquake damaged sites show us a different picture. The liquefaction failure of pile supported bridge piers in the 1989 Loma Prieta earthquake [84], progressive collapse of multiple bridge piers of the Hanshin Expressway during the Kobe earthquake [77], failure of pile supported asymmetric structures during the Nepal earthquake [85] and the deviation in expected site-response behavior from the Mexico city earthquake drew attention to the detrimental effects of SSI. A range of factors ranging from hysteretic behavior of soil, shear wave velocity of layered deposits to structural asymmetry, soil-to-foundation stiffness ratio were responsible for intensifying the structural response. Parametric studies on the inelastic seismic response of bridge piers have revealed a lower ductility demand at the expense of increased drift demands [86]. Similar studies on pile-supported bridge piers considering five synthetic accelerograms revealed that disregarding SSI effects might lead to underestimation of the ductility and drift demands. Large residual displacements were observed for flexible piers due to severe overturning effects at the foundation, which could cause the misplacement of the bridge deck from the connector elements as witnessed during the Kobe Earthquake [77]. The soil flexibility is also capable of causing differential settlements in low rise MRFs especially for heavy and stiff footings due to high inertial effects [87]. Most medium to

large scale earthquakes involve large deformations at the interface. The soil nonlinearity is the most significant factor that influences the structural response under large shear strains [88]. Parametric studies on three dimensional FEA models have shown that the soil-structure effects are enhanced due to foundation embedment, pore water pressure effects, confining pressure and dilatancy behavior, which in turn aggravate the inertial effects in the structure. Inertial effects are regulated by the aspect ratio of the structure and are transmitted to the soil causing an increase in the pore water pressure, thereby intensifying the effects of SSI especially for dry or saturated sands [89]. Response analysis of single story structures revealed that SSI might cause an increase in ductility demands and drift for inelastic structures. Most design codes don't take the increasing ductility demands into consideration and instead reduce the base shear demands. This was addressed by introducing seismic design coefficients which facilitate the structure in attaining its target ductility demands [90], especially for soft soil sites. The stiffness degradation of the soil-structure system is more pronounced in case of soft soil sites as compared to fixed basemat on stiff soil. This results in negative strain hardening which adversely affects the seismic response by increasing the inelastic drift demands and reducing the design strength reduction factor [91].

The ground motion content itself plays a crucial role in determining the influence of SSI on structural response. This has led to the evolution of stochastic processes for determining structural response of multi degree of freedom systems embedded on an elastic halfspace. This was carried out by exposing an idealized MDOF system (representing a multi-story building) embedded on a visco-elastic soil domain resting on a rigid bedrock, to force-controlled boundary conditions at individual story heights. The interaction between the basemat and soil was represented through a stiffness degradation matrix formulation obtained from the non-stationary stochastic processes [92]. The shear beam method was also an effective way of simulating the

propagation of vertically or obliquely propagating harmonic shear waves through a layered soil medium. This method was used to perform a 2D SSI analysis on a system of shear walls placed on a circular basemat while accounting for wave diffraction at the interface. High displacement amplitudes were observed when the applied input frequency approached the natural frequency of the shear wall indicating a cross-interaction effect [93]. A more numerically intensive analysis was performed on a number of rectangular and circular foundation embedded on an isotropic, homogeneous halfspace and subjected to harmonic excitation with Rayleigh waves propagating at random trajectories [94, 95, 96]. The wave scattering effects were observed near the foundation and the angle of incidence of the waves were also altered in the vicinity of the interface. This can be attributed to the spatial variability of the ground motion and multi-phase nature of the soil domain, which explains the drawbacks of using deterministic linear elastic parameters to describe soil-structure interface effects. A better way of addressing this issue is by dividing the variability into stochastic and deterministic components. Frequency domain analysis was performed on a MDOF system with the interaction between the mass and soil being represented through the traditional spring-dashpot formulation. The dynamic interaction behavior was captured using the Wilson-θ method which captured the period elongation of the incoming shear waves [97]. The deterministic component of the shear wave is computed by solving the wave equation for a multi-layered homogeneous soil domain. It involves a planar wave front approaching the soil-structure interface, which upon impinging from the interface scatters into adjoining regions that are delayed repetitions of the original wave front. The stochastic component arises from the spatial incoherence, which causes independent variations of the same wavefront across two different locations in the soil domain [98]. In other words, the wavefronts may deviate away from the interface at different instances with varied angles of incidence while adopting a propagation path which has different

material properties than the other impinging wavefront, while undergoing a shift in its phase and amplitude.

While the Wilson-θ method was used for modelling interactions between soils and shallow foundations, the Greens function approach was used to model the dynamic response of piles in a multi-layered elastic halfspace [99]. The incorporation of non-reflecting boundaries is a key factor is SSI analyses and has been adopted in various finite element analysis codes. We know that waves are reflected, refracted and diffracted from the soil-structure interface due to radiation damping. Similar phenomenon would be observed if we modelled the soil boundaries to be rigid, which could interfere with the waves propagating along the soil domain. Hence, it is imperative to adopt non-reflecting boundary conditions or model the semi-infinite half space with a much larger soil domain as compared to the structure's footprint which would be computationally expensive. Hence, viscous boundaries were proposed to reduce the full-scale soil structure domain [100]. Pure shear [101] and discrete stiffness matrix procedures [102] have also been used to model non-reflecting boundaries of the elastic halfspace for studying the cross-interaction between adjacent structures exposed to vertically propagating shear waves.

The objective of this dissertation is to formulate a well-defined and robust methodology for performing soil structure analyses in the time-domain using the direct method. The interaction and material parameters influencing the structural response are studied individually to effectively segregate and analyze their contributions. The motivation is to be able to rationalize the numerical implementation of the material models, interaction algorithms and boundary conditions in terms of the physics of the problem. Finally, the analysis results are studied to effectively summarize the steps needed to perform an accurate nonlinear SSI analyses.

3. COMPARATIVE ANALYSIS OF CONTACT MODELS FOR SOIL STRUCTURE INTERACTION

The response of a structure to dynamic loading is collectively affected by the interaction between the foundation and the underlying soil surrounding the foundation. SSI can have considerable influence on the calculated structural response due to geometrical and material non-linearities of the interface. The paper aims to establish appropriate contact formulations for the soil structure interface elements through the direct method of analysis. The geometric non-linearities associated with the interface; primarily sticking and slipping are investigated using both kinematic and inertial interaction methods. A series of simulations are performed on a symmetric structure resting on a soil domain with non-reflecting boundaries by applying quasi-static and cyclic loading in MASTODON [7], a MOOSE based software application developed by the Idaho National Laboratory. The tangential behavior at the interface is simulated using a simple Coulomb friction type formulation. The shear stresses and strains are obtained at the interface and compared to the theoretical values. A thin-layer-element based interface formulation is also developed using a phenomenological soil model I-SOIL in MASTODON, which takes material damping into account. Upon establishing the appropriate contact formulation for the interface, a full-scale soil-structure interaction analysis is performed. The response at the interface is compared using algorithms like Lagrange Multiplier, Penalty and Kinematic contact methods in ABAQUS and MOOSE.

3.1 Introduction

The numerical modelling of the contact between soil and structure at the interface is key to obtaining realistic solutions for the foundation response during SSI analysis. The modelling of the interface is based on various deformation modes such as slippage (sliding), no slip (tied), de-

bonding (gapping) followed by re-bonding (rocking); which are incorporated through constitutive models or thin layer elements. The constitutive relationship between the structure and soil is based on the correlation of normal and shear stresses with the displacements at the interface. The degradation of the interface due to sustained loading is governed by a friction model. With the increase in degradation of the soil surrounding the structure, the material non-linearity at the interface also changes which is characterized by softening or hardening of the stress-strain behavior. Hence, there is a need for updating the element interface stiffness matrix obtained from the relative displacements and stresses at the soil-structure interface. Extensive research efforts have focused on emulating this non-linear behavior considering relative motions as independent degrees of freedom to prevent numerical inconsistencies [49]. While some researchers have assumed the shear stress vs. tangential slip displacement to be hyperbolic in nature [103], others have considered it to be elasto-plastic [104] or developed complicated empirical relationships with multiple parameters like grain size, particle roundness, etc. The energy dissipation mechanism of the interface has also been modelled using two [49] or four-noded [52] interface elements using the virtual work principle by applying relevant boundary constraints. The thickness of the interface and the extent of the non-linear zone surrounding the basemat area are crucial towards development of an efficient contact model. The thin layer model for joints and interfaces assumes that the relative motion and degradation of asperity surfaces are localized in a thin layer and the thin layer can be modelled to prevent interpenetration between the soil and structure [53]. However, recent numerical simulations have indicated that the effective non-linear zone surrounding the interface cannot be efficiently modelled by coupling the normal and shear behavior of the thin layer element [105, 106].

The primary motivation of this chapter is to test a few traditional contact algorithms to simulate SSI for small and large scale two-block models subjected to pseudo-static and cyclic loading using two independent finite element schemes. A comparative study of zero-thickness interfacial interaction models and a phenomenological thin layer element model is performed to assess the suitability of the interaction algorithms for large scale non-linear soil structure interaction problems. The response of the two-block soil-structure (concrete block) system was carried out independently in MASTODON and ABAQUS. MASTODON (Multi-hazard Analysis for STOchastic time-DomaiN phenomena) [7] is a finite element application that aims at analyzing 3-D soil structure systems subjected to dynamic loading conditions and is capable of performing extensive simulations ranging from non-linear soil structure interaction, seismic probability risk assessment, fault rupture and non-linear wave propagation problems. It is a MOOSE (Multiphysics Objected Oriented Simulation Environment) based application which is equipped with an effective non-linear hysteretic soil model [107], and a u-p-U formulation which enables coupling of solids and fluids. In our simulations, we use MOOSE based interface formulations [108] and an I-Soil based thin layer element to obtain the stress-strain behavior at the interface. The MASTODON models are used to test and validate the performance of the thin layer element and other contact algorithms against the ABAQUS models. It allows us to physically understand the algorithm behind the contact method and build confidence in the same contact formulation in ABAQUS. Once the contact model of choice is obtained we proceed with the full scale NLSSI modelling of the Fukushima NPP (see Chap 4 and 6) and the TRISEE experiments (see Chap 5) in ABAQUS.

3.2 Benchmarking of SSI models

The benchmarking is performed on a two element model where the top block (assigned concrete material properties) is subjected to displacement boundary conditions and is expected to slide over

the bottom block (soil). The concrete and soil block are both linear elastic in nature. When the concrete block is subjected to pseudo-static and cyclic displacements, inertia is developed in the rigid concrete block which results in stress concentrations at the interface. The flexibility of the soil-structure interface results in energy dissipation via material damping in the form of Raleigh or hysteretic damping. The energy dissipation at the interface is a function of the mass of the structure, intensity or amplitude of the applied displacements, and modulus mismatch at the soil-structure boundary.

The calibration tests are performed by varying the contact algorithm using the same displacement-time histories for all the models. The maximum allowable shear stress across the interface is correlated to the normal pressure exerted on the soil using a Coulomb friction model. The two contacting surfaces can undergo lateral displacement up to a threshold shear stress, before they start slipping relative to each other. The critical shear stress at which the sliding starts is a fraction of the normal contact pressure at the interface determined by the coefficient of friction. For a three-dimensional model, there exists two orthogonal components of the critical shear stress along the interface. For simplicity, the friction coefficient is kept the same in both directions. The lateral loading is mainly controlled by a Dirichlet boundary condition in addition to the normal contact stresses due to self-weight of the structure. The contact pressure for a node-based slave surface equals the normal pressure divided by the total cross-sectional area of the contact node.

3.3 Contact algorithms for modelling interface behavior

Three independent contact algorithms have been used to model the interface:

(i) Penalty contact: A Dirac based penalty algorithm is used where the penalty stiffness is normalized with the nodal area. The penalty parameter is chosen such that it's not too high

where it causes ill-conditioning of the stiffness matrix and not too low which might cause the concrete block to penetrate inside the soil block. MASTODON uses an implicit time integration scheme which might cause convergence issues when the block is subjected to cyclic or seismic displacements. The problem is tested with a somewhat moderate value of the penalty parameter ranging between the bulk modulus of the two materials in contact. It is incrementally increased until convergence is achieved. The shear stress levels are averaged across the interface and compared with the theoretical value we would expect from the Coulomb friction model which is μ times the normal stresses exerted by the concrete block on the soil. The additional stiffness introduced by the penalty parameter can change the stable time increment. Hence it is important to assign a low time-step tolerance while using this formulation. The window of convergence for a penalty based contact algorithm is rather small and although there are some theories stating the usage of an ideal contact parameter, it's more of a trial and error method.

(ii) Kinematic contact: The kinematic contact method uses a predictive algorithm and has no influence on the stable time increment of the simulation. It is best suited to simulate sliding behavior without large penetration effects. A master-slave configuration is specified along with the friction coefficient. The mass of slave nodes in contact is distributed among the master surface nodes to determine the total inertial mass of the interface. A tangential tolerance value is specified to decide whether the nodes in contact will be released when the shear stresses developed at the interface exceed the critical value. The distance over which the contact normal is smoothened is specified to maintain equilibrium. MOOSE also provides us with a *stick_unlock_factor*, which when multiplied by the contact forces, must exceed the frictional capacity to unlock sticking of the two surfaces in contact. It is useful while

simulating the application of cyclic loading on the concrete block when we need to obtain frictional shear stresses for large strains. The MASTODON model is benchmarked against a similar ABAQUS model which uses a hard contact pressure overclosure relationship in the normal direction and a tangential slip relationship governed by the Coulomb friction model.

(iii) Thin layer elements (using I-Soil): I-Soil is a phenomenological, piecewise linearized non-linear hysteretic model which is very effective in modelling soils under dynamic loading conditions. The model is represented by a series of spring-slider components in a 1-D stress space that is analogous to distributed element modelling [7]. The type of yield surface is set on the basis of effective mean stress dependence, which is invariant in the stress space. Hence, there is no requirement for a kinematic hardening rule to model the hysteretic stress strain response. The I-Soil model in MASTODON is analogous to the MAT79 material model (in LS-Dyna) and exhibits numerical stability, which is attained by using Masing-type hysteresis rules for the re/unloading behavior of the shear stress-strain behavior. This imparts numerical stability to the material by allowing it to regain the strength and stiffness lost over a particular cycle [35]. The primary input of the I-soil material model is the shear stress vs. shear strain backbone curve (which can follow a user defined, Darendeli [109] or General Quadratic/Hyperbolic [110] model) at a particular reference pressure. An efficient approach of modelling the thin layer at the interface using I-Soil elements is presented in this paper.

As shown in Fig 3.1, the red layer between the soil layer (in green) and the concrete block (in white) is modelled with user defined I-Soil elements. The thickness of the thin layer elements can be within a range of 5 to 10 percent of the thickness of the surrounding elements in order to obtain accurate results. The properties of the thin layer are modified to simulate Coulomb friction

between the foundation block and soil using a user defined backbone curve. The failure criterion of the thin layer in accordance with the Coulomb friction model is represented in terms of the maximum shear strength $\tau_{max} = \mu\sigma_n$ where μ is the coefficient of friction and σ_n is the normal stress due to the concrete block.

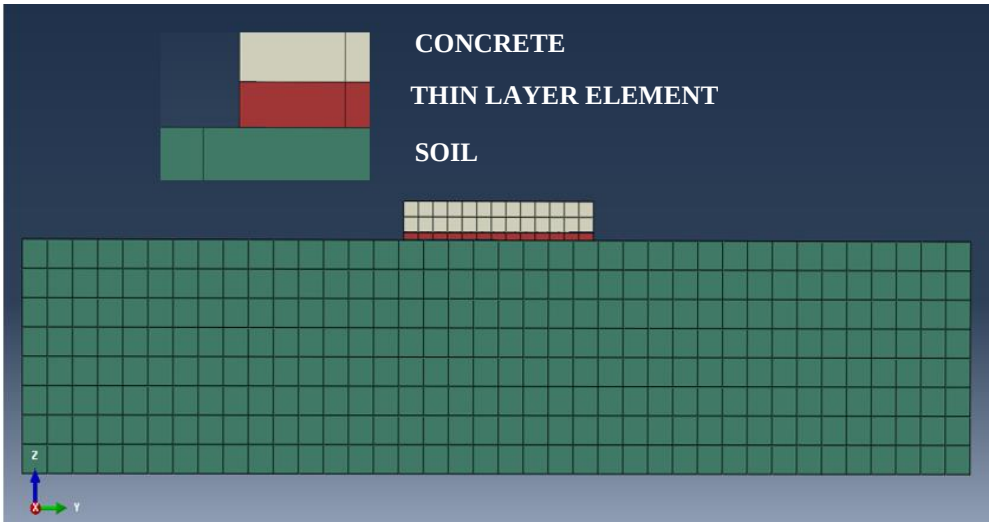

Fig 3.1: The foundation-soil interface modelled with thin-layer I-soil elements

The reference pressure p_{ref} is set to the normal stress due to gravity loads spread across the interface. The user defined shear stress vs shear strain curve is defined to be elastic-perfectly plastic with some hardening. The slope of the backbone curve for the thin layer in case of the foundation resting on the soil should be as high as possible and is chosen between the bounds of the shear modulii for the soil and the foundation. This is done in order to prevent the reduction of the foundation stiffness due to the presence of the thin layer. Any high frequency response is reduced by the almost bilinear stress-strain behavior, which causes gradual yielding of the interface with strain hardening. The Poisson ratio of the thin layer elements is set higher than the foundation and surrounding soil, in order to prevent sudden increase in the volume of the interface once the yield

point is reached. The pressure dependency of the backbone curve is turned on to ensure that the shear strength increases linearly with the normal pressure. The initial stresses needs to be specified in accordance with the approximate normal and shear stresses at the mid-section of the interface elements.

The above stated contact algorithms are compared with the tied case in which the foundation nodes are tied to the soil nodes. The unit element models are calibrated and benchmarked in MASTODON and applied to full scale models which are further verified in ABAQUS [8].

3.4 Small scale verification studies using MASTODON

A number of verification tests were performed on two element models on the basis of the contact algorithm adopted. The bottom element was assigned linear elastic soil property and was fixed at the bottom while the top block was assigned linear elastic concrete properties (all details have been tabulated in Table 3.1).

Table 3.1: Elastic properties of materials

Material	**Elastic modulus (N/m^2)**	**Poisson's ratio (ν)**	**Density (kg/m^3)**
Concrete	6.5E+10	0.25	8792*
Soil	7E+09	0.3	2500
Contact Element (I-Soil)	7.83E+10	0.45	2500

*The density of the concrete is approximately increased 3 times to simulate the weight of a full-scale real structure, which is highly idealized as a rectangular block. The structure height is reduced to avoid overturning effects; as our focus is on the sliding behavior

A function-based Dirichlet boundary condition is applied on a chosen boundary to apply cyclic or pseudo static loading. The blocks are modelled as HEX8 brick elements which are 10*10*10 units in size. In the MOOSE contact module, the concrete face is chosen as the master

surface and the soil block as the slave surface. Glued contact is used to obtain stresses at the interface when the nodes are tied. For the kinematic and penalty contact, a Coulomb based friction model is chosen where the friction coefficient is provided as input, along with the tangential tolerance and tension release threshold. For the penalty contact an additional penalty parameter is specified which is perfected after a few trials.

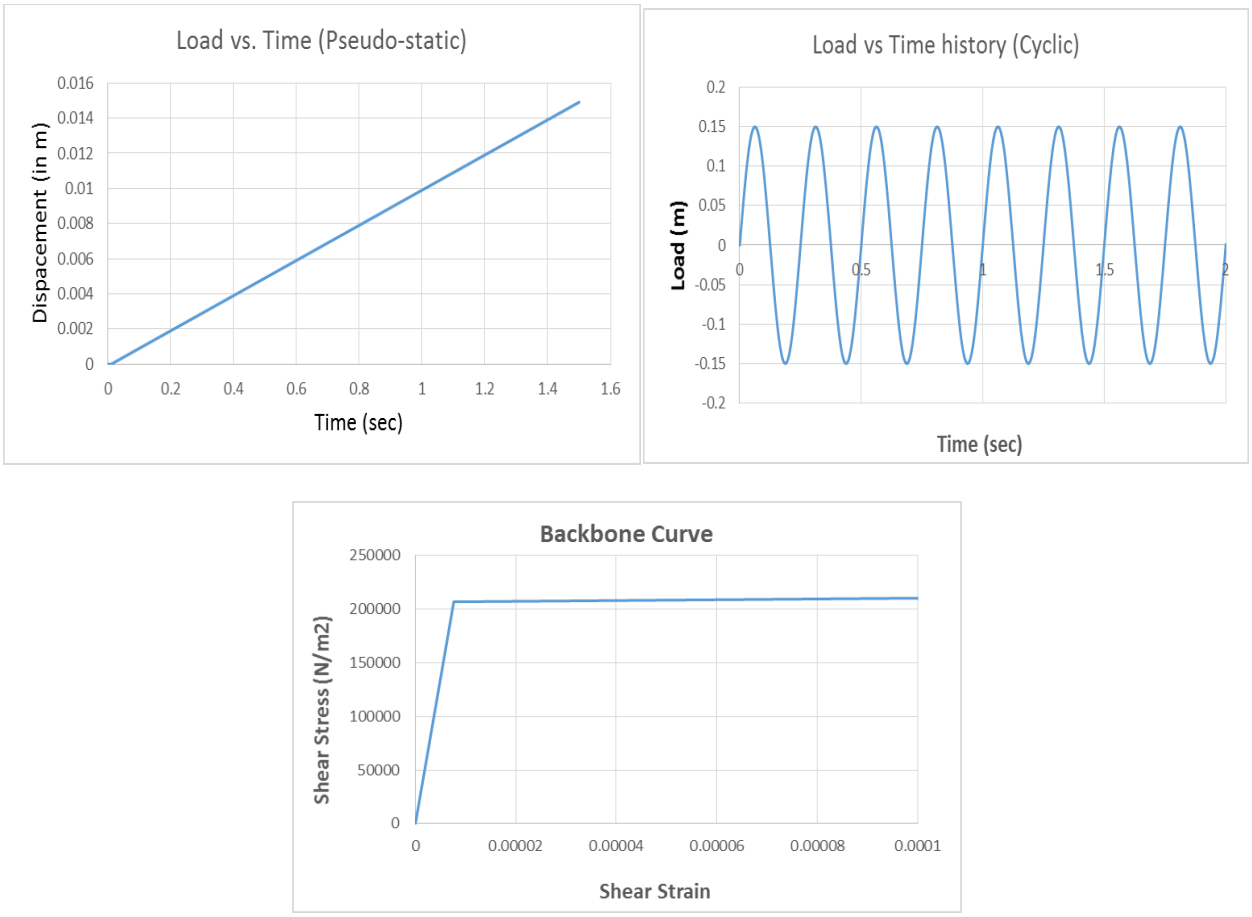

Fig 3.2: Input parameters for the contact models: loading and backbone curves

For the I-soil verification model, there is an additional interface block which is assigned a thickness that is one-tenth of the soil and concrete block. All the unit cells are assigned periodic boundary conditions such that the nodes shared by the cell at a particular face move together, which helps us in simulating the unit cell as a part of an infinite domain. The quantity of translation

is also specified which in this case is the element size. The small strain properties of soils such as the shear wave velocities, shear modulus, etc. change with depth. The depth dependent properties of soil profile are incorporated in the model using layer ids. For a set of horizontal layers stacked on top of each other, the depth of each interface is provided as input, and MASTODON uses the input data to generate a set of layers, referenced by a unique identification number. The layer ids are used to assign material property to each layer.

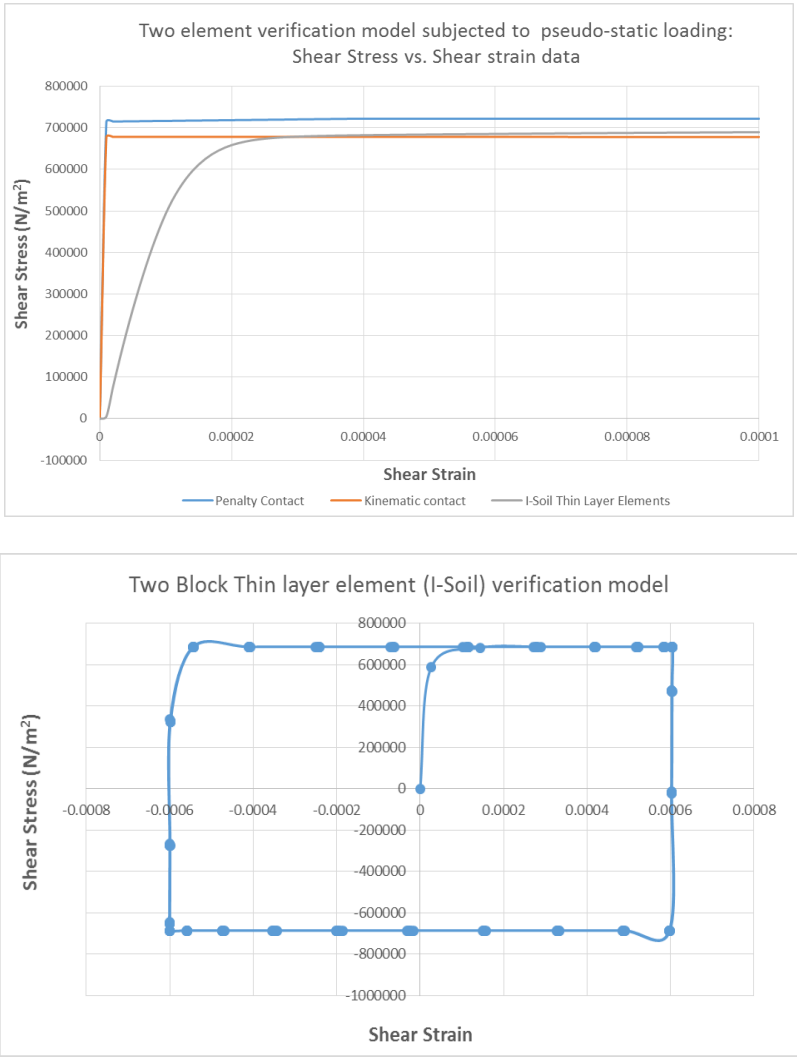

Fig 3.3: Shear stress vs. shear strain curve for the interface element when subjected to (a) pseudo static loading (b) cyclic loading in MOOSE/MASTODON.

In our unit cell calibration tests, we assign a linear elastic constitutive model to the concrete and soil layer (block) and a non-linear hysteretic soil model (I-soil) for the interface layer. The I-soil block in the numerical model takes the user defined backbone curve as input for a particular reference pressure. In our case, we assign an initial stress equivalent to the initial frictional stress at the interface and the strain value is chosen such that the slope of the curve matches the shear moduli chosen (discussed in the previous section). A high value of Poisson's ratio in the order of 0.45 is chosen for the interface element. The pressure dependency is turned on and the initial stresses at the mid sections of each block is specified.

Table 3.2: Comparison of frictional stress data at the interface for small-scale verification models

FEA Environment	Loading	Contact Algorithm	Element type	Shear Stress (Theoretical)	Shear Stress (Stress_ZX)	%age error
MASTODON	Pseudo-static	Thin layer I-Soil	HEX8	685500 N/m^2	689996 N/m^2	0.65%
MASTODON	Cyclic	Thin layer I-Soil	HEX8	Normal Stress (Theoretical)	689996 N/m^2	0.65%
MOOSE	Pseudo-static	Kinematic	HEX8	2285000 N/m^2	690217 N/m^2	0.69%
MOOSE	Pseudo-static	Penalty	HEX8		718236 N/m^2	4.77%

The figures and table above show the correspondence in results obtained from the different contact algorithms used for the unit tests on the basis of a Coulomb friction model assuming a friction coefficient of 0.3. The thin layer element and the kinematic contact methods perform really well in simulation of the sliding behavior within an error threshold of 1%. However, we observe a minor hardening of the stress-strain curve due to the Masing-type hysteretic behavior, which imparts additional strength and stiffness to the interface element, post yielding. This behavior is easier to observe in the cyclic loading case. We observe a slight increase in the shear stress prior

to the un/reloading phase before attaining a constant threshold stress and the slope of the un/reloading curve is parallel to the initial curve. Theoretically, we would expect a slight pinching of the stress-strain curve due to energy dissipation. Hence, a reduction factor based modification on the un/reloading behavior is being implemented to address this issue [37].

In case of penalty contact, when the contact shear stresses across the interface approach the maximum yield stress, it becomes very difficult to determine the stress-strain behavior from the displacements due to an extremely discontinuous force profile. Hence, by overestimating the penalty parameter, the contact function might be replaced with a relatively smooth but highly non-linear function. This causes a slight overestimation of the yield shear stress as seen in Fig 3.3(a).

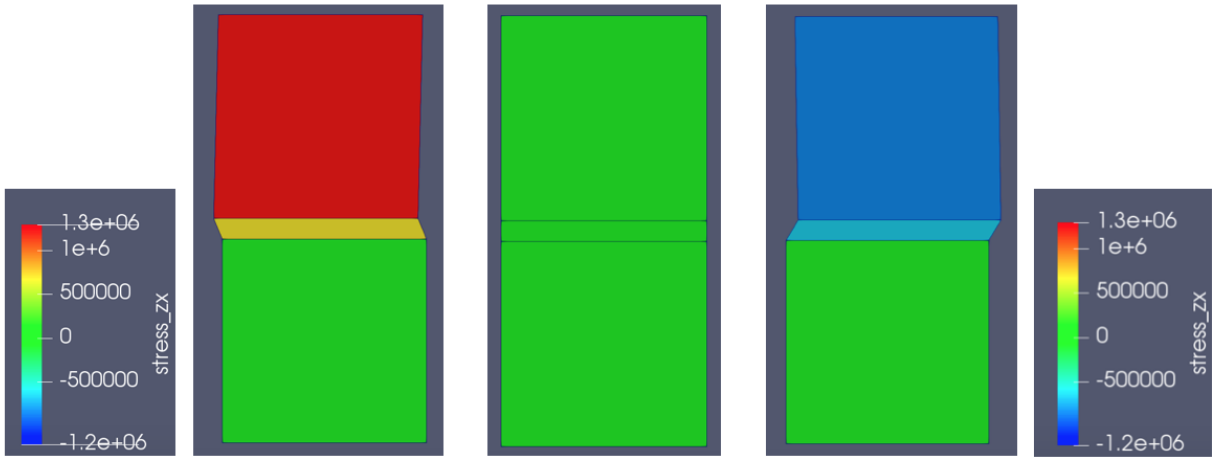

Fig 3.4: Shear stress profile for the thin layer element formulation with the interface element sandwiched between the concrete and soil block.

3.5 Large scale contact modelling using MASTODON and verification with ABAQUS

The verification studies have shown good correspondence for the various contact algorithms. The calibrated friction parameters are now applied to a full scale simplified model. The model consists of a rectangular concrete block (30m*30m*4m) resting on a soil block (150m*150m*30m). The soil domain is five times as large as the concrete block to simulate non-

reflecting boundaries. The thin layer interface is 0.5m thick. The thickness is small enough to facilitate transfer of stresses through the interface but large enough to avoid drastic volumetric changes of the interface at yielding. The material properties are kept the same as small scale calibration models and the input values of reference pressure, initial stress, backbone curve, pressure dependency etc. are modified to be consistent with the small scale calibration models. Periodic boundary conditions are applied only to the concrete and I-Soil block to ensure that the faces along any direction move together.

Table 3.3: Comparison of frictional stress data at the interface for large scale models in MOOSE/MASTODON and ABAQUS

FEA Environment	Loading	Contact Algorithm	Element type	Shear Stress (Theoretical)	Shear Stress (Stress_ZX)	%age error
MASTODON	Pseudo-static	Thin layer I-Soil	HEX8	206787 N/m^2	199997 N/m^2	-3.2%
MASTODON	Cyclic	Thin layer I-Soil	HEX8	206787 N/m^2	199997 N/m^2	-3.2%
MOOSE	Pseudo-static	Kinematic	HEX8	206787 N/m^2	204516 N/m^2	1.09%
MOOSE	Pseudo-static	Penalty	HEX8	206787 N/m^2	153900-220322 N/m^2	-25.5% - 6.5%
ABAQUS	Pseudo-static	Lagrange Multiplier	HEX8	206787 N/m^2	205000 N/m^2	0.86%
ABAQUS	Pseudo-static	Penalty	HEX8	206787 N/m^2	200000 N/m^2	3.28%

For ease of computation time, the mesh size of the soil block is doubled with reference to the concrete and interface block. This is especially important when simulating kinematic and penalty contact. For simulating the master-slave frictional contact, the prescribed displacement at

the nodes of the slave surface of soil block (which is relatively flexible as compared to the concrete block) is projected into the segments of the master surface. If the displacements are small and there is no significant relative motion between the two surfaces, the slave and master nodes are in close proximity and it's easier to implement the friction model. However, in case of large displacements, when the contacting slave node is unknown, the algorithm needs to perform a pattern search for the contacting master segment at every iteration which affects the processing speed significantly.

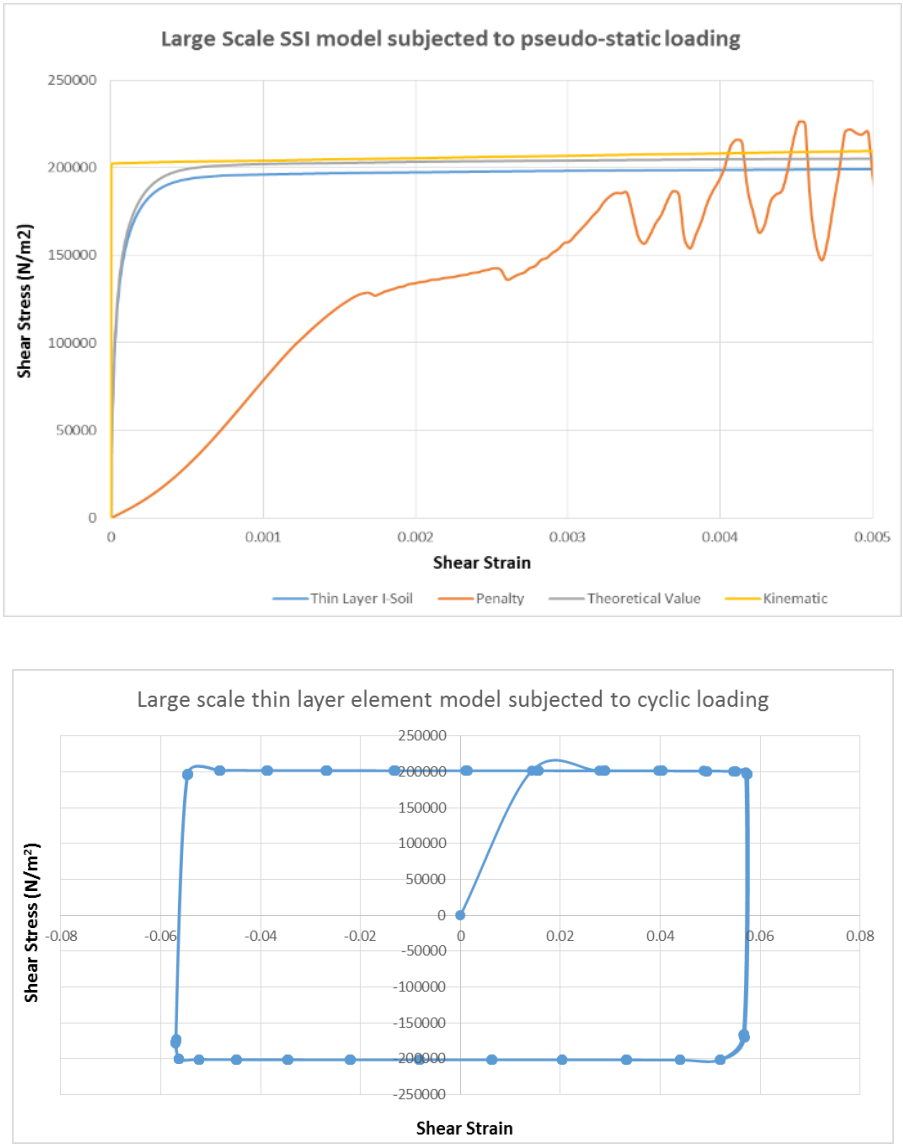

Fig 3.5: Shear stress vs. shear strain curve for the soil-structure interface in the large scale model when subjected to (a) pseudo static loading (b) cyclic loading.

It is observed that the thin layer element model and kinematic contact model show good correlation with the theoretical shear stress vs. shear strain values. However, we observe some convergence issues for the penalty contact. This may be caused by the large displacements exceeding the contact tolerance or the load increment might be large thereby violating the contact constraint. As stated before, a large value of penalty is input into the model to reduce penetration, which might cause convergence issues.

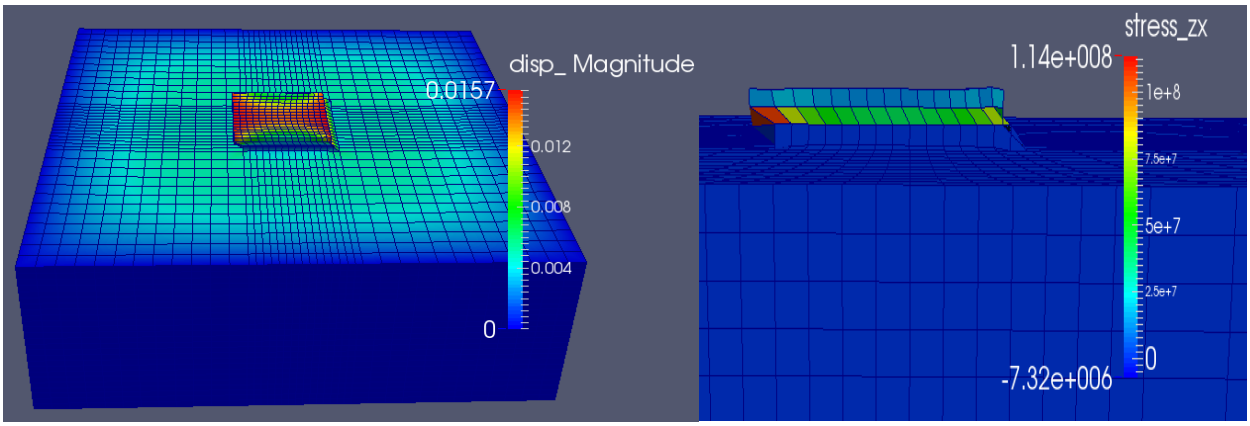

Fig 3.6: Displacement and shear stress profile for the thin layer element formulation for the large-scale model in MASTODON and ABAQUS.

The large-scale models are also simulated in ABAQUS using the Lagrange Multiplier algorithm with consistent material models, loading and boundary conditions and mesh size. The results are comparable with the theoretical values (see Table 3.3).

3.6 Comparative analysis of contact algorithms

The paper discusses four methods (Penalty Contact, Kinematic Contact, Thin-layer elements and Lagrange Multiplier method) to model the non-linear interaction at the soil-structure interface. The penalty contact method checks for slave node penetration in each step. The process is continued till the slave node penetrates the master surface and an interfacial contact force is introduced

between the node and penetrated surface. The contact force is directly proportional to the stiffness of the master surface and penetration depth. If there is a discrepancy in assigning the user defined initial stiffness or penalty parameter, there are convergence issues. The additional stiffness introduced into the model by the penalty algorithm may also influence the stable time increment. Although, the penalty method can imitate the physical behavior of the interface by restricting the penetration of the concrete block into the soil surface, it may completely overestimate the yield shear stresses at failure. Therefore, the penalty contact method may not perform well for large scale models, where the foundation stiffness is unknown.

Kinematic contact is preferred over penalty method when performing cyclic or dynamic SSI analysis as the stress outputs at the interface is less noisy. It follows a predictor/corrector method where the kinematic state is progressed by ignoring contact parameters which results in overclosure or penetration in the predictor phase. During the correction phase of the time increment, the momentum conservation principle is used to apply an acceleration correction to the master and slave nodes. When the predicted penetration is reached, the master nodes are in compliance with the slave nodes. Due to the implicit nature of the kinematic contact algorithm, the contact penetration is eliminated at each stable time increment as opposed to the penalty method, where residual penetration exists at the end of each time step. The kinematic contact definition is not suitable for rigid body contact as reduced deformations result in higher stresses. However, in case of soil structure interface, it yields accurate results due to large variations in the elastic properties of the two materials. The computational cost is also much lesser than the penalty method for large simulations.

The Lagrange Multiplier method imposes the impenetrability condition exactly where the contact forces are independent as opposed to the penalty algorithm where contact force is a

function of deformation. It also ensures that the resultant stresses across the interface is balanced even though the distribution of forces may vary due to discretization. In the kinematic contact method, the Coulomb friction forces are indeterminate when two bodies in contact are stick which means the unique determination of shear stresses at the interface in not possible. Furthermore, there are small elastic deformations prior to slip which requires us to regularize the friction model by imposing normal and tangential damage conditions. The Lagrange Multiplier algorithm implements a large normal stiffness using a hard contact pressure overclosure relationship, while the tangential stiffness criterion is governed by the maximum shear stress which is a function of the friction coefficient. This method is best suited in large scale soil structure interaction models [106].

The thin layer element algorithm using the I-soil material model has some added functionality in terms of pressure overclosure and non-linear stress-strain behavior at the interface under dynamic loading conditions. The shear strength of the thin layer can be modified to account for the degradation of yield shear stresses at each loading cycle. In case of the Lagrange multiplier or kinematic contact method, there is a possibility of high frequency response because it considers pure Coulomb friction (elastic perfectly plastic shear behavior) at the interface, which causes a sudden reduction in the interface shear stiffness. The I-soil model can be modified to include some strain hardening of the shear stress-strain backbone curve to bypass this issue [8]. The pressure dependency option of the thin layer model ensures linear scaling of the shear stress vs. shear strain curve with the normal pressure at the interface. Therefore, the thin layer element model is effective in simulating site soil conditions for assessment of seismic margins of the substructure resting on it. This method can also be used for interface modelling of large scale SSI models in ABAQUS using the recently included Hysteretic Soil UMAT.

3.7 Chapter Summary

The chapter focuses on various contact algorithms to simulate the geometrical non-linearities of the soil structure interface. A novel thin layer element formulation is proposed which can be used for large scale detailed soil structure interaction models. The performance of the thin layer element is comparable to the kinematic contact and Lagrange Multiplier algorithms, generating yield shear stresses within 5% accuracy. Tests on the thin layer element is also carried out for cyclic loading conditions and relatively accurate frictional stresses are obtained. However, the energy dissipation mechanism does not perform as well, due to Masing hysteresis properties. In addition, there is a need to improve the thin layer interface model in the MASTODON environment for simulating gapping and overturning effects, such that it can be efficiently employed to capture non-linear interface responses for complex large-scale models. It also lacks certain element types with hourglass and stiffness controls, which are essential for modeling large-scale NLSSI models of the nuclear power plant. These shortcomings are resolved when we analyze the full-scale models of the Fukushima Daichii NPP in ABAQUS. The hysteretic soil model in ABAQUS is used in conjunction with the kinematic contact model and a softened pressure overclosure relationship to carry out full scale NLSSI analysis which will be discussed in detail in Chapter 6.

The computational efficiency of the individual contact algorithms are tracked for the same number of processors and parallelization environments. The penalty algorithm does not perform as well, primarily because an implicit solver is used in the finite element implementation. However, the thin layer element in MASTODON proves to be computationally efficient and at par with the kinematic and Lagrange multiplier algorithms in ABAQUS.

4. SOIL STRUCTURE INTERACTION ANALYSIS CONSIDERING GEOMETRIC NONLINEARITIES AND LINEAR SOIL PROPERTIES

In Chapter 3, a comparative analysis was performed to analyze which contact algorithm is best suited to simulate the behavior of the soil-structure interface when subjected to cyclic loading. In this chapter, an exploratory study is performed to compare numerical linear soil-structure interaction (LSSI) analyses results with measured ground motions. The goal is to evaluate the sources of geometric nonlinearity (using contact algorithms discussed in Chap 3) contributing to the reduction in peak acceleration between the free-field and basemat response. To achieve this goal, a series of linear SSI analyses is performed using ground motion data from the Tohoku earthquake and site soil profile measured near the Fukushima Daichii nuclear power plant Unit 6. The focus of the analyses is on the evaluation of two specific nonlinear effects attributed to localized soil nonlinearity; gapping and sliding. A full scale finite element model of the NPP-soil assembly is simulated in ABAQUS and benchmarked with linear soil structure interaction (LSSI) models in LS-DYNA [111]. The geometric non-linearities are then introduced to the linear SSI model and the acceleration response is tracked through comparison of the response spectra at the free-field and basemat. The influence of the contact parameters on the variation in structural response is assessed through parametric studies. The parametric study aims to segregate the response of the basemat due to sliding from the gapping behavior.

4.1 Analysis methodology: Direct method vs. Substructuring method

The methods employed to perform soil structure interaction analysis under dynamic loading can be broadly classified into two main approaches; the direct method and the substructuring method. The direct method allows us to simulate the response of the soil-structure system in a single step

in a finite element framework. The system is comprised of a finite soil domain with well-defined boundaries where the interactions between the basemat and soil, material and geometrical non-linearities can be analyzed using a single FEA model. The foundation basemat and the surrounding soil domain share common nodes while a recorded acceleration-time history is applied at the bedrock or as a within motion. In reality the soil domain is infinite, which is incorporated within the model using artificial transmitting boundary conditions at the near field/far field interface. Some models also employ a large soil domain in comparison to the structure to satisfy the radiation damping condition, such that the waves reaching the boundaries are not reflected back, which might interfere with the in-structural response. This approach requires significant computational resources and has often been used to achieve realistic analysis results [112, 113]. In commercially available finite element platforms, the direct method can currently be performed only for vertically propagating compression or shear waves.

The substructuring method on the other hand treats the soil and structure as different substructures and the responses are superposed to obtain the overall response of the structural system. This method, though computationally flexible, does not consider the nonlinearities and interaction properties associated with the interface between the soil and the basemat. The dynamic stiffness of the soil domain is represented in a condensed form at the soil-structure intersection. The substructure method is primarily applicable for linear analysis, though recent programs like DEEPSOIL [68] have used non-linear backbone curves for material definition coupled with Rayleigh damping. The response of the soil domain is computed through site response analysis where the ground motion is input at the bedrock or at a certain level in the confined soil domain. The response output from the site response analysis acts as the input for the structure. This is referred to as the Foundation Input Motion (FIM) which is representative of the basemat response

acceleration had it been devoid of mass and stiffness. The dynamic stiffness of the foundation-soil interface is derived from a massless foundation model, represented in terms of the external harmonic excitation which is composed of a real and imaginary part. The seismic input of the structure accounts for kinematic contact and foundation stiffness coupled with radiation damping known as impedance functions. Impedance functions depict the damping and stiffness characteristic of the soil-basemat system. The dynamic investigation of the structure is performed on a compliant foundation basemat which is represented through a compliance matrix (a combination of rotational and translational springs and dashpots). The dashpots are constituted of two primary sources of damping: (i) radiation damping accompanied by the mobilization of dynamic forces in the superstructure which causes the foundation to deform the granular soil, thereby generating stress waves which move away from the foundation, and (ii) material damping resulting from the inelastic soil behavior, which can substantially increase with the level of strains induced in the soil [9]. Following the determination of the FIM and the foundation compliance matrix, the analysis of the structure can be performed using any commercially available finite element software. The substructuring method can also be used to simulate geometrically irregular boundary conditions using the boundary element method.

4.2 The Fukushima Daichii Nuclear Power Plant

The Fukushima Daichii Unit 6 is considered in this study. It is a boiling water reactor (BWR Mark II) located in the Futaba District of the Fukushima Prefecture, Japan. A schematic cross-section view of a typical BWR Mark II containment is shown in Fig 4.1. A numerical model uses the dimensions of the Fukushima NPP Unit 6 (including the reactor and turbine buildings) with an idealized reactor assembly resting on a non-linear subsoil (linear for this chapter) surrounding the structure and an infinitely large linear elastic soil domain.

Site details including the location of the observation sites and soil profiles are shown in Fig 4.2 [2]. The soil in Fukushima Daichii Unit 6 can be dominantly classified as variations of mudstone. The soil layers present at the site are depicted from the borehole information provided by TEPCO. Table 4.1 summarizes the provided data from the seismometers located near Unit 6. The maximum recorded acceleration in north-south, east west, and up-down directions, shear wave velocities and compressional wave velocities are listed respectively in gals (cm/s^2) and m/s. The elastic soil properties were determined with reference to the Central Federal Lands Highway geophysical methodology [2]. The reported elastic soil properties of the site near Unit 6 are summarized in Table 4.2

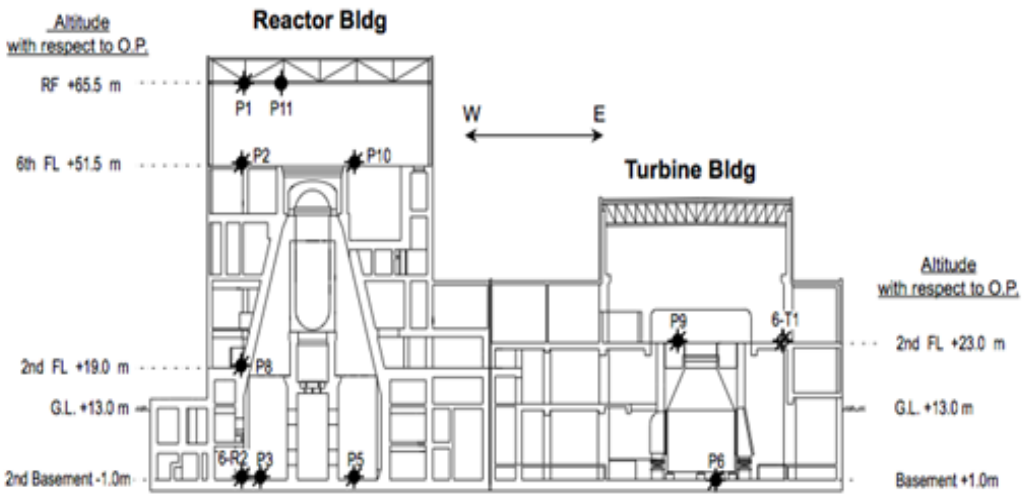

Fig 4.1: Schematic cross-section view of BWR Mark II containment.

Table 4.1: Maximum accelerations recorded for borehole location at Unit 6

Location	Depth (m)	Obs. Pt.	Max Acceleration (Gal)			Shear Velocity (m/s)	Compressional Wave (m/s)
			NS	EW	UD		
Borehole near Unit 6	-31.5	P13	252	405	194	470	1710
	-31.5	P4	209	387	189	470	1710
	-143.5	P14	313	302	113	580	1820

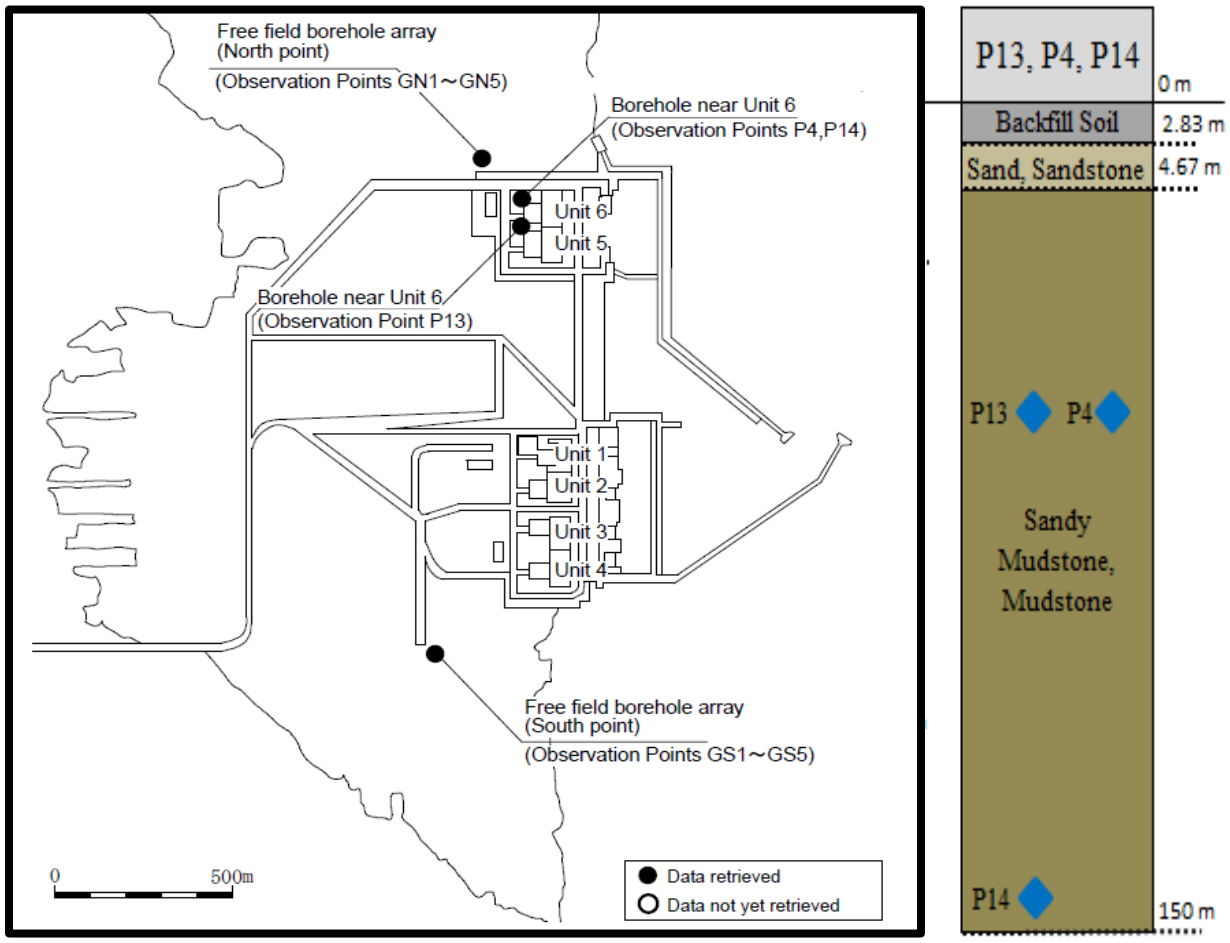

Fig 4.2: Fukushima Daiichi nuclear power plant schematic locations of boreholes on site and interpreted soil layering near Unit 6

Table 4.2: Elastic soil properties for observation point near Unit 6 [3]

Location	Obs. Pt.	Density (kg/m^3)	PR	Young's Mod (Pa)	Shear Mod (MPa)
Borehole near Unit 6	P13	252	0.46	1285090459	440.36
	P4	209	0.46	1285090459	440.36
	P14	313	0.44	1966421665	681.14

4.3 Numerical modeling and analysis

The direct method is used to perform a full scale linear soil structure interaction analysis in Abaqus CAE. The FEA model of the Fukushima Daichii Unit 6 is an idealization of the actual NPP. The entire structure is primarily composed of 8-noded brick elements with the complex reactor assembly and the reinforcement cage being modeled with 10-noded tetrahedral and beam elements respectively. It is common for most nuclear plants to have the reactor building located close to the turbine building and other ancillary structures such as the transmission assembly, the diesel generator building, etc. The adjacent buildings have an influence on each other due to inertial interaction effects, which is referred to as soil-structure-soil-interaction. The analytical studies are performed taking into account (i) the dimensions and location of the power plant building cluster (ii) the location of ground motion input and (iii) dynamic earth pressure underneath the structure.

4.3.1 Finite element model of the NPP for simulation of SSI effects

The primary motivation of the study is to compare numerical LSSI results with the ground motion and site profile data obtained from field, and compute the contribution of the sources of geometric nonlinearities. A detailed model of the NPP assembly is built with a layer of fine meshed soil surrounding the reactor and turbine building basemat which is tied to a large soil strata. The loading is applied to the structure in terms of an acceleration input at the base of the soil strata. The linear in-structure acceleration response is computed to study acceleration attenuation effects and is performed in phases to understand the effect of the geometric nonlinearities individually.

The damping of the soil-structure system for the LSSI analysis is modelled using Rayleigh damping, which is composed of a linear combination of mass and stiffness matrices, modified using the mass (η) and stiffness (ζ) dependent damping parameters. The equation of motion can be given by

$$M\ddot{u} + (\eta M + \zeta K)\dot{u} + Ku = F_{external} \tag{4.1}$$

The degree of damping (ξ) as a function of the frequency is correlated to the mass and stiffness dependent coefficients as [7]

$$\xi(f) = \frac{\eta}{2}\frac{1}{f} + \frac{\zeta}{2}f \tag{4.2}$$

The constant damping ratio is obtained by optimizing the values of η and ζ such that the target ξ(f) can be reached within the frequency range of the ground motion. However, the double mode Rayleigh damping would only account for the ground motion component within the specified frequency range and will overestimate frequencies outside of the range. The frequency range for the two-mode Raleigh damping is obtained by using the natural frequency of the soil and five times the value for the soil column of interest as the lower and upper bound [114]. Although the mass and stiffness damping parameters can be adjusted to obtain a constant damping ratio for short frequency ranges, it varies for large frequency ranges. The material damping for small strain ranges is unaffected by loading frequencies in the range of 0.01 Hz to 10 Hz [115, 116, 117]. The damping formulation is improved for large strain ranges of the soil by using the ABQ_HYSTERETIC_SOIL model, which simulates the energy dissipation due to soil material nonlinearity using a multilinear-inelastic stress-strain backbone curve (discussed in Chap 5 and 6).

LSSI analysis is performed with elastic material properties (elastic modulus, Poisson's ratio, and mass density) and material nonlinearities are ignored. The soil domain, superstructure, mesh properties, loading conditions and boundaries are consistent throughout the analysis process. The mesh size of the structure and the soil domain surrounding the basemat is consistent to facilitate wave propagation at the interface, avoiding mesh deformation effects. The model is primarily split into three parts, viz. (i) Concrete superstructure and substructure which is linear elastic (Elastic modulus (E):30 X 10^9 N/m^2; Poisson's ratio (ν): 0.25; Density: 2400 kg/m^3)

comprising of solid, homogeneous sections and built of C3D8R reduced integration block elements. The structure is simplified by neglecting internal equipment. Additional concrete finite elements are included in the structure to take the mass of the reactor assembly into account. Partial structured meshing with sweep control is used to mesh the complex regions of the reactor assembly using tetrahedral C3D10M elements; (ii) Reinforcement cage: linear elastic with a circular profile (Elastic modulus (E):200 X 10^9 N/m^2; Poisson's ratio (ν): 0.3; Density: 7750 kg/m^3) comprised of B31 beam elements. The steel reinforcement ratio is assumed to be 2% for slabs and walls according to which the spacing was determined (iii) Linear soil: linear elastic (Elastic modulus (E):0.15 X 10^9 N/m^2; Poisson's ratio (ν): 0.3; Density: 2500 kg/m^3) composed of C3D8R elements.

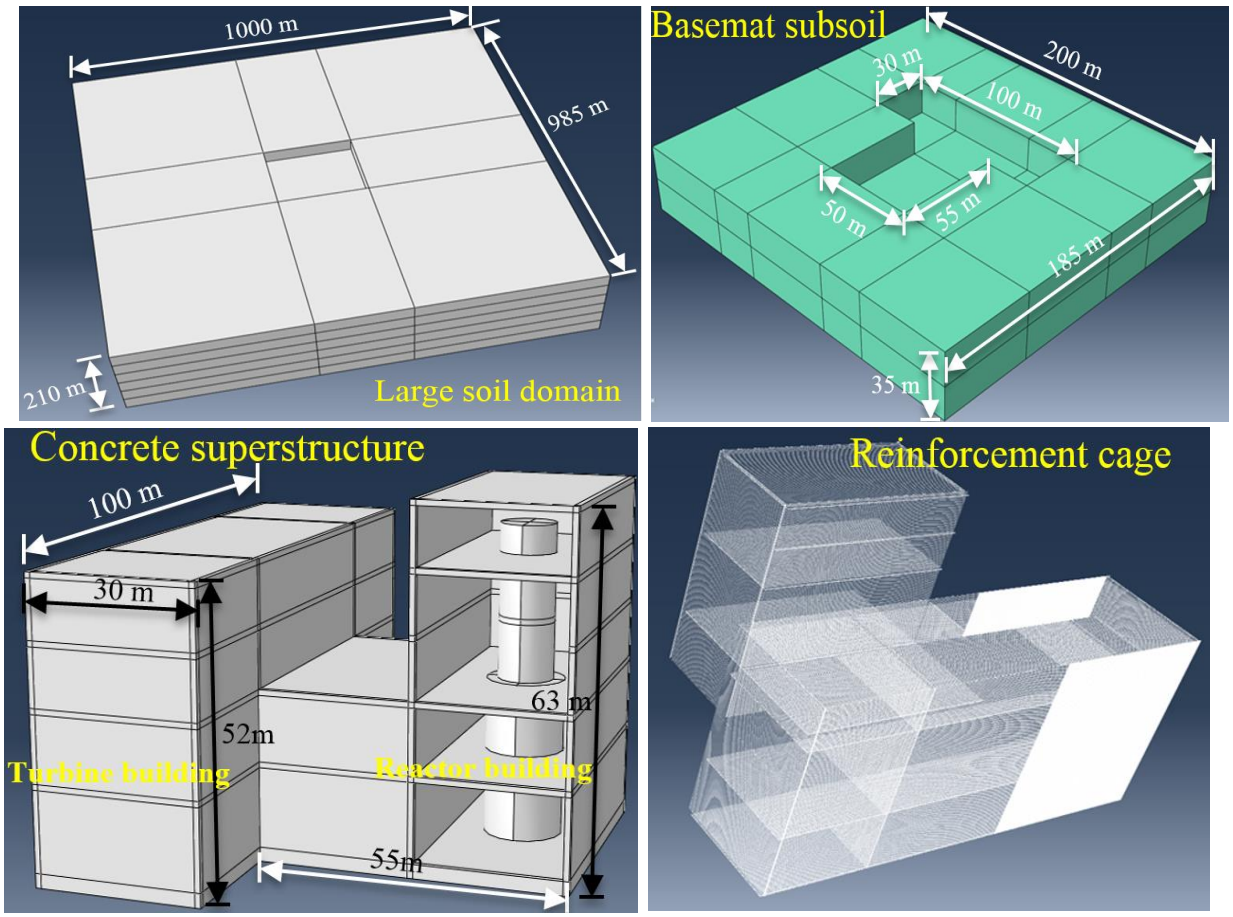

Fig 4.3: FE Model parts of Fukushima NPP, Unit 6

The soil strata surrounding the basemat has a finer mesh (same as the structure) as compared to the rest of the soil domain to maintain continuity of the interactions at the interface. The soil domain is modelled to be six times the size of the structure in plan, such that an infinite domain can be simulated. When the domain size is increased, the computation time increases. The ABAQUS model shows that waves are reflected from the boundaries in spite of a large soil domain. Hence, the boundary conditions are modified to address this issue which has been described in the next section.

4.3.2 Soil Domain and Boundary Condition

A number of boundary conditions are applied in conjunction with several constraint parameters, to study the reflection of waves and minimize the effects of spurious amplifications in computation of the acceleration response. Previous studies show that certain boundary conditions such as the *BOUNDARY_NON_REFLECTING in LS-DYNA [118] are effective in simulating non-reflecting boundaries. Due to absence of similar boundary conditions in ABAQUS, a brief study was conducted to calibrate the finite element model. A set of models with the same material properties and dissimilar boundary conditions are considered for calibration:

(i) Model 1: Boundaries are constrained to move in pure shear using constraint equations. Infinite elements (CIN3D8) surround the external face of the soil domain in all directions to simulate non-reflecting boundaries.

(ii) Model 2: infinite domain along all directions and the bottom face constrained to move with internal nodes. The acceleration is applied at the base

(iii) Model 3: no constraints were defined for this model, with infinite domain in all directions.

(iv) Model 4: node region constrained at edges with infinite domain along all directions.

(v) Model 5: edge constraints without infinite domain.

The ABAQUS infinite element (CIN3D8) was used to simulate the effects of far field stresses on a small region of interest in a large unbounded domain. It is possible to approximate the unbounded domain by expanding the finite element mesh to a large distance such that the influence of the reflected and refracted stress waves can be reduced or considered small enough to be overlooked. It would require a significant amount of computational resources and sensitivity studies to establish the correct mesh sizes and boundary conditions at the truncated edges, especially for dynamic analysis. The CIN3D8 elements have well defined decay functions [100] and are best suited to model the boundaries surrounding the far field region while the region of interest is modeled using 8-node brick elements. The dynamic response of the CIN3D8 elements assumes that the acceleration response in the neighboring elements have low amplitude such that the response of the medium is linear elastic. Infinite elements consider plane body waves striking the boundary at right angles, and can be used to transmit impinging body waves provided the material behavior in the vicinity of the boundary is linear elastic. The equilibrium equations for the infinite elements in terms of the material density (ρ), element acceleration ($\ddot{u}$), stress, shear modulus (G) and Lame's constants is stated as [8]

$$\rho \ddot{u}_i = G \frac{\partial^2 u_i}{\partial x_j \partial x_j} + (\lambda + G) \frac{\partial^2 u_i}{\partial x_i \partial x_j} \tag{4.3}$$

The plane waves are considered along the x-axis. The longitudinal wave solution is of the form

$$u_x = f\left(x \pm v_p t\right), u_y = u_z = 0 \tag{4.4}$$

which gives us the expression of longitudinal wave velocity when substituted in the governing equation

$$v_p = \sqrt{\frac{\lambda+2G}{\rho}} \tag{4.5}$$

Similarly, the shear wave solution is given by

$$u_y = f(x \pm v_s t), u_x = u_z = 0 \; or, u_z = f(x \pm v_s t), u_x = u_y = 0 \tag{4.6}$$

from which the shear wave velocity is extracted as

$$v_s = \sqrt{\frac{G}{\rho}} \tag{4.7}$$

Distributed damping along the boundaries are incorporated to prevent reflection of the longitudinal and shear waves. Normally, we wouldn't expect out-of-plane body waves to impinge from the boundaries at exact right angles and it might also include surface waves like Raleigh waves. However, the infinite elements work well for these general cases, as long as the predominant wave propagation direction is orthogonal to the truncated boundary. The boundaries rely on the solution of the wave equation in its bordering elements to be linear elastic to perfectly transmit longitudinal and shear waves. Hence they should be placed at a reasonable distance from the region of interest, which is around three times the foundation footprint in our case. While infinite boundaries work well for a linear elastic halfspace, it might not perfectly simulate absorbing boundary conditions in the vicinity of non-linear elements. This issue can be resolved by using periodic boundary conditions for individual soil layers and is implemented through constraint equations in the FE model. The constraint equation can be used to simulate pure shear across each layer by allowing the boundary elements to move together. It should be noted that only the translational degrees of freedom at the boundaries are constrained for the model while the rotational degrees of freedom are released. Hence, the seismic response of the NPP is most accurately described by Model 1. In Model 2, the bottom face was constrained to move with the superstructure assembly and resulted in large amplifications of the structural response. When the model is surrounded by infinite

boundary elements without constraints, as in the case of Model 3, similar amplifications in basemat response is observed, which do not comply with the expected results. In case of Model 4; where the entire node region in individual layers are constrained to move with the boundaries, the observed acceleration amplifications in the soil are much lower than expected. This is primarily due to the fact that the individual layers behave as rigid plates. The individual surfaces have a node to surface coupling with the influence region extending to outermost points of the domain. If pure shear boundary condition is implemented along the lateral boundaries without infinite elements in the bottom face (in case of Model 5), there are oscillations in the response acceleration history which is more pronounced in the vertical direction primarily due to reflection and interference of plane body waves from the bottom face.

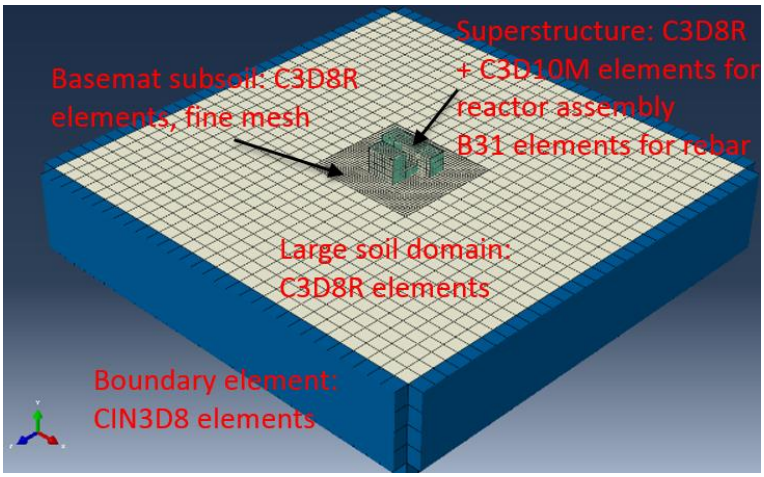

Fig 4.4: Element types used in the FE model including infinite boundary elements

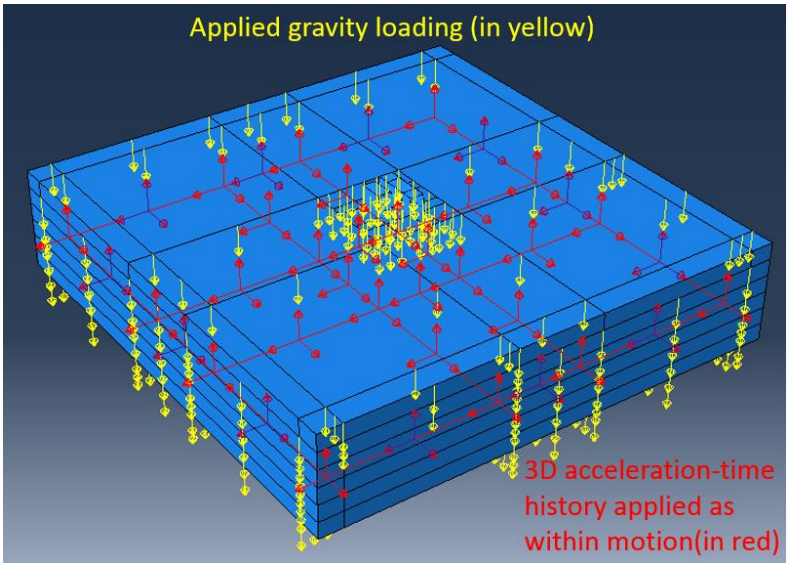

Fig 4.5: Applied gravity loading and scaled ground acceleration with tabular amplitudes

Since input ground motions are predominantly waves propagating in the vertical direction, it is applied at the base of the soil. However, in this case a within motion is available [2]; which is the acceleration data obtained from site, when the bottom soil domain or rock is assumed to be rigid. The simulation is performed in two steps. In the first step, static gravity loading is applied for a brief instant and propagated to the next step where the acceleration is scaled with respect to its amplitude and applied above the infinite element layer in terms of an acceleration-time history obtained from site. The acceleration input must be applied at elements which don't share its nodes with the infinite boundaries, as it might cause non-linear stress localization in the vicinity of the infinite elements causing some body waves to reflect back from the truncated boundaries. However, this effect is minimal for a relatively large soil domain. The linear or modal response of the system is performed using a pseudo-static analysis and the natural time period is found to be acceptable. In case of outcrop motions, the load input has to be assumed as a force-time history dependent on

the shear wave velocity, surface area and velocity-time history; with absorbing boundary conditions.

Table 4.3: Summary of ground motion input

Location	Location Vertically	Max acceleration (g)		
		NS	EW	UD
P14	-130 m	0.44	0.531	0.288

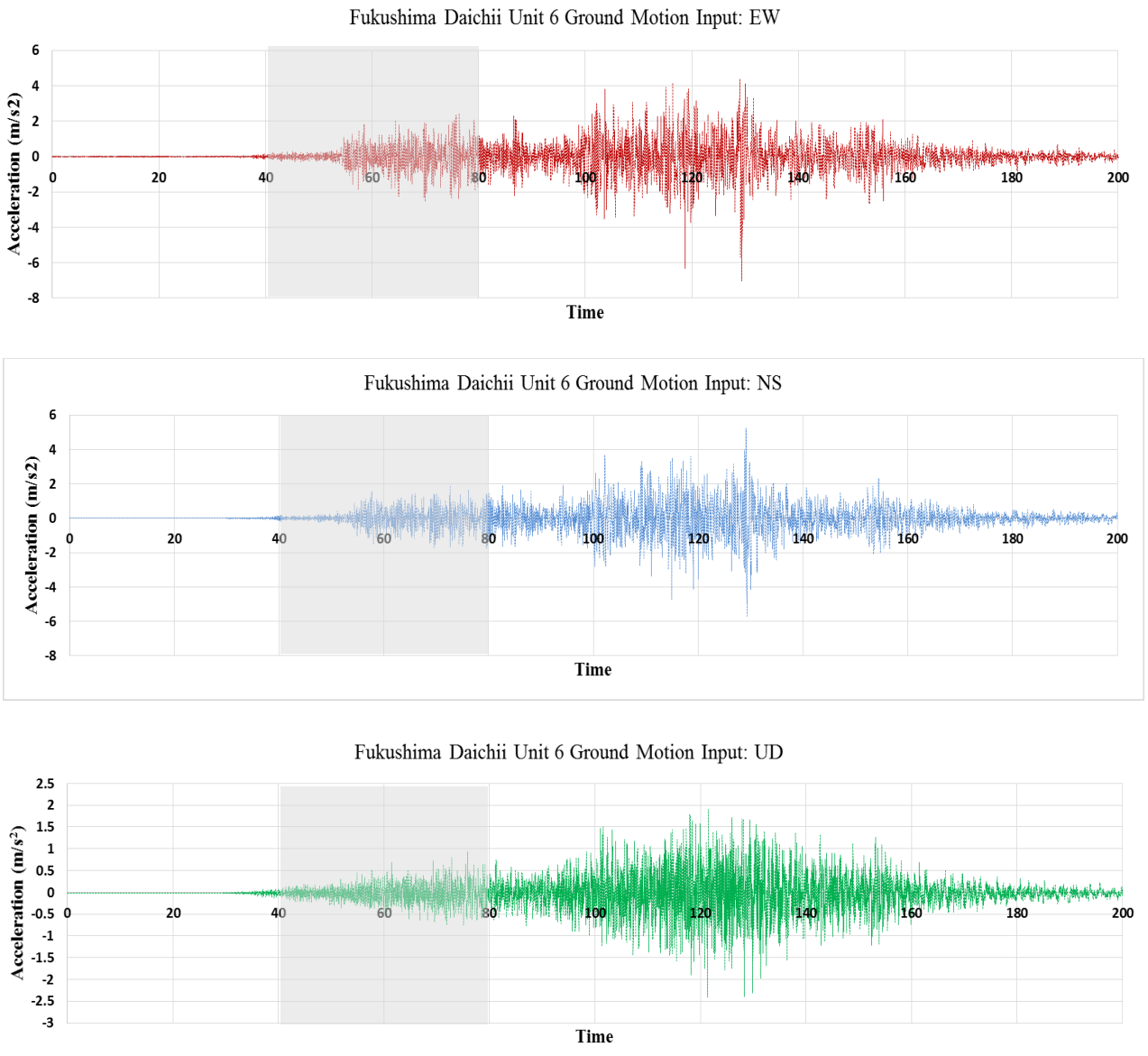

Fig 4.6: Ground motion data used in simulations in: (a) EW, (b) NS, and (c) UD directions

4.4 Linear Soil Structure Interaction Analysis (LSSI)

The linear soil structure interaction analysis is performed without any material or geometric nonlinearities and then compared with the actual field data [2]. The basemat is tied to the soil domain for the initial LSSI analysis and the interaction parameters are modified in the subsequent steps. The soil domain, superstructure, mesh properties, loading conditions and boundaries are consistent throughout the analysis process. In case of linear analysis, only elastic material properties are used for the simulations. The mesh size of the structure and the soil domain surrounding the basemat are consistent to facilitate wave propagation across the interface, avoiding mesh deformation effects.

The response acceleration-time history is obtained at the basemat of the reactor and turbine building in contact with the soil as well as the free-field motion, to give us a clear idea of the attenuation effects, as waves travel through the interface into the superstructure. The free field motion used for the simulations captures the acceleration response every 0.02 sec. Hence, the field history output for the in-structure response acceleration is collected at the same frequency. A direct comparison of acceleration time history responses may not reflect the true behavior of the trends in results. A response spectrum analysis has been performed to compare the frequency content and peak pseudo spectral accelerations at the basemat and the top floor of the reactor building. This allows us to compare the trends in the attenuation of the in-structure response with respect to the free-field motion.

4.4.1 Comparative analysis of ABAQUS results with field data

The acceleration-time histories at the basemat below the sub-structure and the free field are compared in three different directions. The reduction in maximum acceleration from the free-field (LIN_Freefield) to the reactor building (RB_BM) and turbine building basemat (TB_BM) is

compared with the data gathered from the seismometers installed at Fukushima Daichii Unit 6 [2]. They do not follow well-defined trends, and there is a wide variation between the recorded acceleration and LSSI analysis results.

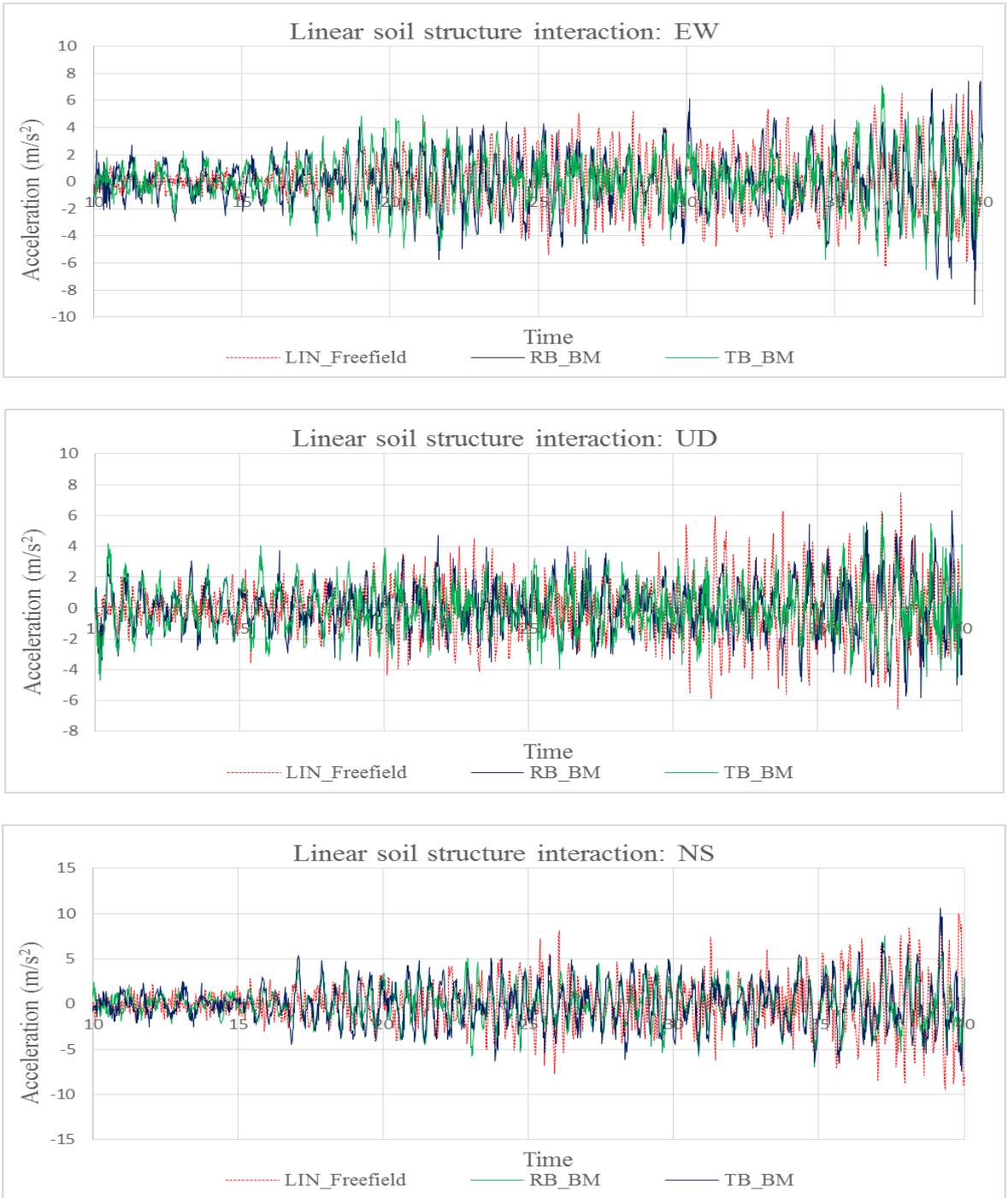

Fig 4.7: Response acceleration-time history of the free field and at the basemat for LSSI

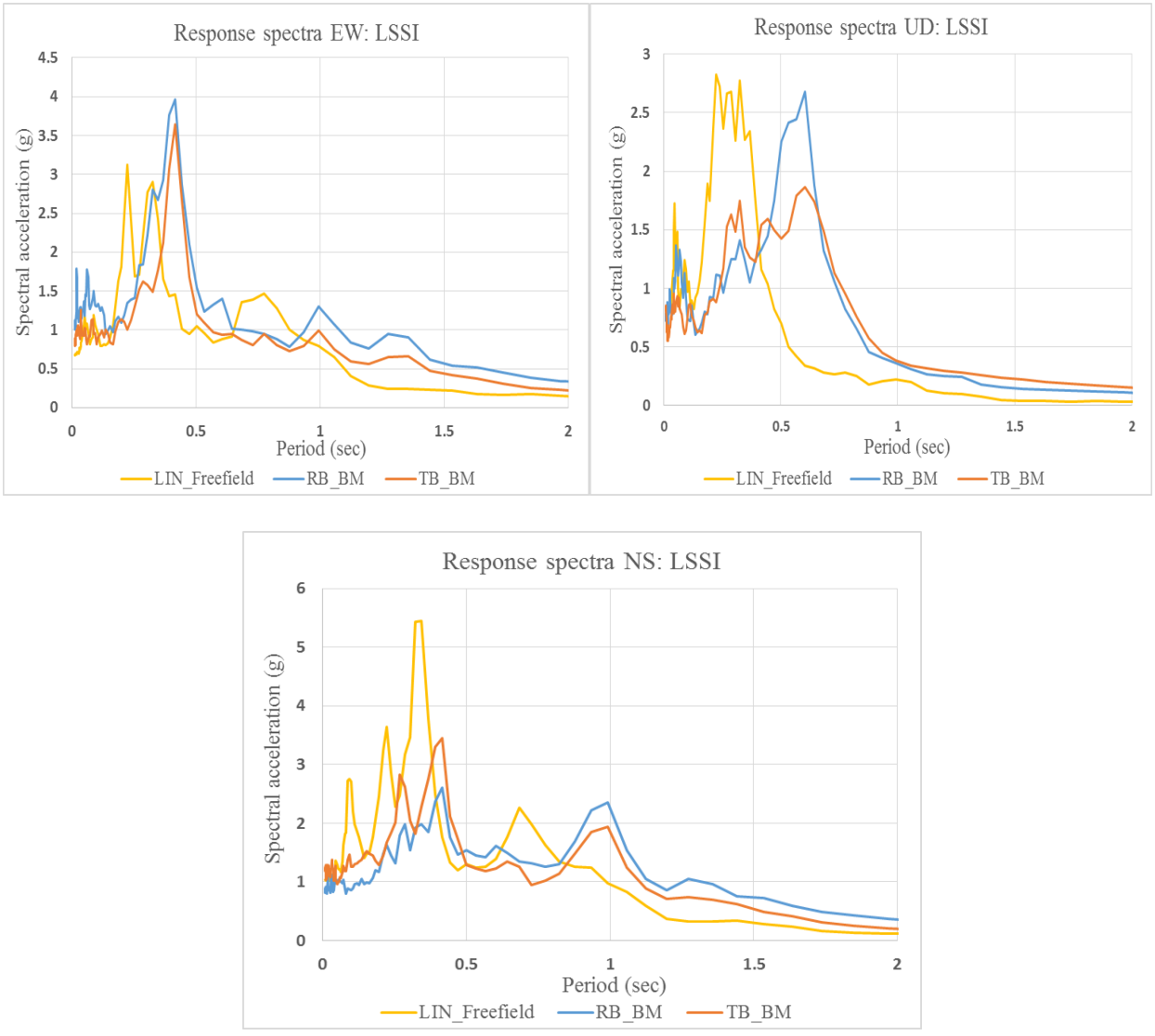

Fig 4.8: Response spectrum from LSSI analyses

Table 4.4: Summary of LSSI results

	Maximum acceleration (g)					
Locations	EW	%age change w.r.t. F.F.	NS	%age change w.r.t. F.F.	UD	%age change w.r.t. F.F.
Free field (TEPCO)	0.405		0.25		0.194	
Free field (ABAQUS)	0.7		0.9		0.75	
RB-Basemat soil (ABAQUS)	0.9	+28.6%	0.75	-16.7%	0.83	+10.6%
TB-Basemat (ABAQUS)	0.65	-7.14%	0.84	-6.7%	0.81	+8%

As observed in Table 4.4, the values at the reactor building basemat (RB_BM) are increased by 28.6 % in the EW direction and 10.6% in the UD direction, and reduced by 16.7 % in the NS direction. The ABAQUS models overestimate the free field motion as well as the basemat response by more than 100 percent. The large variations in data is due to lack of proper interaction parameters, material nonlinearity, time integration and meshing schemes. The dependence of the dynamic properties of the foundation soil and the basemat on the interaction between the two entities is crucial to analyze the reduction in the amplitude of structural response of seismically excited structures. The overestimation of the free field response can be attributed to the linear elastic soil domain which fails to account for the hysteretic characteristics of the soil and computes the response on the basis of a single set of linear elastic parameters. It was observed that the RB basemat had an amplified response in the EW and UD direction as compared to the free field while attenuation was observed for the NS case. It is also important to note that the vertical shear waves were amplified because the basemat was tied to the soil resulting in large inertial effects, which substantially increased the acceleration response in the UD direction. The radiation damping at the interface and the reduction in inertial effects was not captured due to the absence of tangential and normal contact definition at the soil structure interface. In spite of the lack of

accuracy of the LSSI analyses, it can be considered as a good benchmark for the NLSSI models which simulate the effects of geometric and material non-linearities at the interface.

The response acceleration time history is converted to response spectra with 5% damping introduced to the model using the Newmark method. A comparison was made between the response at the basemat and at the top floor level. The objective is to observe the amplification in the structural response with reference to the basemat and compare the net in-structure response when combined with the attenuation effects at the foundation-subsoil interface. As observed in the response spectrum analysis, the peak spectral accelerations (PSA) occur at lower periods or high frequencies, owing to high stiffness of the soil. The symmetric points at each level in the turbine and reactor building exhibit the same response. Higher stories of the reactor and turbine building experience higher pseudo spectral accelerations than the basemat.

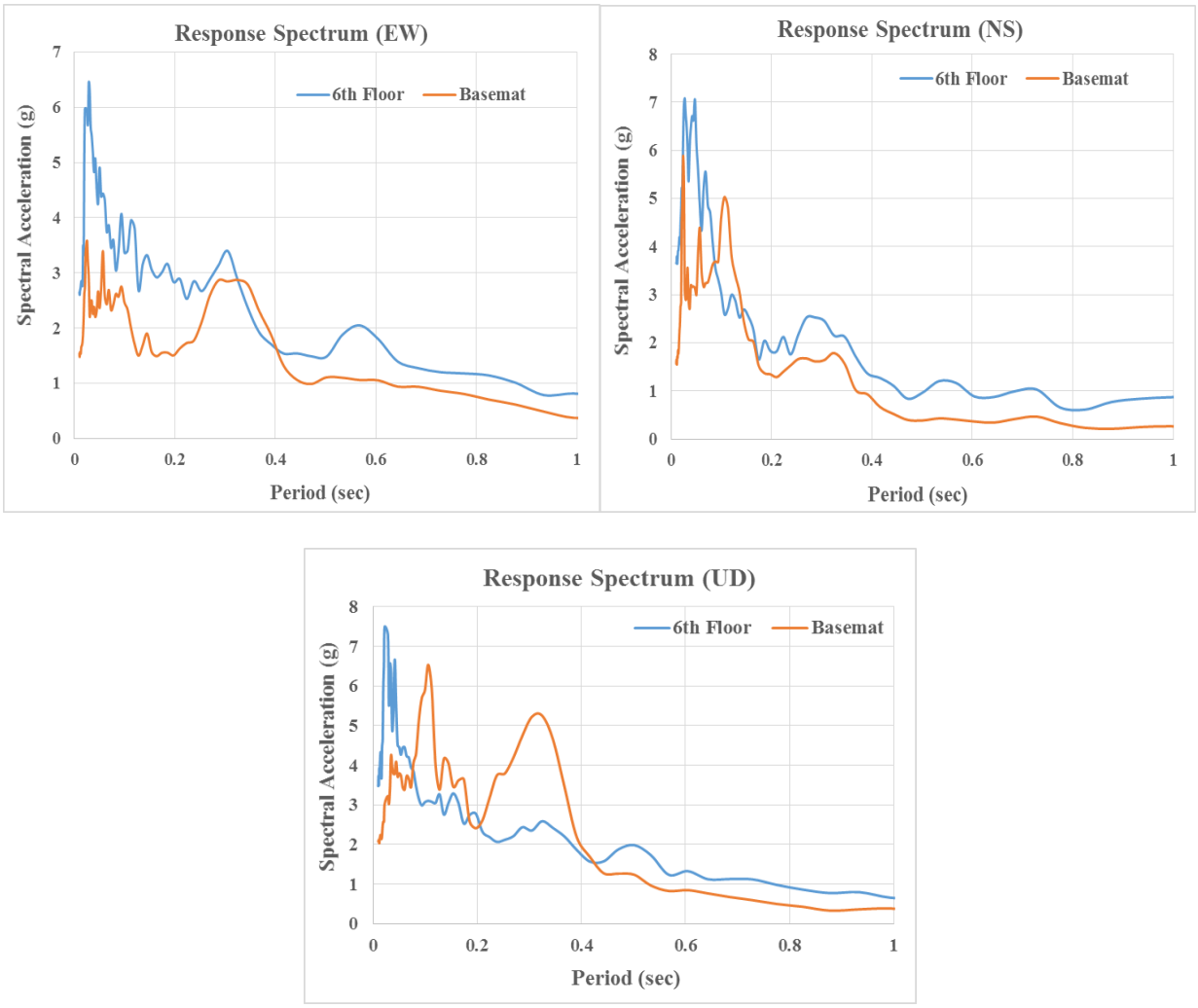

Fig 4.9: Response spectra from LSSI analysis in ABAQUS (a) EW, (b) NS, and (c) UD direction

For LSSI, the two adjacent structures didn't have any significant influence on the dynamic response of each other. However, past investigations suggest that the PSA of a group of structures resting on inelastic soil is reduced with respect to a single structure [119]. The distance between adjacent buildings also have a minor influence on the structural response. The in-structure amplification and the basemat attenuation effects are a function of the mass of the structure, intensity or amplitude of the ground motion content, and modulus mismatch of the soil-structure

interface. It should be noted that the structure was modelled with .linear elastic parameters which overestimates the PSA.

4.5 Linear soil structure analysis with an account of geometric nonlinearities at interface

In this section, geometric nonlinearities (gapping and sliding) across the soil-structure interface are considered in addition to the linear elastic material model for the soil. The results from LSSI case is used to compare the influence of nonlinear interface on the reduction of the maximum acceleration. A series of NLSSI analyses on the NPP considering material and geometric nonlinearities were performed in LS-DYNA to simulate geometric nonlinearities across the interface [111]. A thin layer of elements with zero thickness were used to simulate gapping effects using the *MAT_BRITTLE_DAMAGE material model. The *automatic_surface_to_surface tie-break contact was also used to simulate gapping and sliding effects resulting in high amplification of the acceleration-time output of the response which could not be explained. In this chapter, the kinematic contact formulation is used to implement the Coulomb friction criterion to simulate sliding across the interface. The maximum possible shear stress is also specified. Gapping is simulated through a hard pressure overclosure relationship.

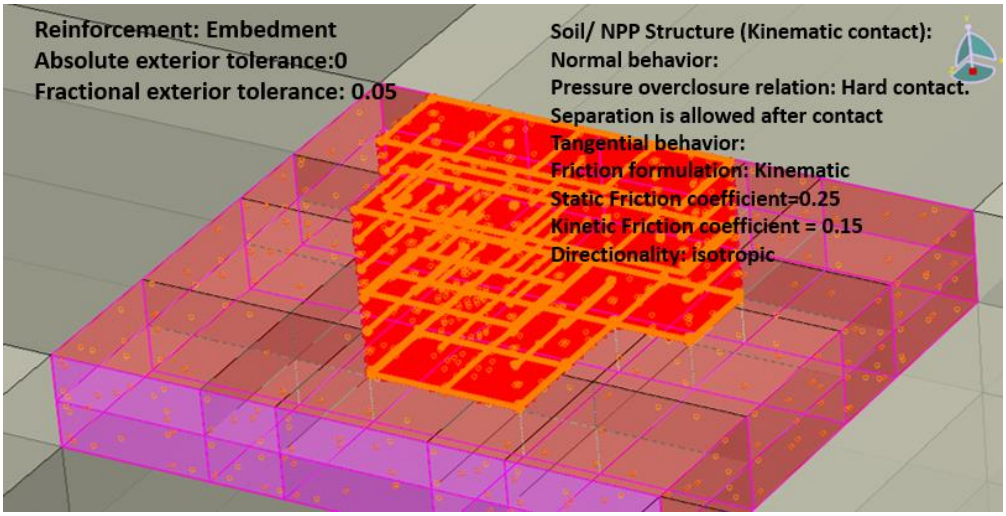

Fig 4.10: Nonlinear interaction and contact formulation in ABAQUS

According to the Coulomb formulation, the yielding across the interface is governed by the critical shear stress after which the contacting surfaces start sliding with respect to each other. The critical stress is expressed as a fraction of the normal contact stress represented by the friction coefficient. For a dynamic analysis, the friction coefficient determines when a particular node transitions from sticking to slipping and vice versa. The LSSI models adopt a node-based contact which distributes the normal force across the cross sectional area of the nodes in contact. The friction coefficient can be specified for the orthogonal direction of the shear stress. The models under consideration here use an isotropic formulation (same friction coefficient along all directions). In addition to the tangential behavior, it is crucial to model the normal behavior across the interface. Since both the contacting materials in this analysis are isotropic elastic, the hard pressure overclosure relationship is used. The penetration of the foundation into the linear elastic soil domain is arrested for this formulation. This may not be an ideal representation of the actual interfacial behavior, but is effective for simulating the stiffness reversal across the loading cycles. However, the ideal normal contact would be represented by a softened contact relationship, which

will be utilized in the comprehensive NLSSI models in Chapter 5 and 6, as the non-linear soil takes care of the stiffness variations with the change in confining pressure. For the sake of simulating gapping, separation was allowed after contact. This suggests that the clearance between the surfaces reduces to zero when the separated surfaces are in contact and when the surfaces separate the contact pressure is zero.

The LSSI analyses is carried out in three phases to segregate the effects of the individual sources of nonlinearity. In phase A, the basemat is tied to the soil domain and contact hasn't been activated as described in Sec 4.4.1. In phase B, the nodes of the basemat are constrained to move together in the lateral (X-Z) direction with hard pressure overclosure relationship in the normal direction. In Phase C, the kinematic contact is activated in the lateral direction with hard pressure overclosure in the normal direction.

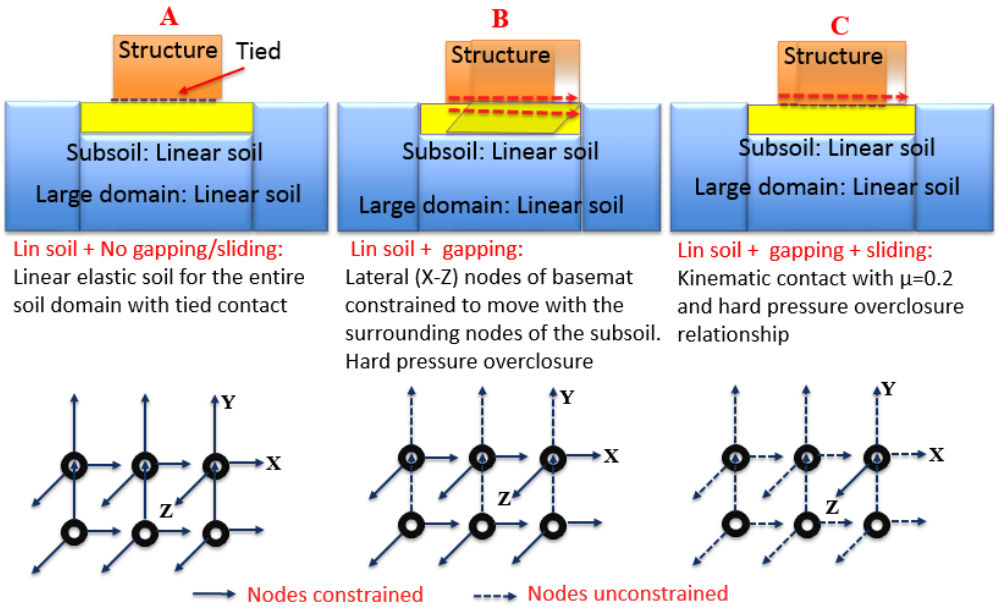

Fig 4.11: The phases of LSSI analyses for analyzing effects of gapping and sliding

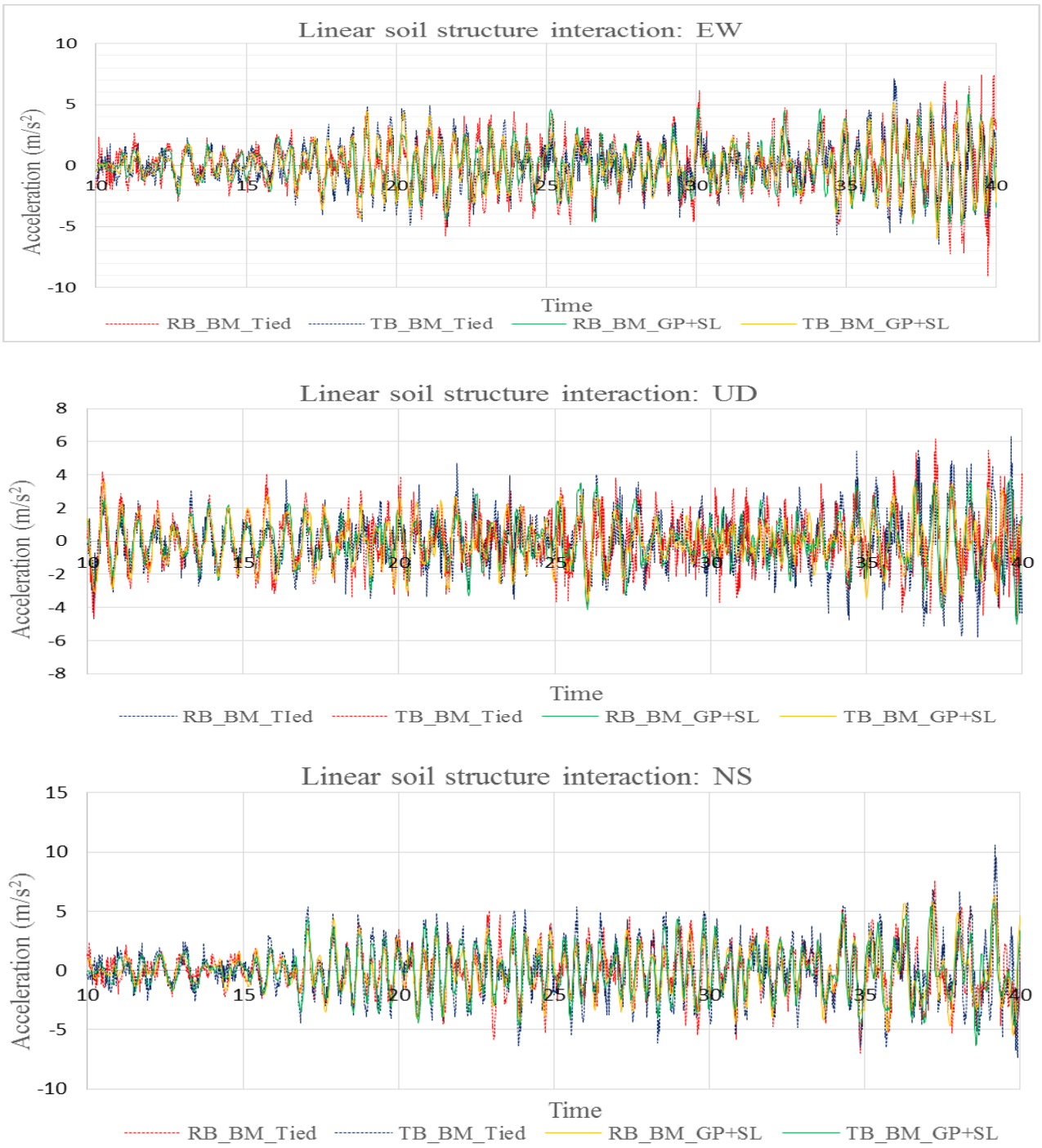

Fig 4.12: Response acceleration-time history for LSSI analysis with geometric nonlinearity

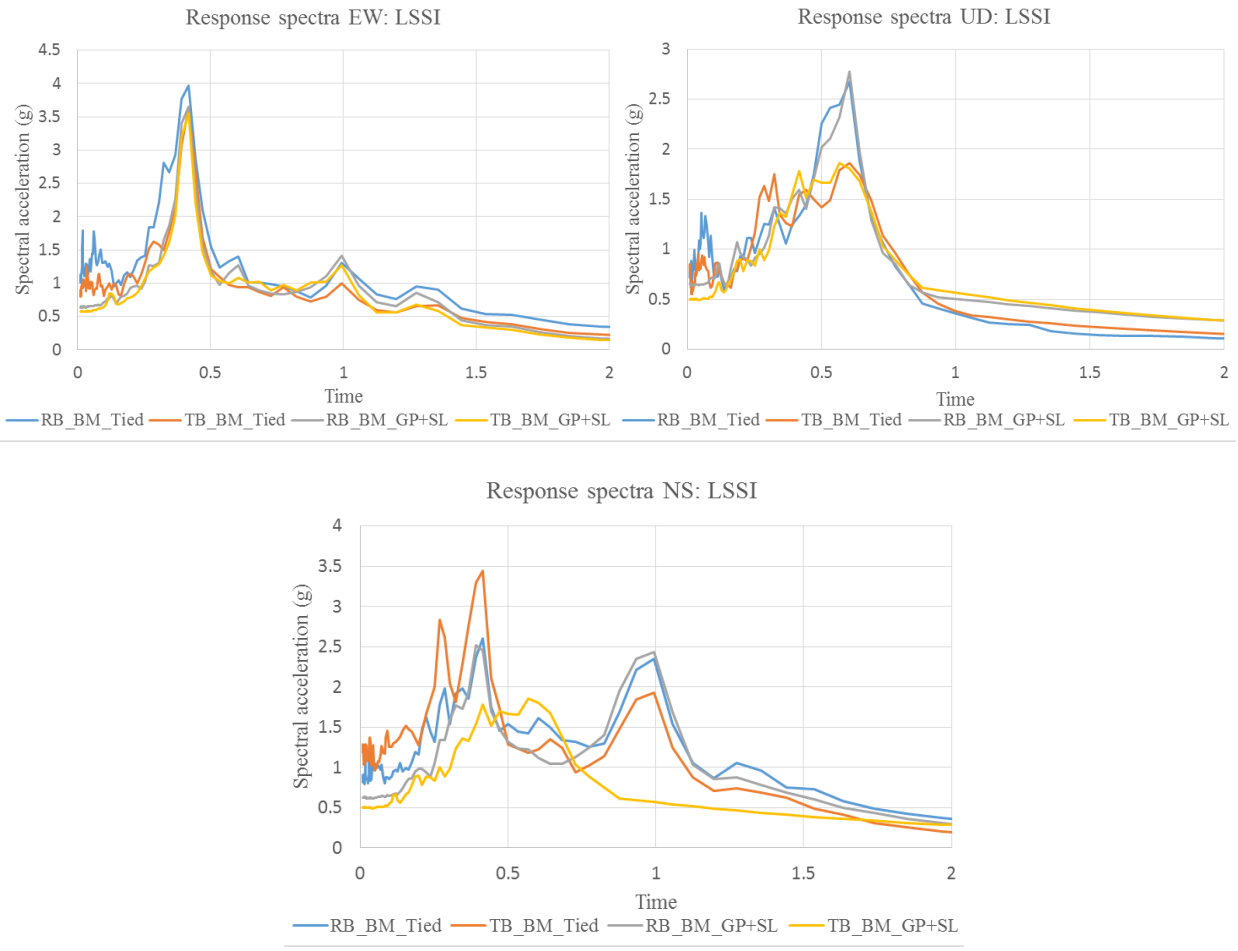

Fig 4.13: Response spectrum from LSSI analyses with geometric nonlinearity

Overall, the inclusion of contact in the LSSI analyses results in a reduction of the basemat response. The peaks of the response spectrum also reduce as a result of interaction effects. The reduction in the PSA is more pronounced in the lateral direction than in the vertical direction. There are two peaks in the response spectrum for the NS component for the tied case which plateaus for the GP+SL case. The interaction model helps in smoothing out the structural response by limiting the transmission of stresses between the soil and basemat through its sliding and pressure overclosure formulation. Table 4.14 summarizes the results of the SSI analysis when geometric nonlinearities are considered. There is a significant reduction in the basemat response

when compared with the linear free field data. A reduction of 3.4%, 28% and 5% was observed in the peak response accelerations at the RB basemat when gapping was introduced into the system for the EW, UD and NS component respectively. The PRA was further reduced by 31%, 12% and 11% respectively for the EW, UD and NS components respectively when sliding was added. It should be noted that sliding nonlinearity has a greater impact on the acceleration attenuation for the EW and NS component while the attenuation in UD direction is governed by the gapping nonlinearity. This is consistent with the fact that the UD component is responsible for producing overturning effects in the structure and is reduced when the hard pressure overclosure relationship is implemented in the normal direction. Similar trends were observed for the TB basemat as well. This behavior is more accurately represented by the soft pressure overclosure relationship which is used in Chapter 5 and 6. Although the trends of acceleration attenuation at the reactor building basemat is improved by introducing geometric nonlinearity at the interface, the EW, UD and NS components still exceed the actual TEPCO free field accelerations by 46%, 157% and 150% respectively. Similar trends were also observed at the turbine building basemat. The results are better than those obtained from LSSI analysis modelled without contact parameters, but still overestimate the basemat response by a large margin due to lack of material nonlinearity.

Table 4.5: Summary of peak accelerations from SSI analysis considering geometric nonlinearity

Component	**FF TEPCO**	**FF LIN**	**RB_BM TIED (A)**	**RB_BM GP (B)**	**RB_BM GP+SL (C)**	**TB_BM TIED (A)**	**TB_BM GP (B)**	**TB_BM GP+SL (C)**
EW	0.405g	0.7g	0.9g	0.87g	0.59g	0.65g	0.61g	0.54g
UD	0.194g	0.75g	0.83g	0.60g	0.5g	0.81g	0.45g	0.36g
NS	0.252g	0.9g	0.75g	0.71g	0.63g	0.84g	0.68g	0.36g

Fig 4.14 draws a comparison between the maximum accelerations computed for the linear SSI model with the interaction-based LSSI model. The labels A and C correspond the cases depicted in Fig 4.11.

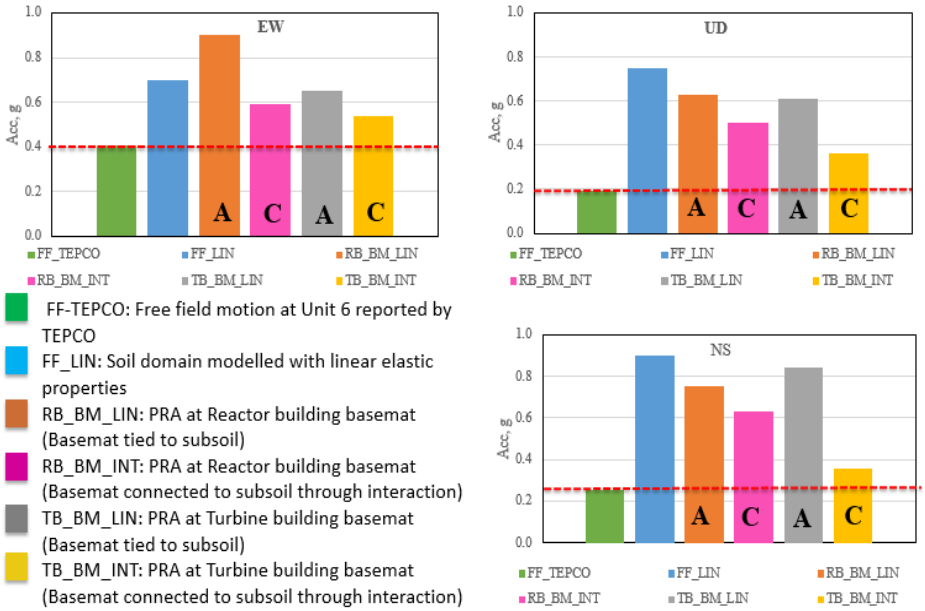

Fig 4.14: Summary of maximum acceleration from LSSI and LSSI-interaction analysis

Rayleigh damping of 5 to 10 percent was adopted across all LSSI-interaction models. The introduction of damping doesn't dramatically reduce the structural response, but a reduction of the peak spectral accelerations was observed at low frequencies. Preliminary investigations also revealed that the response at the basemat was amplified for lower soil depths. At low damping, the response of the basemat was observed to increase marginally with the increase in the ratio of elastic modulus between the structure and soil. However, this effect is negligible for higher Rayleigh damping. When the kinematic interaction is introduced to the LSSI analyses, higher kinematic and inertial effects were observed. This was identified by altering the mass of the structure by changing its density, which resulted in a spike in the basemat acceleration response. The size and mass effects have a predictable impact on the response spectral acceleration, which cannot be neglected.

The shear stresses in the lateral directions were in the range of 10^7 Pa, which exceeds the expected values. Stress concentrations were also observed along the edges of the basemat footprint in the range of 10^8 Pa. The observed shear strain values in the vicinity of the basemat occur in the range of 0.01-0.02 which exceed the computed values [120] by a factor of 10. This is primarily due to the lack of hysteresis properties in the linear elastic soil.

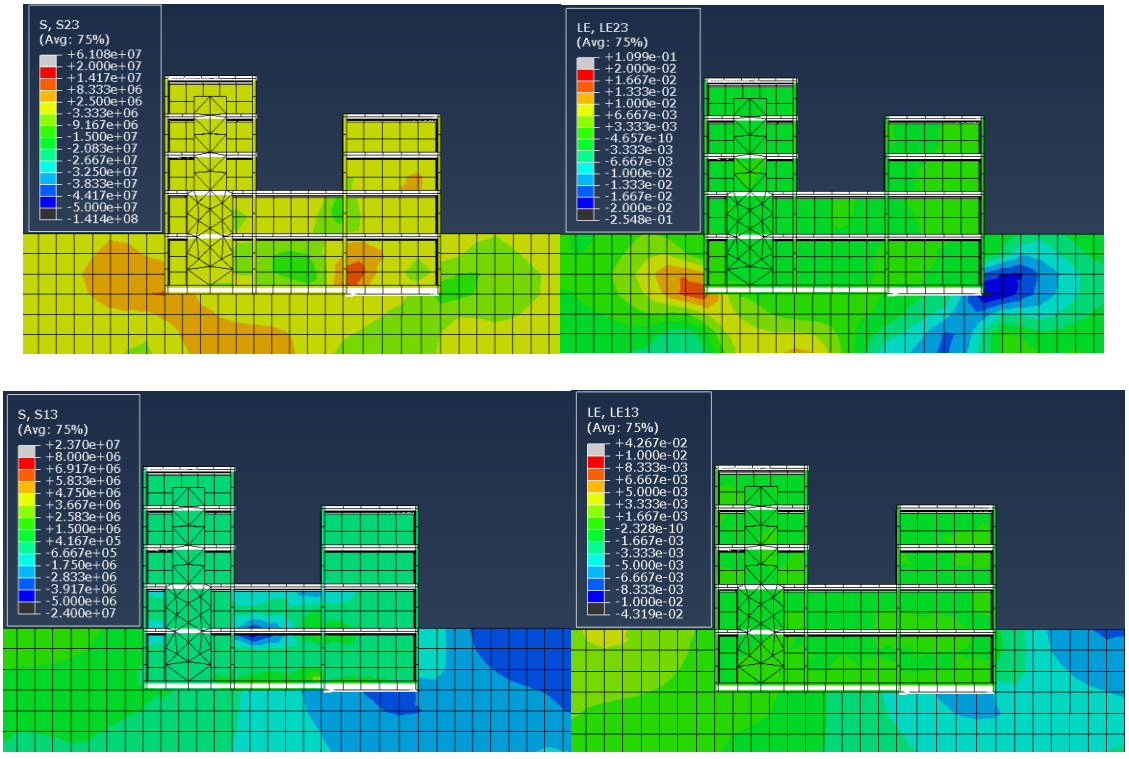

Fig 4.15: Shear stress and strain profiles in the vicinity of RB and TB basemat for LSSI

4.5.1 Parametric studies for comparison of sliding and gapping effects

The structure resting on soil exhibits inertial and kinematic effects when subjected to ground motion. When the wave propagates from one medium to another, kinematic effects are observed due to change in elasticity and density of the media, resulting in reflection and refraction of

incoming waves and a change in the wave propagation velocity. These kinematic effects primarily represent the change in response of the structure under the influence of free field motion. To simulate gapping behavior, hard contact pressure overclosure relationship is implemented as discussed in the previous section. The zero-penetration condition is enforced when the surfaces separate and the contact pressure reduces to zero. The meshing is performed in a way such that the nodes shared by the two adjacent parts move together.

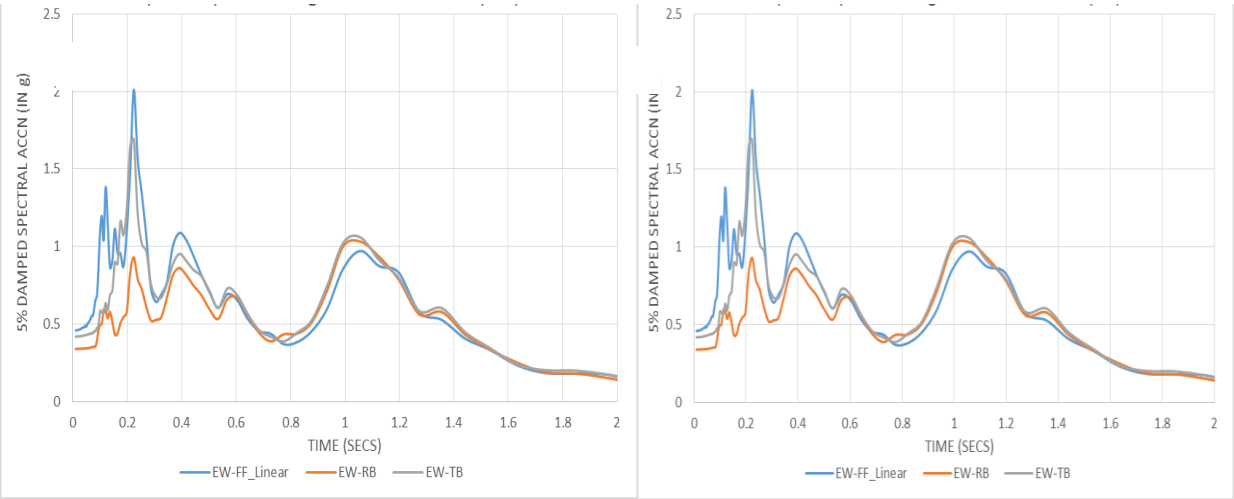

Fig 4.16: Response spectra from NLSSI-gapping analysis in (a) EW, (b) NS direction (PSA in g)

The response spectrum at the free field, the bottom of reactor building basemat (RB-BM), and the bottom of turbine building basemat (TB-BM) are compared in Fig 4.15. From the response spectrum, it is observed that there is a reduction of the maximum pseudo spectral acceleration values at the reactor building basemat (RB-BM) and turbine building basemat (TB-BM). A sensitivity study is performed to compare the gapping and sliding formulation with the case when the structure is tied to the soil (gapping and sliding is arrested) (refer Fig 4.11). Separation is permitted after contact for all simulations. Upon performing the response spectrum analysis, we

observe that the structure experiences higher spectral acceleration at lower frequencies when the basemat is tied to the soil suggesting a steady growth in the in-structure response.

When gapping effects are introduced, the peak accelerations are found to occur at high frequencies owing to the loss of contact between the basemat and subsoil for certain ground motions with high frequency content. The pseudo spectral acceleration (PSA) is reduced when gapping effects are introduced as compared to the tied case. When the friction (sliding) component is introduced in addition to gapping, there is further attenuation of the acceleration response. The nonlinear interface helps in reducing the peak spectral acceleration by a small amount due to its softening characteristics. The highest PSA is observed for the no-gapping (tied) case, as the basemat experiences greater inertia effects and behaves as a single unit with the soil.

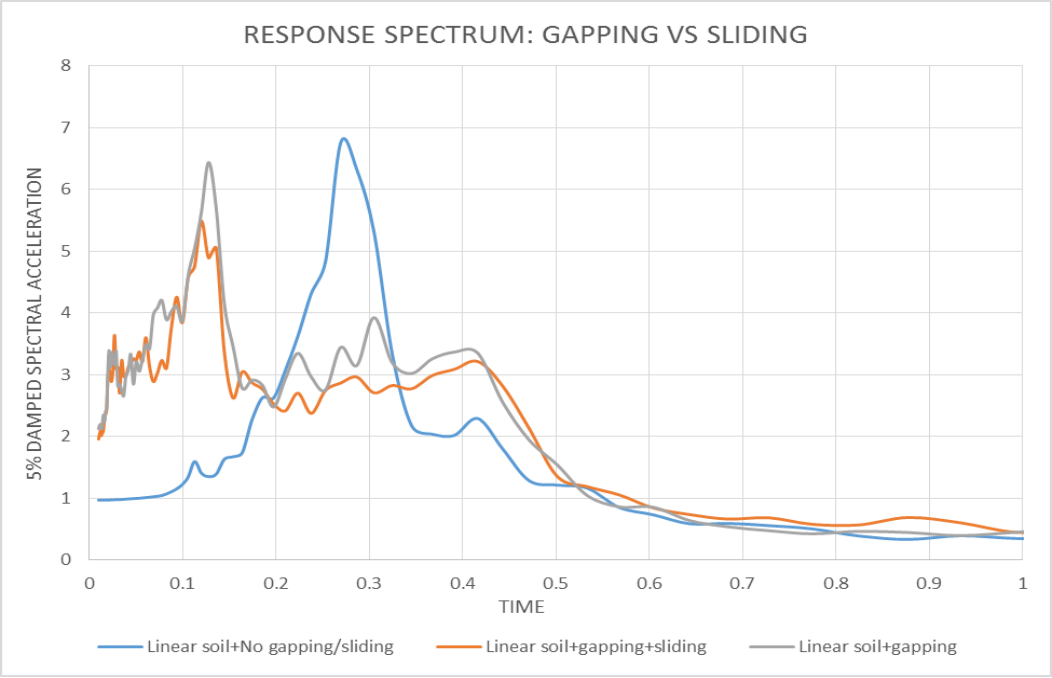

Fig 4.17: Response spectra for gapping and sliding vs. tied case

4.5.2 Parametric studies on the basis of friction formulation

Shear forces are transmitted across the interface during contact apart from normal forces. The tangential or shearing behavior of the FE model is governed by a kinematic friction formulation, based on the classical isotropic friction model in ABAQUS/Explicit. The two contacting surfaces carry shear stresses up to a certain magnitude before they start sliding with respect to each other. This is determined by the critical shear stress which is dependent on the coefficient of friction between the surfaces in contact. The coefficient of friction (μ) is varied to study its impact on the sliding behavior.

For a three dimensional model, there exists two orthogonal components of the critical shear stress along the interface. For simplicity, the friction coefficient is kept the same in both directions. The lateral loading is mainly controlled by the ground motion in addition to the normal contact stresses due to self-weight of the structure. The contact pressure for a node-based slave surface equals the normal pressure divided by the total cross sectional area of the contact node. However for ABAQUS/Explicit, the cross sectional area is always 1.0. Fig. 4.17 shows the acceleration response behavior at the basemat due to variation in the friction coefficient. The peak spectral acceleration at the basemat is reduced as compared to the free field response spectra. It is observed that the peak spectral acceleration is higher at lower periods for higher friction coefficients. As the period increases, the peak spectral acceleration increases for lower friction coefficient. This is consistent with the fact that when the friction coefficient is higher, the interface is relatively stiff at higher frequencies. Hence, the acceleration response is higher. However, the probability of slippage increases at low friction coefficients. Hence, the energy dissipation across the interface occurs over a greater time period, thereby reducing the peak spectral acceleration response.

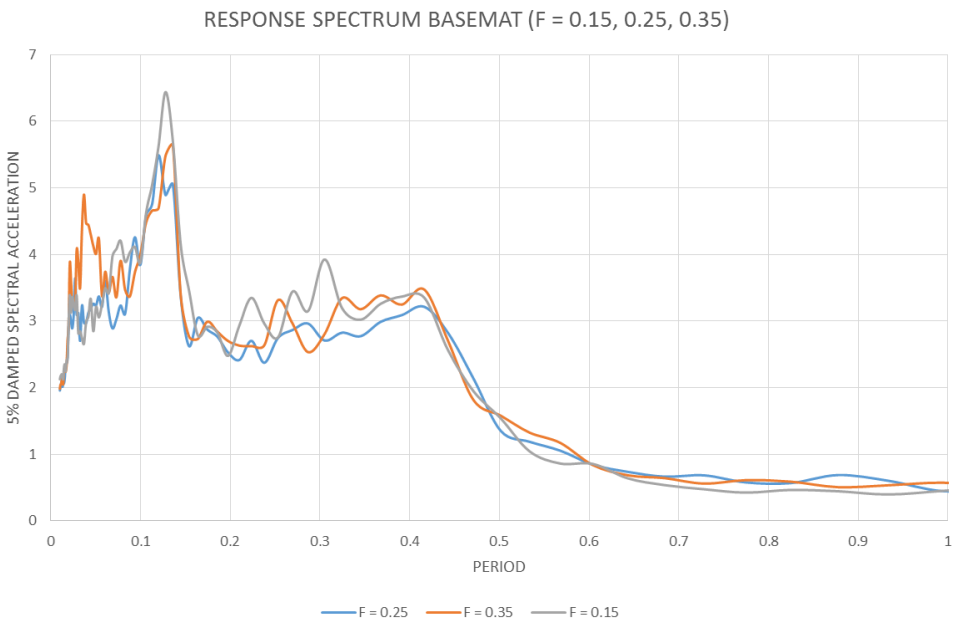

Fig 4.18: Acceleration response spectrum for friction coefficients of 0.25, 0.35 and 0.15 at the basemat (PSA in g and time period in sec)

4.6 Chapter Summary

A series of linear soil-structure interaction analyses was performed to explore the influence of geometric interfacial nonlinearities on the seismic response of nuclear power plant structures. The study was motivated by the hypothesis that these nonlinearities could potentially reduce the maximum accelerations at the basemat with respect to the free field motion. Only geometric nonlinearities were explored in this study: (i) gapping, and (ii) sliding between soil and structure. Linear soil-structure interaction (LSSI) analysis was first performed in the time domain with isotropic elastic material properties. The geometric nonlinearities were incorporated into the LSSI model through a kinematic frictional contact formulation and a hard contact overclosure relationship. The FEA analyses performed in ABAQUS point to the fact that the interface nonlinearities reduce the peak acceleration response at the basemat. The change in friction parameters also impact the spectral acceleration which vary with the period of the structure. The

tied contact overestimates the structural response by a large margin. However, this was an exploratory study, which highlights the need for more detailed and focused investigations with due consideration of: (i) the ground motion content (frequency and amplitude), (ii) better modeling of soil material nonlinearities, (iii) updating the nonlinearity at the soil-structure interface with respect to site conditions, and (iv) formulation and benchmarking of material models using experimental data. Experimental calibration of the interface model using direct shear test data is performed in the next chapter. A multilinear inelastic model is used to model the soil and verification studies are performed to analyze the applicability of the material model to full scale dynamic non-linear soil structure interaction analysis.

5. CALIBRATION OF NONLINEAR SOIL MODEL USING CYCLIC DIRECT SHEAR TESTS

The dynamic soil structure interaction analysis of nuclear structures and components during a seismic event is mostly carried out using the equivalent linear analysis in the frequency domain (ELFD). The ASCE 4-1998 [121] lays down a detailed set of instructions to perform the linear SSI analysis in the frequency domain. While the ELFD method produces acceptable results for low to medium scale seismic events and helps in assigning damping parameters for the structural response in accordance with the strong motion frequency ranges, it falls short of accounting for the material and geometric nonlinearity at the interface. Understanding the nonlinear soil behaviour of shallow foundations under high amplitude seismic loading is crucial for determining the seismic margins of critical infrastructure facilities.

The assessment of non-linear soil parameters is a key prerequisite for modelling the behaviour of the soil-structure interface subjected to seismic excitation. Although there is a plethora of sophisticated constitutive models in literature to model the soil domain, their utilization is limited because (i) they require a large number of parameters for calibration (ii) the dynamic test data needed for calibration is not easily available for most soil types (iii) their applications are limited to certain soil types and conditions (iv) implemented through specialized analytical frameworks. The linear time domain SSI analysis method discussed in Chapter 4 utilizes isotropic elastic material parameters to obtain the seismic response at the basemat of the Fukushima Daichii NPP. As mentioned in Chapter 1 and 2, soil structure interaction effects are a combination of the material and geometric nonlinearities at the interface. It was observed that the LSSI models overestimated the basemat and free-field response when compared with the response accelerograms obtained from the Fukushima NPP Unit 6 site. This calls for the development of a

fairly exhaustive nonlinear material model for the soil, which accounts for its hysteretic behavior and is sensitive to variations in pressure. It should also be capable of replicating the low-strain stiffness of the soil in addition to the post-yielding behavior at high strains.

The chapter aims to develop a comprehensive nonlinear material model for modelling the cyclic response of shallow foundations, by simulating the force-displacement response of a concrete footing resting on dense sand. The material model is encoded in ABAQUS through a user defined subroutine and validated against a series of large scale, cyclic direct shear type tests, carried out at the European Laboratory for Structural Analysis (ELSA) under the TRISEE project [1].

5.1 Description of the TRISEE experiments at the ELSA facility in ISPRA, Italy

The experiments conducted at the ELSA facility in Italy consisted of a large concrete sandbox, filled with coarse to medium grade Ticino sand [122] and a rigid steel slab, prototypical of a typical shallow foundation. The interface of the slab with the sand was made of concrete to ensure substantial frictional resistance. The sandbox had dimension 4.6 m by 4.6 m in plan and 4 m in height. The foundation was 1 m by 1m in plan. The lateral boundaries of the sandbox was impermeable and rigid. The foundation being in close proximity to the walls of the sandbox, could have experienced reflection of shear waves from the boundaries causing a variation in the stress profile beneath the foundation. However, our finite element models show negligible contrast in the stress profile. The foundation was placed in a trench surrounded by a formwork of 1 m which was meant to retain the surrounding sand and create an overburden pressure of about 20 kPa. The soil sample was deposited through pluvial deposition in layers, using a travelling sand spreader which ensures a high degree of spatial uniformity in density and grain size distribution. The spreader consists of a hopper moving at a steady pace over the sample supported on a fixed platform. The

relative density for the sample is regulated by varying the width of the hopper which controls the deposition intensity or the mass of sand being deposited in each layer for a certain interval of time. The travelling speed of the spreader is also controlled to avoid accumulation of sand along the boundaries. After deposition of the final layer of sand, the sample is saturated by injecting water through a grid of hoses embedded at the bottom gravel layer, which is separated from the layer of sand using a geotextile. The soil properties had measured relative densities of 85% for high density tests and 45% for low density tests. The properties of the soil specimen was determined by instrumenting the sample with a set of geophones to measure the degree of saturation and soil density, and thermo-electric probes for local check.

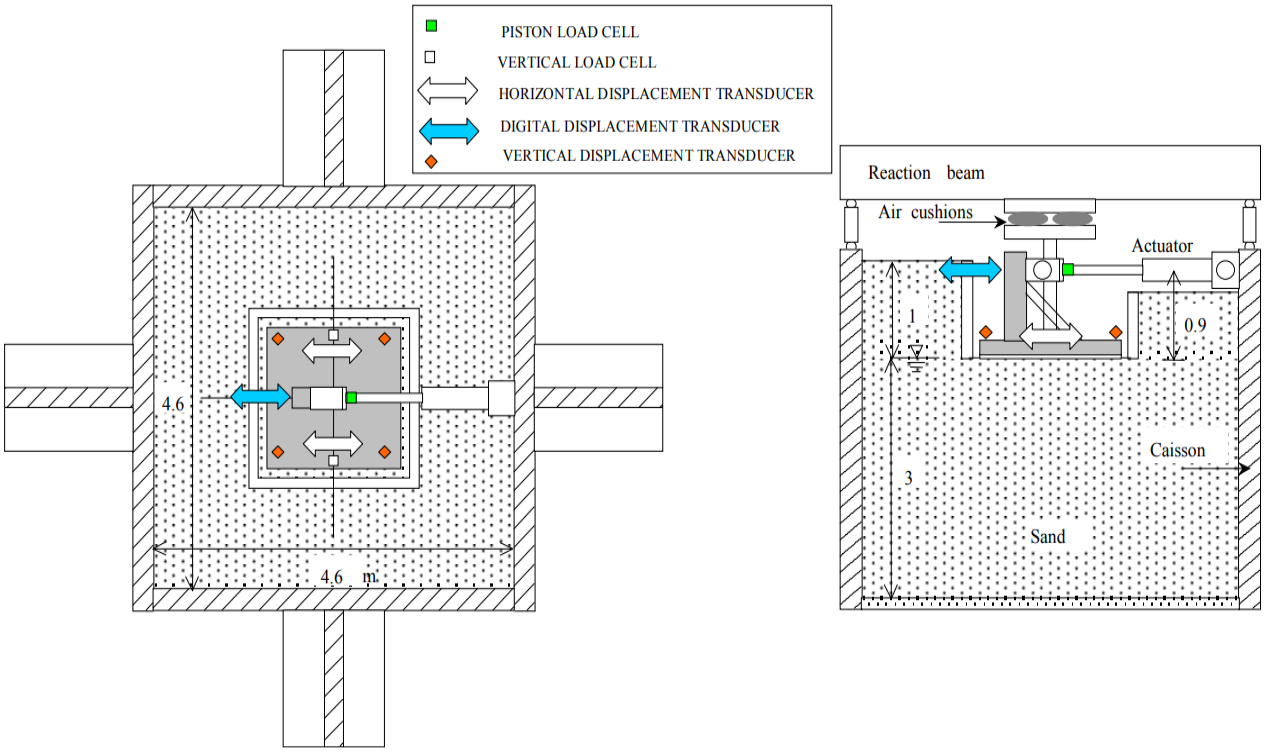

Fig 5.1: Prototype of the TRISEE cyclic direct shear-type experiments [1]

A vertical load of 100 kN for low density and 300 kN for high density sand, was continually transmitted to the foundation through an air cushion system. The load was constant during the course of experiments and represented the design pressure levels of structures for shallow foundations. A hydraulic actuator was installed 0.9 m above the foundation to transmit cyclic lateral loading to the foundation through a steel formwork. The applied forces, vertical and horizontal displacements and the effective soil pressure beneath the foundation were measured with a system of transducers, load cells and piezometers. The tests were conducted in three phases of slow cyclic load packets. In the first phase small amplitude force controlled load cycles were applied to the foundation, followed by a typical seismic time history. In the third phase, the foundation was subjected to sinusoidal displacement controlled load cycles of increasing amplitude till the lateral capacity of the foundation was mobilized. The Phase 3 experiments for high density sands are used for comparison of the numerical models to the experimental data.

5.2 Hysteretic material model for the soil

The non-linear soil is modelled using a multi-linear inelastic hysteretic soil model in ABAQUS defined as ABQ_HYST_SOIL [8], which is similar to the MAT_HYSTERETIC model in LS-DYNA [118] or the I-Soil model in MASTODON [7]. The soil model is comprised of a shear stress-strain backbone curve and the material damping is represented through the post-yielding shear stress vs. shear strain behaviour. The first point of the backbone curve is (0, 0) by default while the other stress-strain pairs individually represent an elastic-perfectly plastic "layer" with varying yield stress-strain values. With the yielding of each layer, the stiffness associated with the layer fades away thereby causing a reduction in the overall macroscopic shear stiffness. The response of the all these individual layers is summed up to generate a post-yielding shear stress vs shear strain curve which is valid for a single hydrostatic stress in the element. The hysteretic shear

stress vs strain behavior is generated as a response to a cyclic shear strain amplitude exceeding the lowest yield strain of a particular layer and follows the Masing's hysteresis rule unless the damping ratio vs. shear strain relationship is available for the soil under consideration. Therefore, the nested elasto-plastic layers yield at different stresses resulting in the observed hysteresis behavior.

The backbone curve is applicable at the confinement or reference pressure at which the experiments were performed. The shear stress vs shear strain data is primarily obtained from dynamic experiments like the Resonant Column Test or the Torsional Shear Test and the Cyclic Shear tests as described in section 2.1. Besides the backbone curve and the reference pressure (p_{ref}), the constitutive model includes pressure sensitivity parameters (a_0, a_1, a_2 and b), dilation constants and cut-off pressure (p_0); which can be calibrated from experimental data.

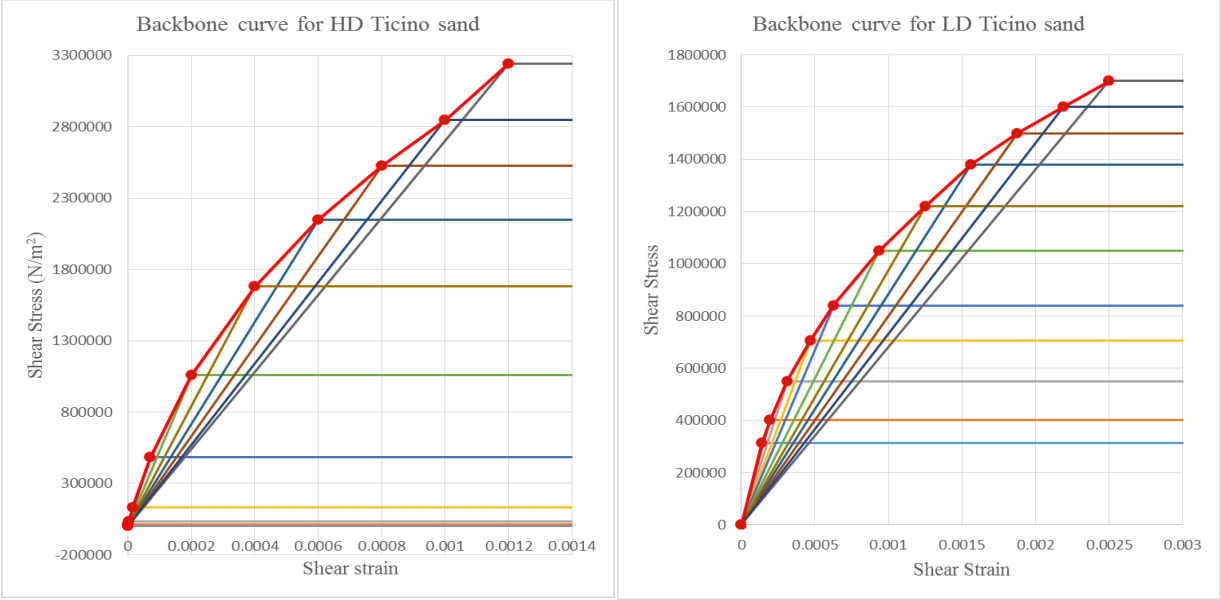

Fig 5.2: Multilinear inelastic backbone curve as a combination of elastic-perfectly plastic stress-strain pairs for Ticino sand

The shear and bulk modulus are pressure sensitive and are scaled with respect to the reference pressure (p_{ref}). The stress-strain behaviour of Ticino sands were obtained from a set of resonant column and monotonic loading torsional shear tests [123, 124] on solid cylindrical

specimens isotropically consolidated at varying void ratios. The shear modulus from the tests was plotted against the log of shear strain, and a well-defined plateau was observed for the shear modulus, G at strains less than 0.001%. This data was used to obtain the shear strain vs shear stress backbone curve for the TRISEE experiments. As discussed before, the backbone curve is formulated by combining the modulus reduction curve with the damping ratio vs shear strain relationship. If the variation of damping with shear strain data is not available for the soil sample, the backbone curve can be formulated with Masing's hysteresis rules. The elastic shear and bulk modulus are pressure sensitive governed by the constants a_0, a_1, a_2 and b. The ratio between these values determine how the backbone curve is scaled when the hydrostatic pressure changes during the simulation. The cut-off pressure p_0 determines the point below which shear stresses are set to zero. In other words, when the current pressure goes below the cut-off pressure, the soil has no stiffness in tension. However, for clayey soil or sticky interfaces, a non-zero cut-off pressure might be helpful in replicating the normal stick slip behaviour. The reference pressure was scaled up with respect to the operating pressure (p) of the experiment and the datum pressure (p_0) as [118]

$$\frac{\tau(p,\Upsilon)}{\tau(p_{ref},\Upsilon)} = \sqrt{\frac{[a_0+a_1(p-p_0)+a_2(p-p_0)^2]}{[a_0+a_1(p_{ref}-p_0)+a_2(p_{ref}-p_0)^2]}} \tag{5.1}$$

The stiffness in compression is correlated to the pressure changes with respect to the relative volume (ratio of original to current volume) V as [118]

$$p = p_{ref}\left[-\frac{K_0}{p_{ref}}\ln(V)\right]^{\frac{1}{1-b}} \tag{5.2}$$

where b is the pressure sensitive moduli exponent which varies between 0 to 1 and K_0 is the initial bulk modulus.

The dependence of the initial shear modulus on void ratio and confining stresses was defined on the basis of resonant column tests [125] as

$$G_{max} = C_g . F(e) . {\sigma'_m}^n . p_a^{1-n} \quad (5.3)$$

where,

C_g	= 710	Dimensionless soil constant
$F(e) = (2.27 - e)^2/(1 + e)$		Void ratio function ($0.579 \leq e \leq 0.930$)
n	= 0.43	Modulus exponent
p_a		Atmospheric pressure
σ'_m		Mean effective stress

The initial shear modulus at varying reference pressures was used to formulate the backbone curve. The deviatoric stresses are computed for each layer and the energy dissipation occurs when the amplitude of a strain cycle exceeds the lowest yield strain of the shear stress-strain curve which defines the layer under consideration. When the deviatoric stresses attain the pure shear state, the maximum shear stresses exceed the input backbone curve by a factor of $\sqrt{1.33}$. The yield surface defined by each elasto-plastic layer (denoted by *i*) is defined in terms of the second stress invariant under a uniaxial stress state, which is converted from the maximum shear stress as [8]

$$J_{2i} = \left(\sigma'_I : \frac{\sigma'_I}{2}\right) < \frac{4}{3}\tau^2_{max} \quad (5.4)$$

5.3 Material properties of Ticino sand

The non-linear soil in the ABAQUS models was modelled using the ABQ_HYSTERETIC_SOIL material. The primary input parameters for this model include the user-defined backbone curve, the initial shear modulus, reference pressure and pressure dependency coefficients. Ticino sand was used for the cyclic shear experiments, which is predominantly a feldsparic sand with 30% quartz and around 5% mica content. The particles have high sphericity in the range of 0.7 to 0.8

with small roundness and is descried as sub-angular [126]. A wide range of monotonic and cyclic shear testing was performed on Ticino sand to determine its anisotropy and dynamic shear behavior [127, 128, 129].

Table 5.1: Physical properties of Ticino Sand [122]

Υ_{max}	Υ_{min}	e_{max}	e_{min}	Specific gravity
1700 kg/m^3	1390 kg/m^3	0.934	0.582	2.69

The shear modulus of pluviated deposits of Ticino Sand was measured in a resonant column and torsional shear apparatus and the measured values were compared for the monotonic loading tests and the cyclic shear tests [125]. The stiffness of sands at small strains is a key parameter for the hysteretic soil model used in the analysis and it is effective for determining the seismic response of deep soil deposits and design of foundations with stringent displacement serviceability requirements.

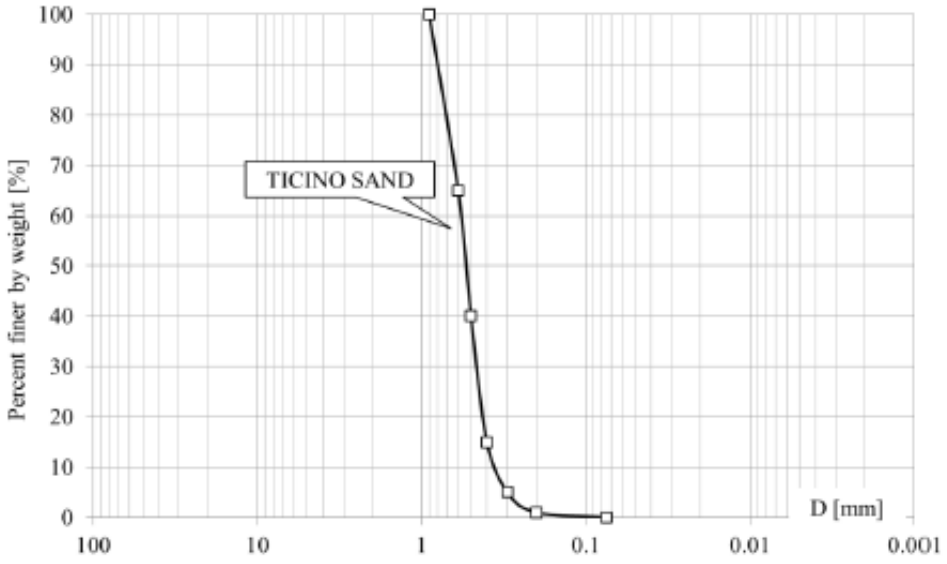

Fig 5.3: Grain size distribution of Ticino Sand [125]

Although the strain levels in soils surrounding shallow foundations is quite small for monotonic loading conditions [130, 131] in the range of 1%, the strain levels tend to vary drastically when subjected to cyclic loading or ground motions. The response of uniform, well-graded coarse-to-medium sands remain elastic at strain levels below 0.001% while the behavior becomes highly nonlinear in the range of 0.001 to 1%. The behavior of Ticino sand subjected to such high strain levels were obtained from dynamic tests such as the resonant column test or seismic wave tests. While the conventional monotonic tests fail to accurately determine the small strain stiffness, the RC tests fail to control the number or loading cycles or strain rates in tandem [132, 133]. Cyclic triaxial and RC tests operating within a frequency range of 0.1-1 Hz were used to determine the shear modulii of soils. The dynamic unloading-reloading behavior was expressed through the secant shear modulus which is the slope of the line joining the peaks of the unloading-reloading points (as described in section 2.3.1). For medium-to-coarse grained Ticino sands, the shear modulus is constant at small strains (< 0.001%) and represents the maximum shear modulus (G_{max}). The maximum shear modulus is dependent on state parameters such as the mean effective stress and void ratio, determined from monotonic tests on isotropically consolidated specimens [32, 134]. However, the propagation of seismic body waves [122] revealed that the body wave velocities depend primarily on the normal effective stress along the particle motion in the direction of wave propagation. The effective stress ratio, number of loading cycles and the loading frequency do not have a significant influence on the maximum shear modulus. The secant shear modulus depends on the effective consolidation stresses and levels of operating shear strain [31]. The secant or equivalent shear modulus is marginally affected by the cyclic prestraining or the principal stress ratio, except during the initial quarter load cycle when the influence is higher [135]. Monotonic and cyclic loading tests result in the same maximum shear modulus varying with void ratio and

consolidation stresses. However, the secant shear modulus obtained from monotonic loading tests deviate from the cyclic shear tests at strain levels greater than 0.001%.

A set of 80 RC tests were performed on isotropically consolidated cylindrical specimens of Ticino sands [125]. Similar soil samples were tested using the monotonic torsional shear tests at void ratios and confining stresses close to the RC tests [136].

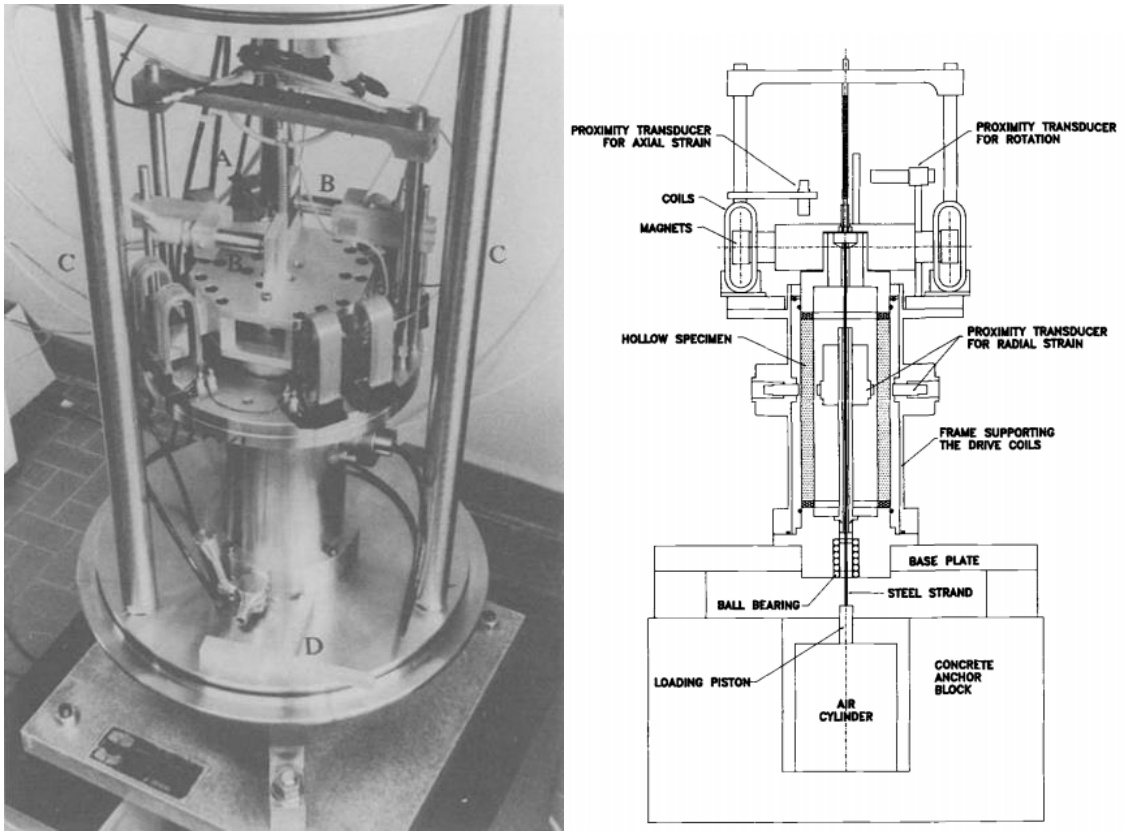

Fig 5.4: (a) General view of the apparatus: (A) proximity transducer for axial strain; (B) proximity transducers for top rotation; (C) tie rods; (D) aluminum element for correctly positioning proximity transducers. (b) Schematics of experimental setup

The test matrix involved around 18 tests on normally consolidated specimens, 5 tests on isotropic pre-consolidated specimens and 4 cyclically pre-strained specimens. The tests on Ticino sand specimens were reconstructed by pluviation technique [136] and were carried out within 5-

10 mins of application of the consolidation stresses. The monotonic torsional shear stresses revealed that the shear stress vs strain relationship was linear under strain levels of 0.001%. When the specimen was subjected to cyclic loading, the slope of the reloading curve was found to be parallel to the slope of the initial virgin loop [125]. This allows us to apply Masing's rule to formulate the backbone curve if the variation of damping ratio with shear strain is not available.

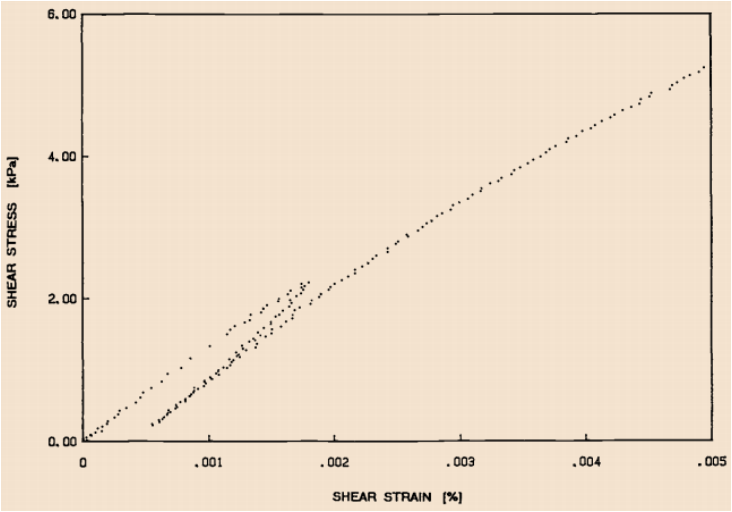

Fig 5.5: Shear stress-shear strain curve from monotonic torsional shear test for Ticino sand [129]

The maximum shear modulus for Ticino sand remained the same across the RC and the monotonic torsional loading tests. The values of maximum shear modulus obtained from isotropically pre-compressed and normally consolidated specimens agreed well with the empirical relation for G_{max} in Sec 5.2. However the experimental values obtained from the cyclically pre-strained specimens exceeded the empirical values by 20%.

The G_{max} obtained from dynamic tests often exceed the G_{max} obtained from monotonic loading tests primarily due to particle crushing of the sand which increases the surface area in contact. The pre-consolidation mechanism has a significant impact on the shear modulus once the threshold elastic shear strain is reached. The correlation of the normalized shear modulus with the

mobilization factor (ratio of the mobilized shear stress to peak shear stress) helps us in obtaining the relationship between the dynamic secant shear modulus which has been observed to be hyperbolic for coarse to medium sands [137]. The deviation from hyperbolic relationship is observed at strains higher than 0.01% after a large number of loading cycles due to strain hardening.

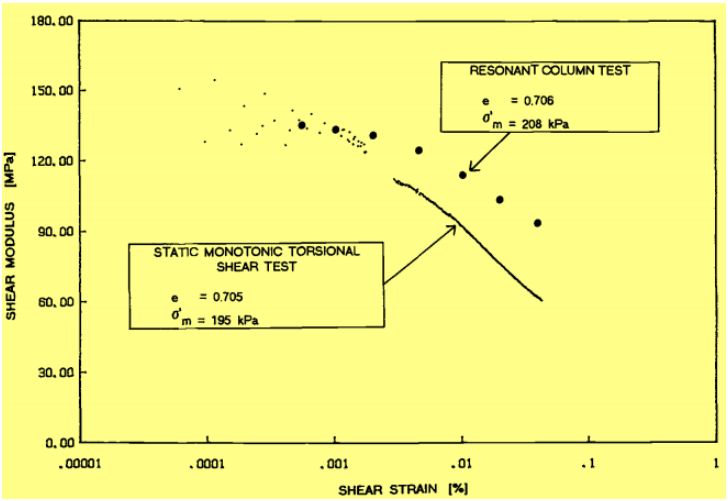

Fig 5.6: Variation of shear modulus of Ticino sand with shear strain for static monotonic and resonant column tests [125]

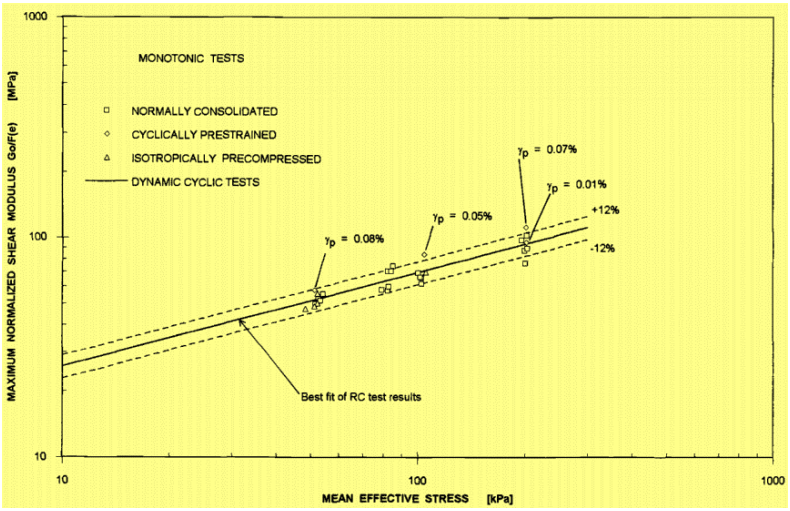

Fig 5.7: Variation of normalized shear modulus with mean effective stress [125]

5.4 Finite element modelling procedure

The primary motivation of the study is to compare numerical NLSSI results with the experimental data from the TRISEE experiments. The hysteresis behavior of the non-linear soil is generated by using a two-element finite element model which imitates the behavior of the linear elastic soil model. The reference pressure at the soil structure interface and the operating shear strain range for the displacement controlled load cycles is obtained from a linear SSI analysis without any material or geometric nonlinearity. The numerical backbone curve is derived from the experimental G/G_{max} vs. Υ curve, and element tests are performed to verify the hysteresis behavior. When the behavior of the soil element is observed to mimic the shear stress vs. shear strain behavior of the backbone curve, the material model parameters are input to the large scale experimental prototype. The parameters a_0, a_1, a_2 were set to activate pressure dependency, such that the backbone curve could scale with the reference pressure.

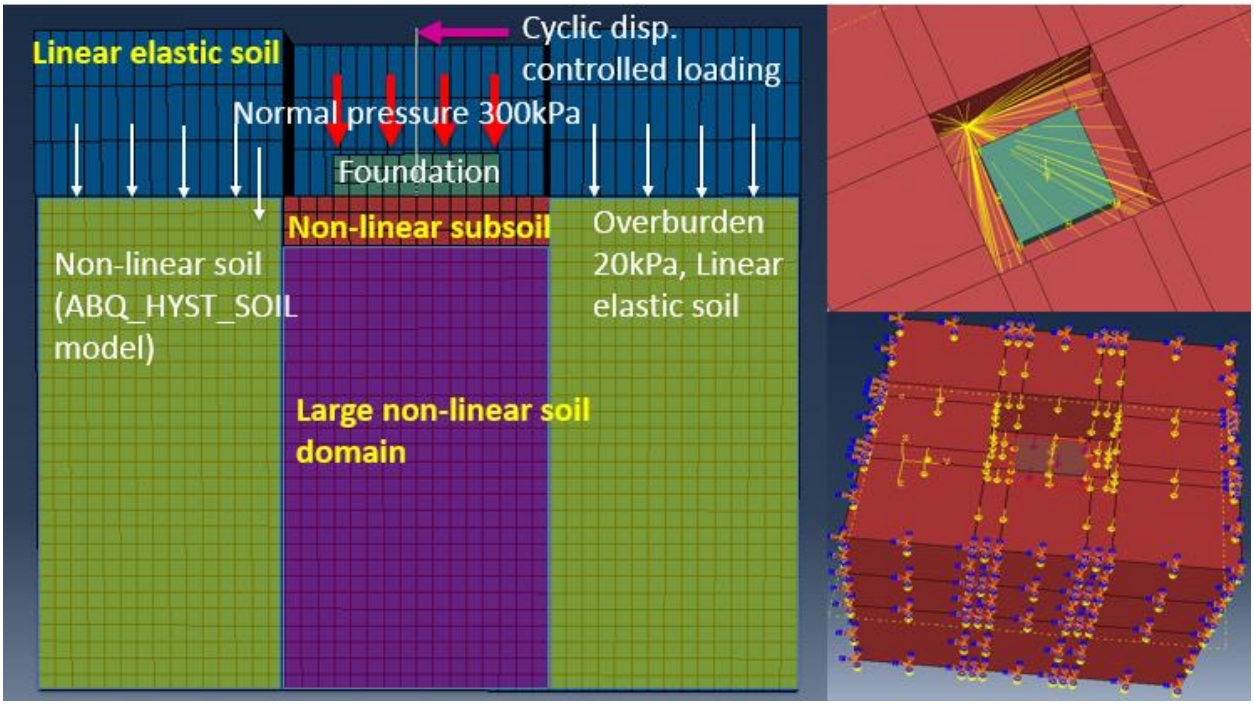

Fig 5.8: Finite element model of the TRISEE experimental prototype

A detailed model of the TRISEE experimental prototype is built with a layer of fine meshed non-linear soil surrounding the foundation (in red) which is tied to the surrounding soil domain, also non-linear in nature. The backbone curve for the underlying soil domain was scaled according the confinement pressure. The steel foundation and formwork have isotropic linear elastic properties. The loading is applied to the structure in terms of sine shaped displacement cycles of gradually increasing amplitude, through a rigid steel column which is embedded in the foundation. A constant uniform load of 300 kN is applied on top of the foundation and maintained throughout the simulation. The unsaturated layer of sand surrounding the foundation exerts an overburden pressure of 20 kPa and is retained through a 1m formwork surrounding the sand. This is simulated by constraining the nodes of the trench boundary surfaces to move together. The edges of the soil domain are fixed to ensure soil confinement.

Fig 5.9: Displacement-time loading history for sliding of foundation on high density and low density Ticino sand

The soil domain, foundation, mesh properties, loading conditions and boundaries are consistent throughout the analysis process. Enhanced hourglass control was adopted for the non-linear soil elements for improved coarse mesh accuracy and ensuring better performance of non-linear material response at high strain levels. The reduced integration elements account for the linearly varying part of the incremental displacement field for calculation of the increase in physical strain, while the non-linear part is expressed in terms of hourglass modes [4]. Excitation of the hourglass modes results in heavy mesh distortion, which is controlled by activating the stiffness control factor.

The interaction between the soil and structure is controlled by a softened contact overclosure relationship in the normal direction, in which the contact pressure is an exponential function of the clearance between the contact surfaces. The contact pressure increases exponentially as the clearance between the two surface decreases which captures the phenomenon of increasing soil stiffness for increased penetration. The tangential behavior is efficiently implemented through the non-linear hysteretic soil model along with a kinematic friction formulation.

5.5 Results from small-scale test models for simulating direct shear tests

The small scale tests were setup by stacking two elements of the same scale as the experimental prototype on top of each other. The backbone curve for the non-linear soil element was defined for the initial hydrostatic stress which corresponds to the reference pressure using the ABQ_HYSTERETIC_SOIL model.

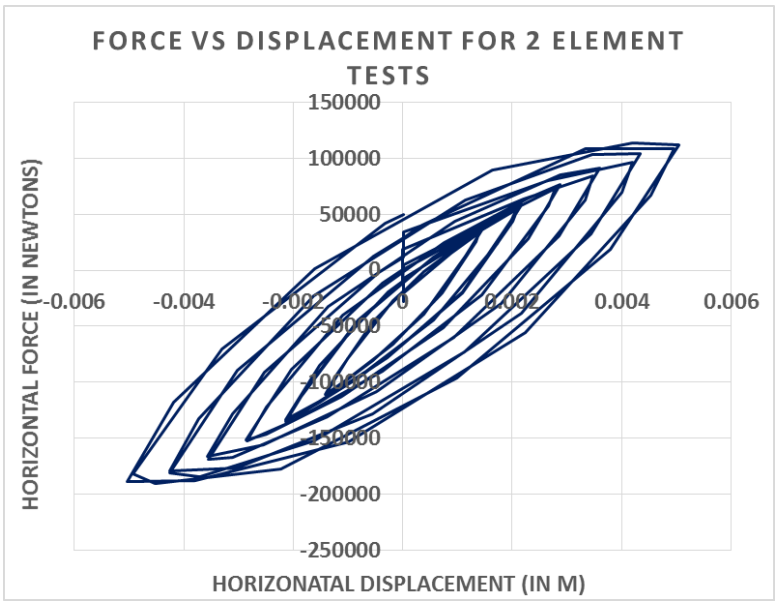

Fig 5.10: Force vs. displacement response of the 2-element tests

The hydrostatic stress is obtained by performing a pseudo static gravity test on the two-element model. The lateral displacement load is applied on top of the foundation element and the model is restrained to allow shearing only in the X-direction. Under the operating strain range, the pattern of the load-displacement history from the simulations was found to closely resemble those from the experiment as seen in Fig 5.10.

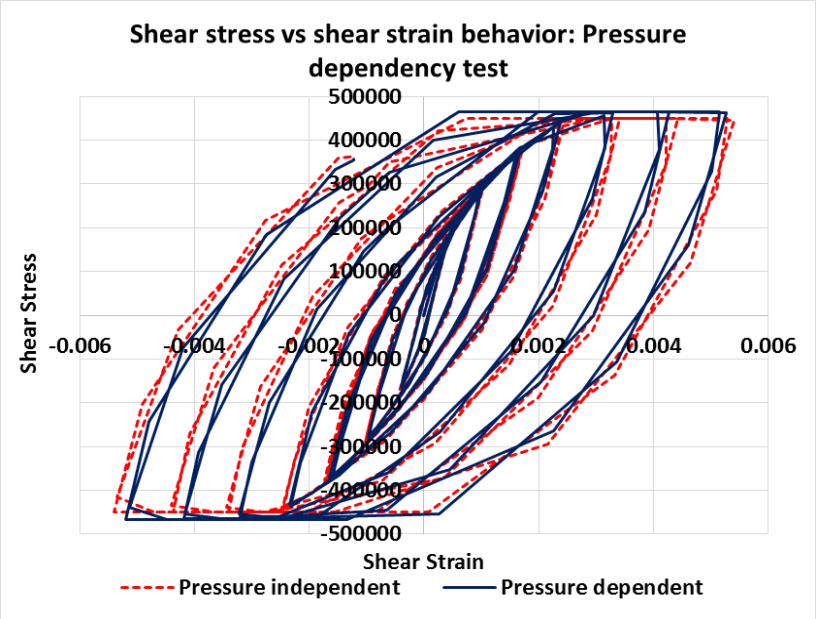

Fig 5.11: Sensitivity study on the basis of pressure dependency

The yield stresses of the individual 'layers' or shear stress-strain pair of the backbone curve varies with the change in pressure, which is implemented through the pressure dependency coefficients a_0, a_1, a_2 and b. The backbone curve scales itself with respect to these coefficients. The parameters a_0, a_1 and a_2 are responsible for scaling the shear stresses at a particular strain level when the pressure changes. The intermediate slope between two successive stress-strain points in the backbone curve also changes with changes in the confining pressure governed by the coefficient b. A pressure dependency sensitivity study was performed on the two element models. There was no significant difference in the shear stress vs. shear strain response of the soil element. A similar trend was observed for the large scale experiments as well which were pressure dependent, to allow scaling of the shear moduli and the slope of each section of the shear stress-strain backbone curve. The pressure dependency however plays a crucial role in determination of the non-linear response of the underlying soil strata. It should be noted that pressure sensitivity could introduce noise in the numerical solutions, especially for soil layers where the variation in

pressure is negligible compared to the initial stress state. In such cases, it is advisable to use the pressure from initial stress state of the soil domain rather than the current pressure [118].

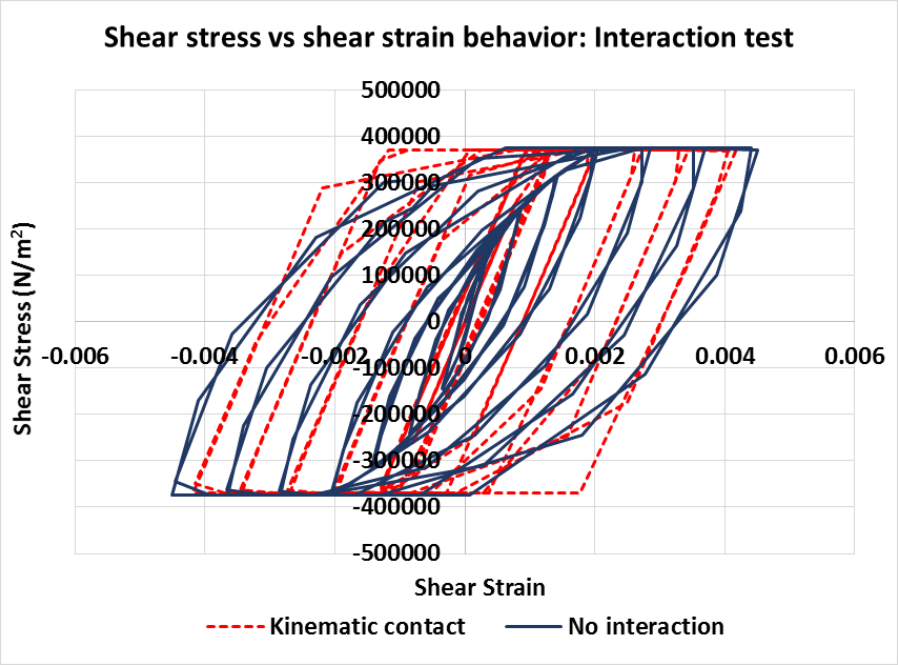

Fig 5.12: Idealization of shear stress vs. shear strain response of the non-linear interface using Coulomb friction

The interaction definition for the test models was defined using the 'softened' pressure overclosure relationship. The softened pressure overclosure relationship allows us to model the increase in soil stiffness as the overclosure between the soil and structure decreases. The formulation will be discussed in detail in chapter 6. The tangential non-linearity was effectively represented through the hysteretic soil model in the vicinity of the interface along with kinematic friction formulation with a friction coefficient of 0.2. The tangential behavior in the vicinity of the foundation was dominated by the hysteretic soil behavior while the kinematic contact was adopted for numerical stability and to avoid convergence issues. This was based on the assumption that the sliding of concrete/steel foundations on soil cannot be solely represented by a friction-based

interaction algorithm; primarily due to the change in the stresses at the nodes of the non-linear soil surrounding the interface when subjected to dynamic loads.

The hysteretic soil model is an Iwan-type [38, 107] model, where the material properties are distributed over the nodes which dictate the hysteretic behavior. Depending on the strain level at a particular element, the nodes at the interface might undergo yielding due to higher shear stresses in accordance with the backbone curve. Similarly, a node which does not reach the threshold shear stress at a particular cycle may respond elastically. The combination of the behavior of these individual nodes represents the behavior of the interface. On the other hand, a simple kinematic contact algorithm enforces frictional contact when the shear stresses of the surfaces in contact exceed the critical shear stress. It doesn't take the scaling of stresses with the confining pressure or the differential yielding of the nodes across the interface into account. Hence, it is difficult to model the true tangential behavior of the nonlinear soil surrounding the interface with a friction based contact algorithm. However; if we are just concerned with the margins of the ultimate shear stresses and strains at the interface and not the hysteresis behavior, an equivalent friction based model (which has been calibrated with the non-linear material model) might be computationally more efficient. The implementation should be performed after thorough calibration with the full scale nonlinear prototype and may perform well in simulating the response of shallow foundations. It won't be able to accurately capture the hysteresis behavior but would be effective in determining the margins of the non-linear dynamic response. However, it is not ideal for modelling contact of deep foundations due to pressure dependency stipulations.

A sensitivity study is also performed on the basis of the bulk modulus on the Ticino sand. It was observed the dissipation of energy occurred more for the lowest bulk modulus or least volumetric change, and gradually increased as the bulk modulus increased.

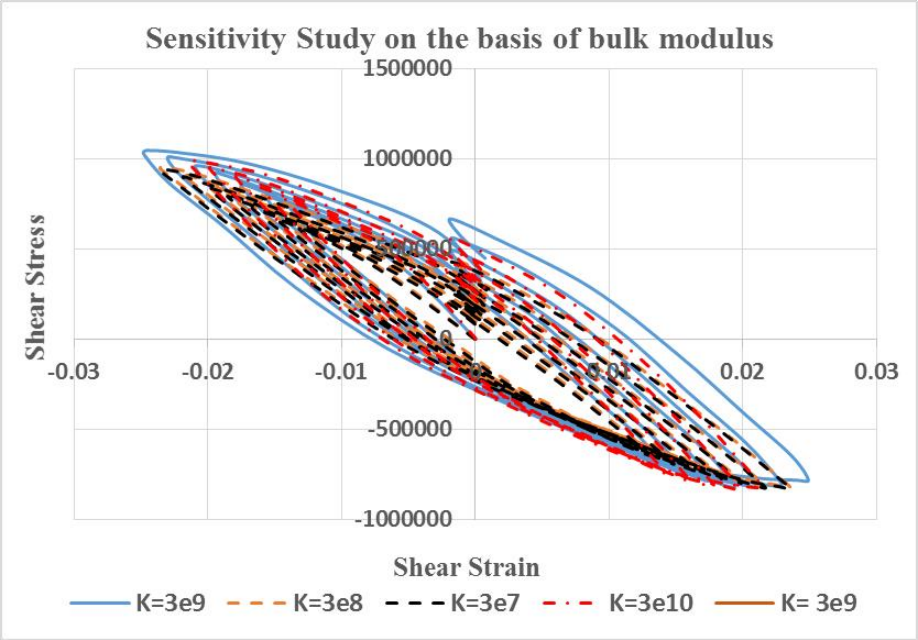

Fig 5.13: Sensitivity study on the basis of bulk modulus for Ticino sand

5.6 Verification of finite element analysis results with experimental data

The non-linear full scale models were observed to have good agreement with the experimental hysteresis behaviour. While analysing the output, it should be noted that each point in the shear stress vs shear strain backbone curve is treated by the material model as [9]

$$\sigma_{ej} = \sqrt{\frac{3}{4}}\tau_j \tag{5.5}$$

$$\Upsilon_{ej} = \sqrt{\frac{3}{4}}\Upsilon_j \tag{5.6}$$

where, τ_j and Υ_j represent the maximum shear stress and shear strain which is reached when the deviatoric stress state is close to pure shear and, σ_{ej} and Υ_{ej} represent the data points for the input backbone curve. The initial hydrostatic stress state is expressed in terms of the normal stress which is a combination of the applied vertical pressure and gravity load. The soil domain is partitioned

in terms of its initial hydrostatic stresses through a pseudo static gravity analysis and the backbone curve is specified for the partitioned soil domains.

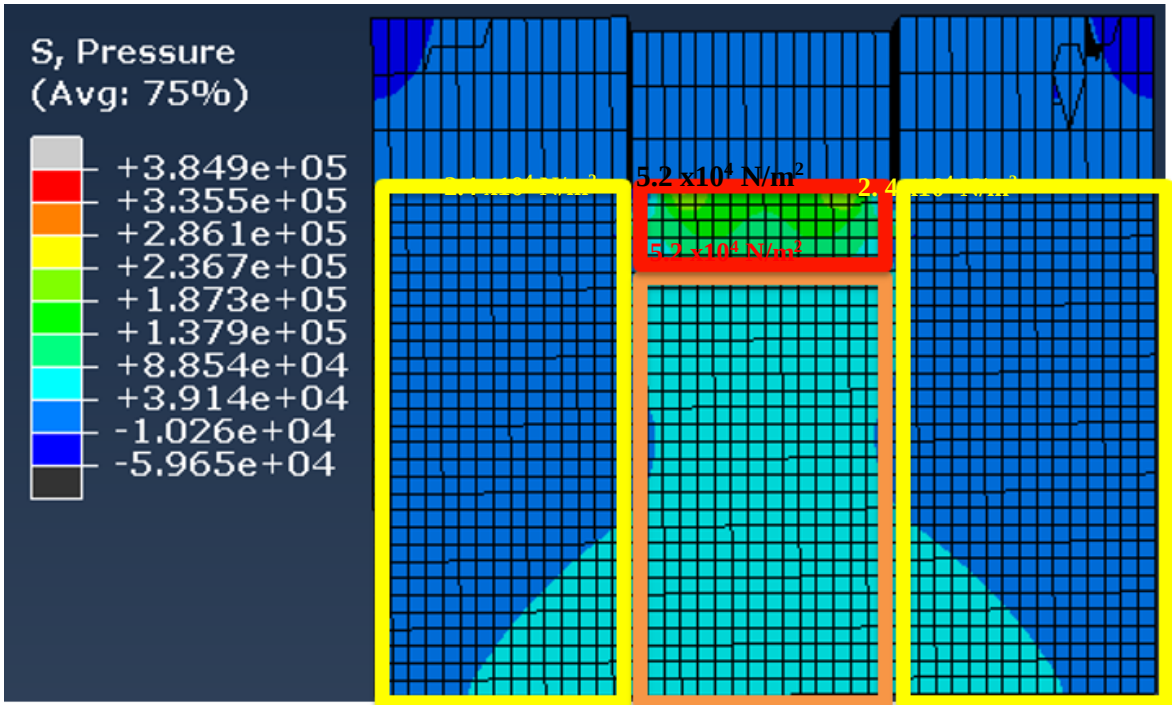

Fig 5.14: Partitioning the soil domain on the basis of initial hydrostatic stresses

The numerical analysis was performed in three stages to differentiate the effects of geometric nonlinearities from the material nonlinearity, as depicted in Fig 5.14. In GEOM_SLI case, the nodes of the soil are constrained to move with nodes of the basemat in lateral direction and hard pressure overclosure relationship is applied in the normal direction. This case slightly over-predicted the response as compared to the GEOM_SL2 case, where a friction formulation was adopted. The best results were obtained for the GEOM_GP+SL case, where a slight reduction in the force-displacement response was observed due to inclusion of the softened exponential pressure overclosure relationship. However, the material nonlinearity plays the key role in accurately describing the soil-structure interface behavior.

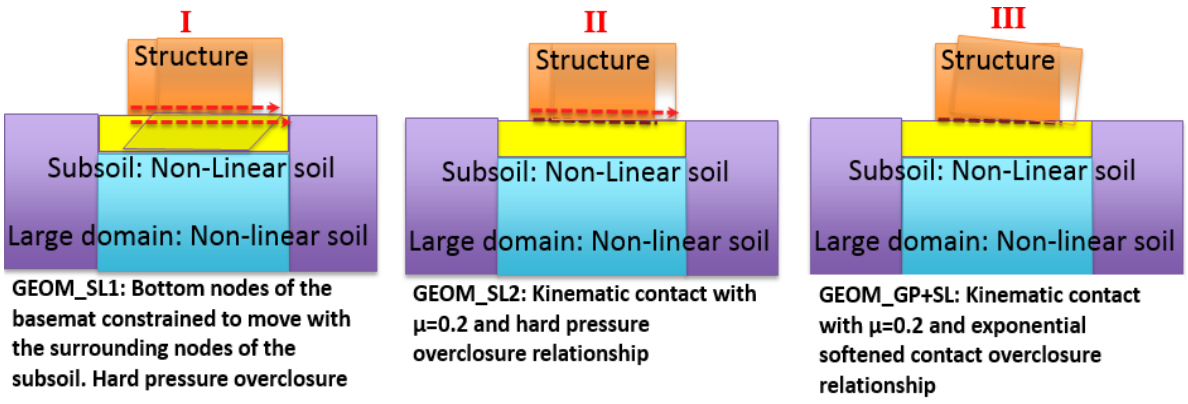

Fig 5.15: Phases of NLSSI analyses of the TRISEE experiments

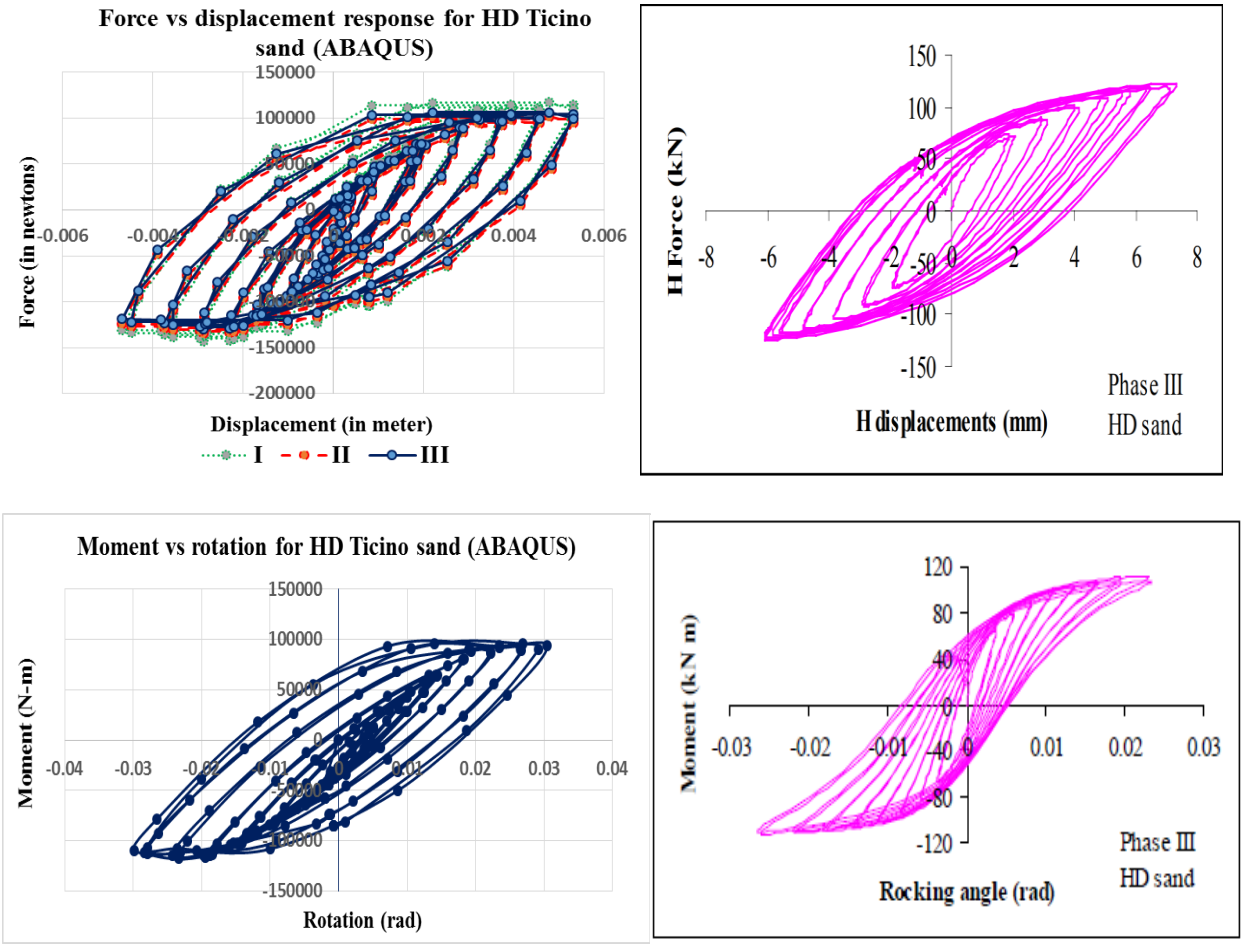

Fig 5.16: Comparison of the force vs. displacement (for case I, II and III) and moment vs. rotation curve from numerical analysis results against the TRISEE large scale tests

The finite element models capture the initial stiffness of the force-displacement response and its degradation with increasing shear strain with reasonable accuracy. The force-displacement response is mostly symmetric and reaches a maximum displacement of around 6 mm for the high density Ticino sand, which is corroborated by the experimental data. Most of the horizontal displacement of the foundation is recovered while the load amplitude is increased. This can be attributed to the high strength capacity of the Ticino sand. The numerical model captures the gaining of lateral capacity of the foundation at an ultimate moment of about 100 kNm. The rotational stiffness of the system gradually decreases with the increase in rotation, as depicted by the hysteresis loop in Fig 5.15. The moment-rotation curve obtained from the experiments is S-shaped, signifying an uplift-controlled response. The pinching of the hysteresis loop is not captured efficiently by the numerical model. The model marginally over-predicts the energy dissipation at the interface.

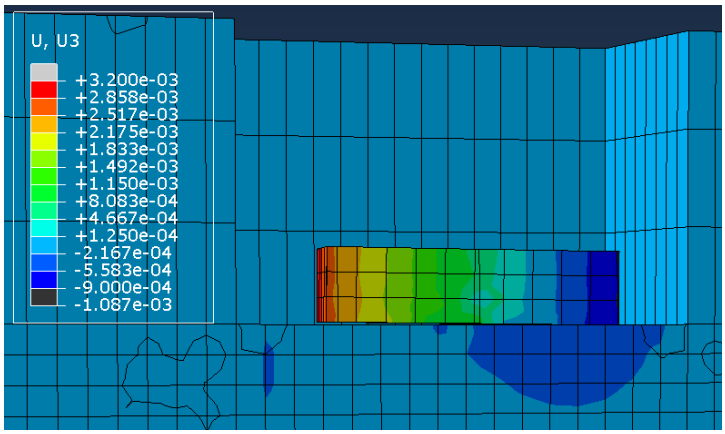

Fig 5.17: Gapping behavior at the interface

The softened pressure overclosure relationship can be modified to account for the stiffness-penetration relationship and model the uplift behavior more accurately. The uplift behavior of the foundation is reversible for the high density Ticino sand, characterized by the symmetric hysteretic loop. However, the possibility cannot be ruled out for low density sands or if the vertical pressure

is not high enough or applied asymmetrically; which might result in overturning effects, producing gapping behaviour at the soil-structure interface.

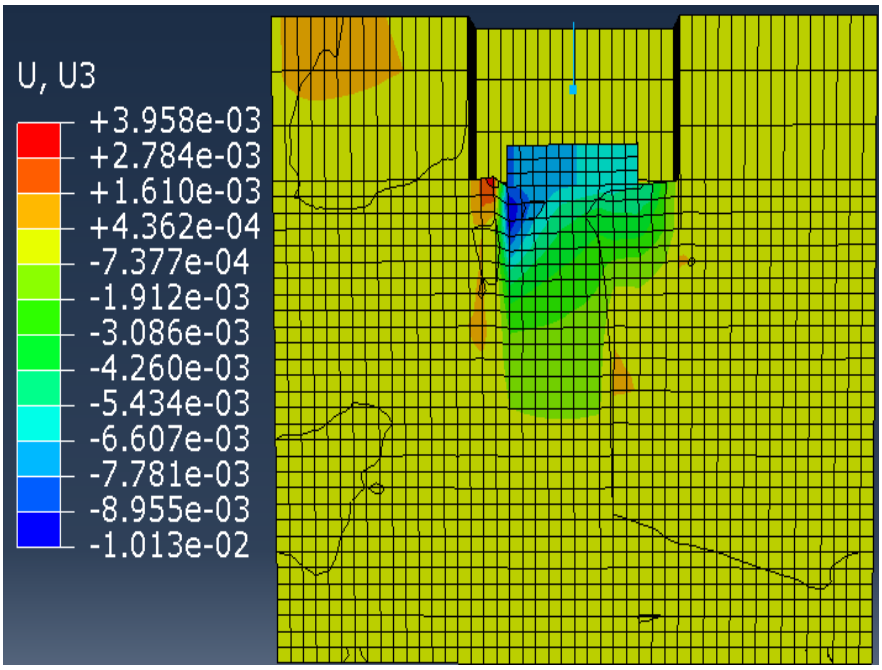

Fig 5.18: Lateral displacement behaviour at the soil-structure interface

5.7 Chapter summary

The chapter demonstrates NLSSI analysis of cyclic direct shear tests, which focuses on the calibration of the non-linear hysteretic soil model parameters which is used in the full-scale NLSSI analysis of the Fukushima Daichii NPP in the next chapter. The numerical results are validated against the force-displacement and moment-rotation relationship of the foundation obtained from experiments [1]. Small-scale tests were performed to test the nature of shear stress vs. shear strain hysteresis loop in addition to pressure dependency tests and a sensitivity study on the basis of the bulk modulus. The pressure dependency parameter didn't have a significant influence on the hysteretic response of the foundation. This is due to the fact that we are dealing with shallow

foundations, which is the case for most SSI analysis. The increase in bulk modulus resulted in bulging of the hysteresis loops which eventually ceases at a threshold value. The force-displacement response of the full-scale cyclic shear test models and the hysteretic behavior obtained from the numerical analysis is found to be in close correspondence with the experimental results. However, the pinching of the moment-rotation curve is not efficiently captured by the material model. The peak lateral stresses in the vicinity of the interface at maximum shear strains is governed by the post yielding shear stress vs shear strain backbone curve, which also controls the hysteresis behaviour. The tangential contact formulation provides numerical stability for modelling the interface. However, the non-linear behavior of the soil in the vicinity of the foundation is depicted by the hysteretic material model, while the kinematic contact algorithm has minimum influence. For large scale FEA models of NPPs subjected to seismic loads; an equivalent kinematic, friction-based contact formulation can be calibrated with the backbone curve to determine the shear stresses at failure. This is useful when the exact hysteresis behaviour of the interface is not important, and we are interested only in determining the seismic margins of the structural response.

6. FULL SCALE NON-LINEAR SOIL STRUCTURE INTERACTION ANALYSIS OF THE FUKUSHIMA DAICHII NPP

For most nuclear structures resting on a stiff soil mass, the natural frequency of the soil-NPP assembly is reduced as compared to a fixed base structure. The stress waves that reach the ground are partially transmitted into the structure and a part of the incident shear waves are reflected back resulting in radiation damping which dissipates energy across the interfaces. Radiation damping tends to reduce the overall damping of the soil-structure system as compared to the structural damping. This would imply that SSI reduces the in-structure response of the system. However, the overall displacement of the structure might increase because of rotation and translation of the foundation, which is a critical aspect of drift-driven seismic design.

Normally, the effects of soil structure interaction is more pronounced on heavy structures resting on soft soils as compared to light structures on stiff soil. Nuclear power plants are large stocky structures housing critical mechanical components like control rods, turbines, steam generators, etc. which function simultaneously to generate power from nuclear fission and are frequency rated. The response of heavy or stocky structures resting on stiff soils needs to be analyzed on a case by case basis because SSI can have largely varying effects on the seismic behavior of different structural systems. The variability in the structural response can be attributed to kinematic interaction effects which is responsible for modifying the free field motion and inertial interaction effects which changes the behavior of the non-linear soil on which the superstructure is supported. Kinematic interaction induces torsion and rocking behavior in the structure while inertial interaction effects result in translation and differential settlement of the structure when subjected to cyclic loading. The inertial and kinematic interaction effects are

represented through geometric nonlinearities at the interface and the non-linear behavior of the soil surrounding the basemat.

Chapter 4 focused on simulating the response of a structure to three dimensional ground motion with geometrical nonlinearities at the interface. It was observed that the response acceleration was much higher than the free-field motion. Additionally, there were certain anomalies in some components of basemat response. Even though the inclusion of contact parameters reduced the response acceleration when compared to the numerical free field motion, the numerical values exceeded the actual free field motion recorded at the Fukushima Daichii Unit 6 by more than 100%. This called for an investigation into the material nonlinearity at the interface and the overall soil domain. In Chapter 5, the hysteretic soil model was used to model the nonlinear soil for a set of cyclic shear experiments. The material model was successful in capturing the acceleration response in the vicinity of the basemat. The normal contact algorithm was also modified from its initial formulation in Chapter 4. This chapter will focus on a full scale nonlinear SSI analysis incorporating material nonlinearity in the soil surrounding the basemat and the large soil domain as well.

6.1 Modifications to the finite element model

The same finite element model is used for the NLSSI analysis except for modifications to the interaction parameters and the soil domain. The lateral boundaries are constrained to move in pure shear by assigning constraint equations to each layer to prevent spurious reflections of the stress waves. The bottom-most layer of the soil domain is composed of CIN3D8 infinite elements to prevent reflection of waves from the bedrock layer, resulting in amplifications of the input motion. The soil domain is subdivided into four zones of non-linear soil on the basis of initial hydrostatic stresses at the top of each soil layer determined from a pseudo-static gravity analysis. This allows

us to obtain the in-situ shear stress vs shear strain behavior of the soil concurrent with the no-deformation/equilibrium phase, before the application of ground acceleration.

The attenuation of response acceleration is primarily attributed to the non-linear soil zone in the vicinity of the soil-foundation interface. The soil surrounding the basemat soil has slightly varying properties in terms of the reference pressure and initial shear modulus. A sensitivity study was performed with non-linear soil surrounding the basemat with isotropic elastic soil making up rest of the soil domain and a full-scale NLSSI analysis (the whole soil domain modeled with nonlinear soil).

The interaction parameters adopted for the soil-structure interface is aimed at simulating the geometric nonlinearities at the interface which includes gapping or uplift (in the normal direction) and sliding (in the tangential direction). In Chapter 4, gapping was simulated through the hard pressure overclosure relationship. This formulation performed reasonably well for two isotropic elastic materials in contact by controlling the penetration between the master and slave nodes before activating contact restraints and facilitating transfer of tensile stresses before deactivating contact restraints. For coarse to medium grade sands, there is no transfer of tensile stresses during gapping or uplift behavior. Furthermore, with the progression in cyclic loading there might be differential penetration of the foundation into the soil, which is not effectively captured by the hard contact algorithm. The softened contact relationship is used to model the gapping nonlinearity of the interface. In this algorithm, the normal contact forces are assumed to increase exponentially with the overclosure or penetration. The algorithm specifies the contact between two surfaces in terms of the clearance vs. contact pressure. The surfaces transfer contact pressure when the clearance or gap between them is reduced to the specified value along the normal direction. The transmitted pressure continues to increase exponentially as the clearance between

the two surfaces start reducing. The contact stiffness can be limited to a maximum threshold value in order to alleviate the effects of large stiffnesses on the stable time increment when enforced through penalty constraint. The soft contact is effective in reproducing the phenomenon of increasing stiffness of the interface with increasing penetration of the foundation. It is also effective in modelling of thin-layer contact elements by making it easier to attain numerical convergence. However, one should be wary of residual stresses at the interface that might result from the softened contact formulation. Certain facts must be considered while applying the softened contact algorithm in ABAQUS Explicit or Implicit for performing dynamic SSI analysis. In ABAQUS/Implicit, the softened contact is not meant for transmission of impact loads, where the kinetic energy of the nodes across the interface is eliminated when the impact occurs. It will presume an elastic collision between the two surfaces which will cause the slave nodes to spring back immediately after impact with the master surface. This might result in substantial noise in the analysis output and convergence issues pertaining to low time increments [8]. This is especially important to keep in mind while modelling the response of heavy structures to high frequency ground motions or modelling gapping in foundations subjected to accidental loads.

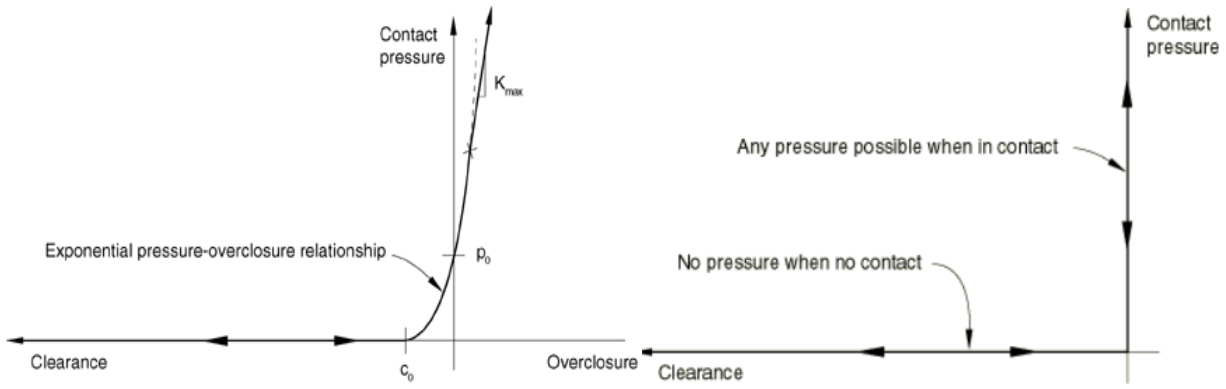

Fig 6.1: Exponential softened pressure overclosure relationship vs hard pressure overclosure [8]

The tangential behavior of the interface is taken care of by the nonlinear soil surrounding the basemat. In Chapter 3, the thin layer element was used to simulate Coulomb friction between the soil and foundation. In the full scale NLSSI simulations, we will be using the shear stress vs. shear strain backbone curve of sandy mudstone in addition to the kinematic friction formulation (similar to the procedure discussed in section 5.5 and 5.6), which is more accurate in predicting the sliding behavior of the foundation. The reference pressure of the non-linear soil surrounding the interface is set to the normal stresses from gravity loads or overburden pressure. The hysteretic backbone curve is pressure dependent and facilitates the yielding of individual nodes in accordance with the strain levels at that node and scales it with the change in confining pressure. It also helps in reducing high frequency response when the kinematic Coulomb friction model is implemented, caused by abrupt changes in the interfacial shear stiffness. The pressure dependency condition also helps in adjusting the shear stress vs strain relationship of the backbone curve with the change in normal pressure. A separate non-linear soil model is adopted for the larger soil domain. The non-linear material properties of mudstone/sandstone that have been used to derive the backbone curve, will be discussed in the next section.

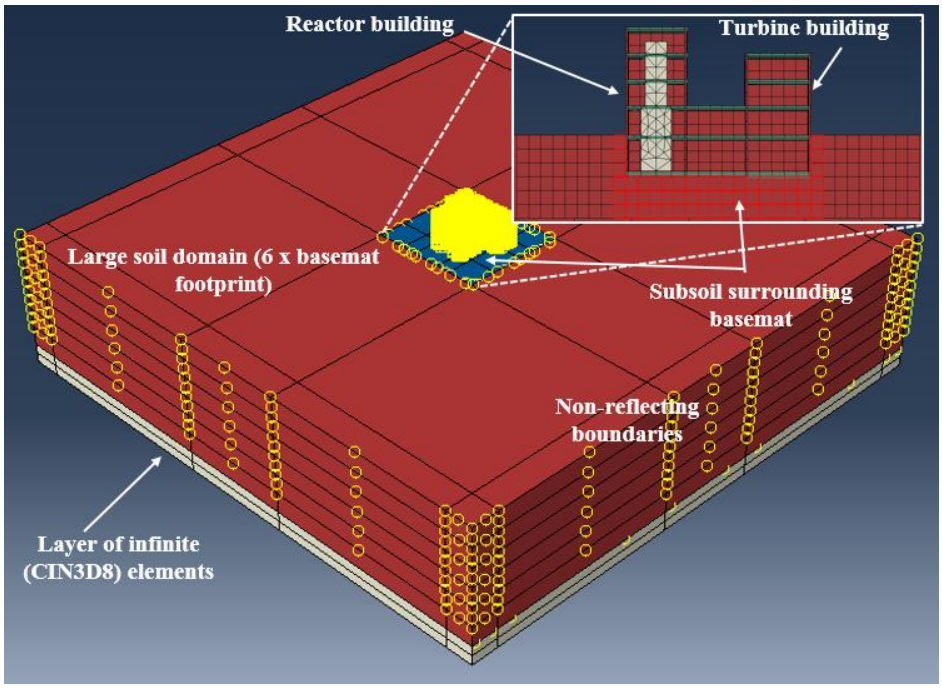

Fig 6.2: Full-scale NLSSI finite element model

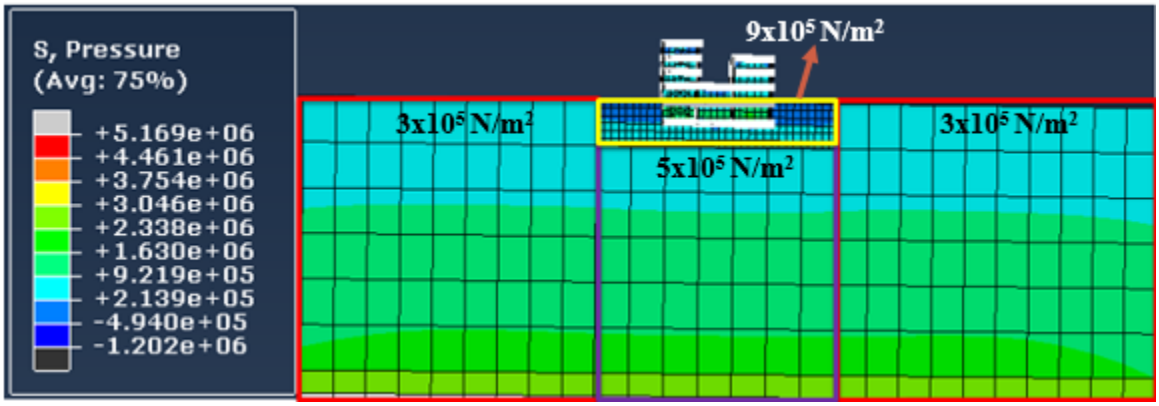

Fig 6.3: Partitioning the non-linear soil domain on the basis of initial hydrostatic stresses

In terms of the mesh, structured meshing is used to mesh the soil-superstructure assembly with reduced integration 8-noded brick elements and 10-noded tetrahedral elements. The infinite elements are meshed using the sweep method and the sweeping path must face towards the direction where we want to simulate the infinite domain. It's also important to ensure that the

nodes of the infinite elements are aligned with the nodes of the larger soil domain. Similarly, the nodes of the basemat should align with the nodes of the surrounding nonlinear soil for accurate results. The basemat soil is tied to the larger soil domain, which is composed of larger elements. However, it is important to ensure that there are a minimum of 10 nodes per wavelength along the direction of propagating waves. Reduced integration elements are ideal for explicit dynamic analysis. They have a faster analysis time, are robust under high levels of strains and resistant to shear locking which might stiffen the response. When reduced integration elements are used in conjunction with nonlinear material, it is prone to hourglassing effects. Hourglass modes are zero energy modes which can impact the accuracy of the solution by interfering with the structural response. They do no generate additional stresses or strains but might lead to inaccurate displacements or acceleration response. The simplest way of addressing hourglassing effects is by refining the mesh or spreading the loads over a greater contact area (pressure loads are more effective than point loads).

6.2 Dynamic properties of mudstone

The soil stratigraphy present at the Fukushima Daichii Unit 6 was described in the borehole information provided by TEPCO [120]. The location of the sites where the geotechnical profiling was performed is shown in Fig 4.2, in addition to the thickness of individual soil layers and approximate depths of each layer. The soil site consisted of mudstones, gravel, sandy loams and sandstone and can be primarily classified as variations of mudstone. The dynamic properties of mudstone are essential to derive the backbone curve which is input in the full scale FE model. It couldn't be directly gathered from the Fukushima site and was obtained from the cyclic torsional shear and triaxial tests performed on mudstone deposits in surrounding areas of Makinohara and Fujeida [138]. The experimental data was also compared with an array of dynamic triaxial tests on

red mudstone in the Sichuan province of China, to observe similarities in the behavior of the soil at varied strain levels.

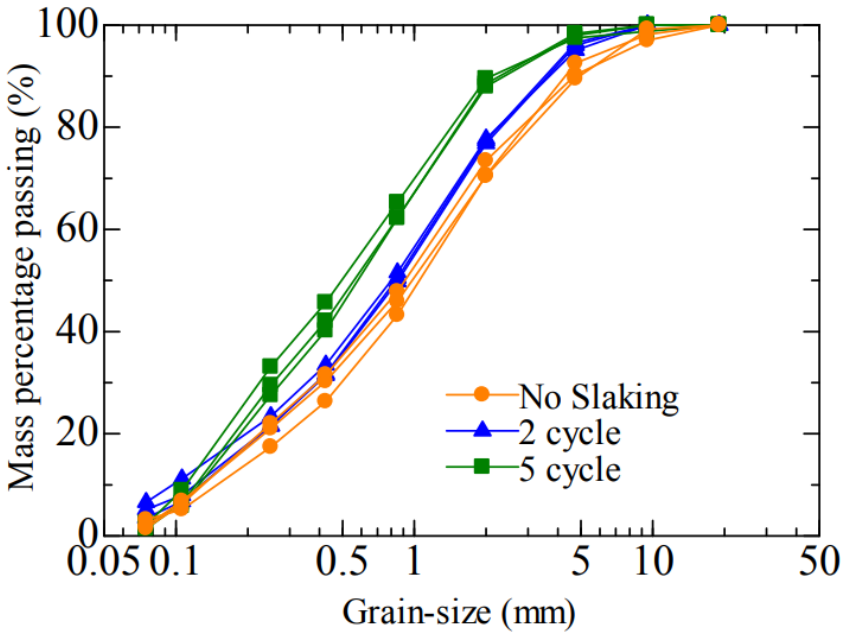

Fig 6.4: Particle size distribution of weathered mudstones

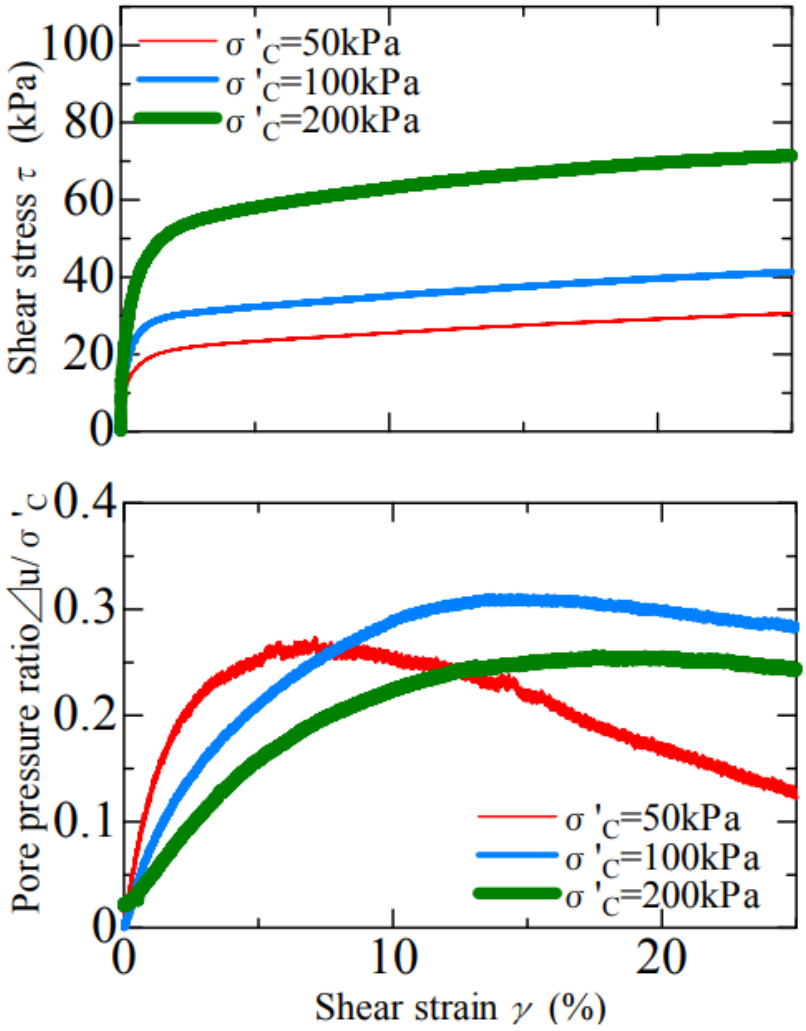

Fig 6.5: Variation of shear stress and pore water pressure with shear strain after 5 cycles of weathering [138]

The mudstone was artificially weathered through heat treatment followed by submerging in water. The particle size of the crushed mudstone had an upper bound of about 20 mm and was filled in a cylindrical mold about 10 cm in diameter. It was then consolidated upto 99.5% degree of compaction followed by slaking the mudstone through repeated cycles of heating at 110 degrees in an oven alternated with wetting the specimen in a pool of water. The grain size distribution of the particles reduce due to slaking which is a common phenomenon in site.

The static and dynamic shear stress vs. strain relationship was obtained under different confining pressures. The shear stresses increased gradually with increment in shear strain while the pore water pressure increased at low strains and started decreasing at higher strain levels. The behavior is analogous to course and medium grade sands. The static shear resistance decreased with the slaking process (about 30% to 50%) while the effective stresses gradually increased at small strains for different levels of confinement. For the dynamic shear tests, the undrained specimens were subjected to 20 cycles of loading at 0.1 Hz under confining pressures of 100 kPa. The shear stress vs shear strain correlation, dynamic shear modulus and damping ratio were obtained for the specimens.

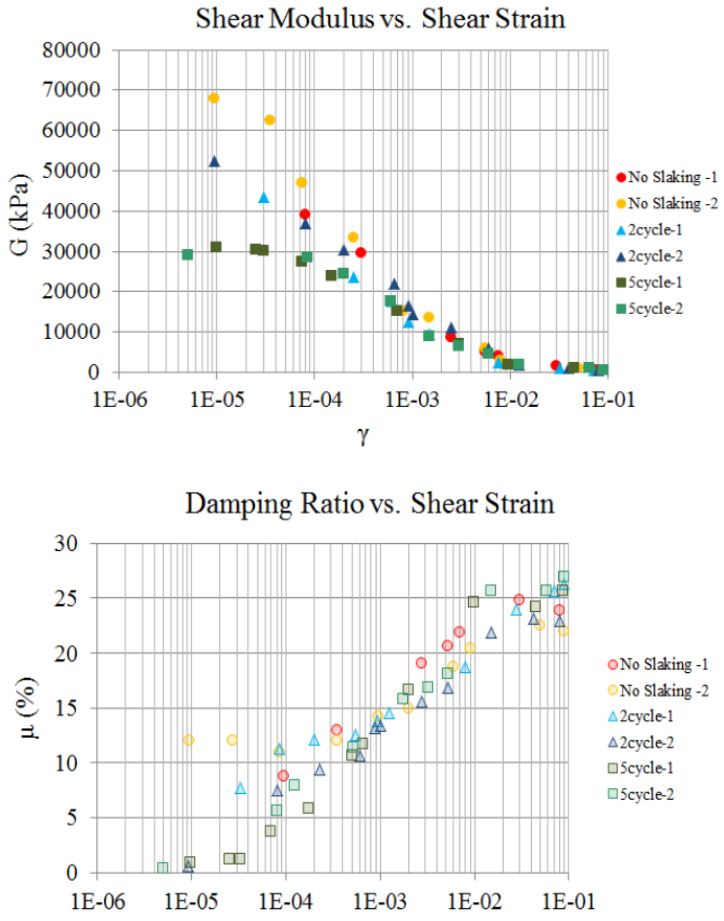

Fig 6.6: Variation of shear modulus and damping ratio with shear strain for mudstones

Another set of cyclic shear tests and triaxial tests were performed on red mudstone in Sichuan province in China. The cyclic load was applied at a frequency of 5 Hz under confining pressure of 25, 50 and 100 kPa [139]. The maximum shear modulus for the range of consolidation pressure (σ_m') and void ratio (e) is given by [140]

$$G_{max} = 426\left(\frac{1+0.37e}{1+e}\right)(1.70-e)^2\sqrt{\acute{\sigma}_m} \tag{6.1}$$

The tests were performed in three stages by initially applying a constant confining pressure, followed by adjustment of the principal stresses with the dynamic stress amplitude and finally loading the specimen to failure. Similar patterns were observed in the variation of deviatoric and shear stresses, which increased gradually under low strain ranges (0% to 1%) followed by non-linear behavior and plastic deformation at high strain levels.

The stresses tend to exhibit an increasing hardening tendency with the increase in confining pressures. The secant modulus portrays an inverted S shape attenuation behavior with increasing shear strain. The minimum axial stress was set to effective confining pressure to avoid the mobilization of tensile stresses in the specimen. The shear stress vs strain behavior tends to be linear elastic at low cyclic strains and develops plastic strain beyond 0.58%. The aggregate strain increases for high stresses under larger confining pressures. The dynamic shear modulus displays an inverted S attenuation behavior with increasing strain levels. It also increases with the confinement pressure.

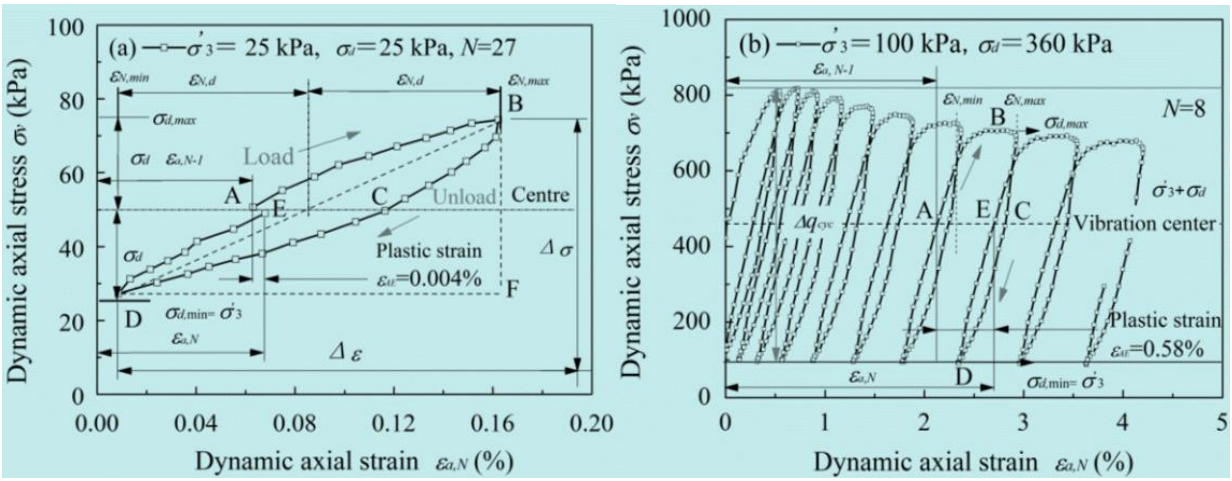

Fig 6.7: Hysteretic behavior of red mudstone for (a) Confining pressure = 25 kPa, dynamic loading stress amplitude = 25 kPa; (b) Confining pressure = 100 kPa, DLSA = 360 kPA [141]

The soil mass also experiences some degradation in its bearing capacity and the dynamic shear modulus with increments in the number of loading cycles. The initial shear modulus grows with the increase in confining pressure, implying the escalation of lateral restraint due to reduction of void spaces between the particles. The plasticization of the mudstone is arrested and the dynamic shear modulus increases. The ratio of secant shear modulus to the maximum shear modulus reduces with the increase in dynamic strains, which is more pronounced at higher confinement pressures (see Fig 6.7).

On the other hand the damping ratio increases with the increase in dynamic strains and reaches a threshold value at strains of 0.01%, as indicated in Fig 6.8. For small strains, the confining pressures don't have a significant impact on the damping ratio. However, at higher strains the damping ratio reduces with the increase in confining pressure and the relationship is linear. This is due to the densification of the soil domain which reduces the dissipation of energy.

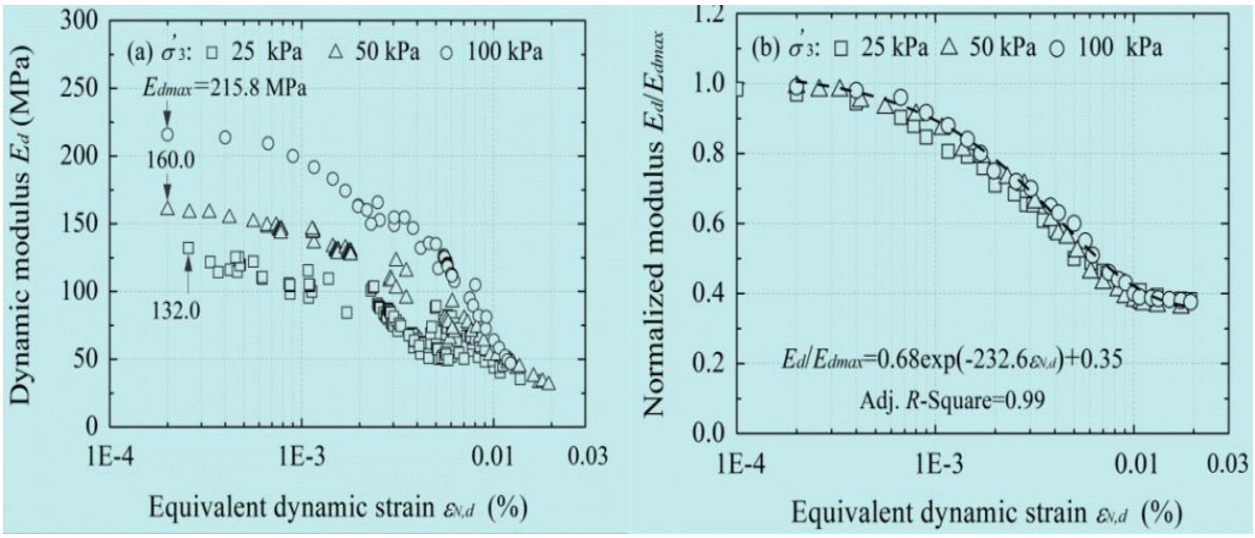

Fig 6.8: Variation of the modulus reduction with the dynamic strain for red mudstone [141]

The behavior of the mudstone is quite similar to that of medium grade and coarse sands like the Ticino sand. The modulus reduction and damping ratio vs shear strain data are used to formulate the ABQ_HYSTERETIC_SOIL model for the full scale NLSSI analysis of the Fukushima NPP.

6.3 Results from full scale nonlinear soil structure interaction analysis

Full scale NLSSI analysis was performed on the Fukushima NPP in multiple phases to assess the contribution of the sources of non-linearity to the attenuation of the basemat response. Non-linear site response analysis is performed to highlight the decline in the free field motion (when compared with linear site response analysis) due to introduction of material nonlinearity. Subsequently, a full scale SSI analysis is performed by introducing material nonlinearity to the basemat soil followed by modelling the entire soil domain with non-linear soil; and a comparison was made with the LSSI data. Lastly, geometric nonlinearities are introduced to the soil-structure system to assess its impact on the basemat response and compare the attenuation with material nonlinearity-based SSI analysis. The results have been discussed in Sec 6.3.2, 6.3.3 and 6.3.4.

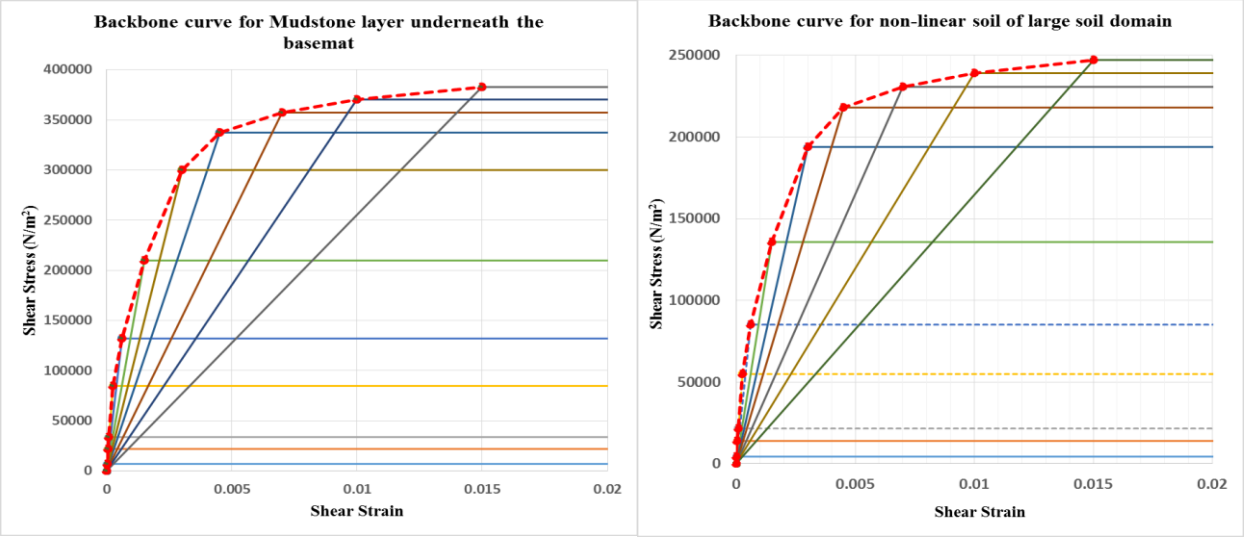

Fig 6.9: Backbone curves of mudstone for full-scale NLSSI analysis

The PGA was computed from the response acceleration time history at the basemat and the numerical free field motion. These values are compared with the values obtained from LSSI analysis and actual data obtained from site [120].

6.3.1 Comparison of free field motion from linear and non-linear site response analysis

The free field motions obtained from LSRA overestimate the value of the basemat response. The spectral accelerations are amplified by more than 100% between time periods of 0.1sec - 0.5 sec. Site response analysis should account for the varying stiffnesses and damping characteristics of the individual soil layers, where the vertically propagating shear waves are either reflected or transmitted. The shortcomings of the LSRA were overcome when the entire soil domain was modelled with the ABQ_HYSTERETIC_SOIL material model.

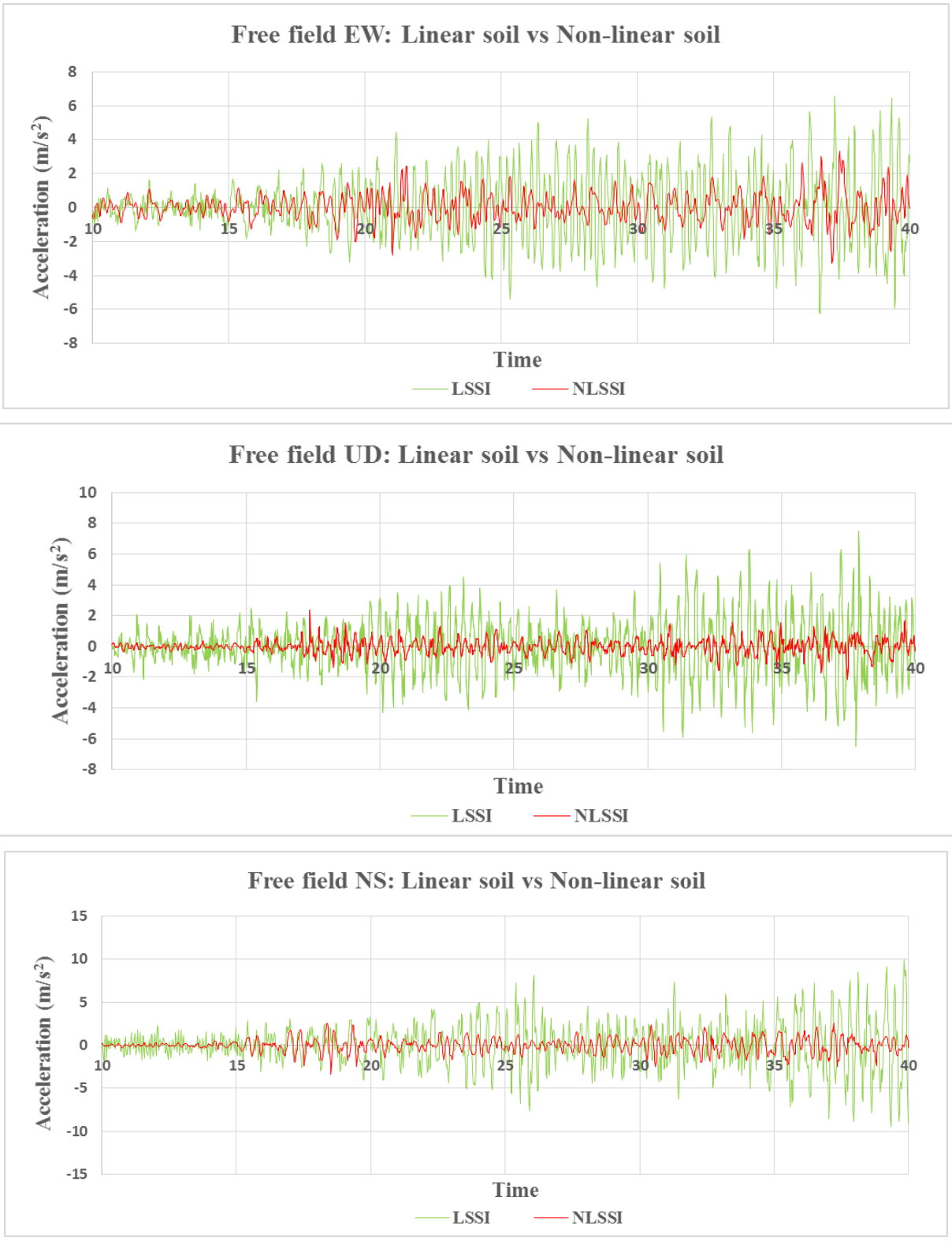

Fig 6.10: Comparison of free field motion from LSSI and NLSSI

The linear approach assumes the maximum shear modulus and the damping to be fixed during the course of the entire ground motion. But, the levels of strain in each soil layer vary during the earthquake. Since, the time history of ground motions is characterized by multiple peaks in its shear strain amplitude, the strain compatible soil parameters should account for the fluctuations in peak shear stresses or strains. However, as the shear modulus and damping ratio is kept constant during the duration of the entire ground motion, LSSI is ineffective in capturing the variations in soil stiffness during the earthquake.

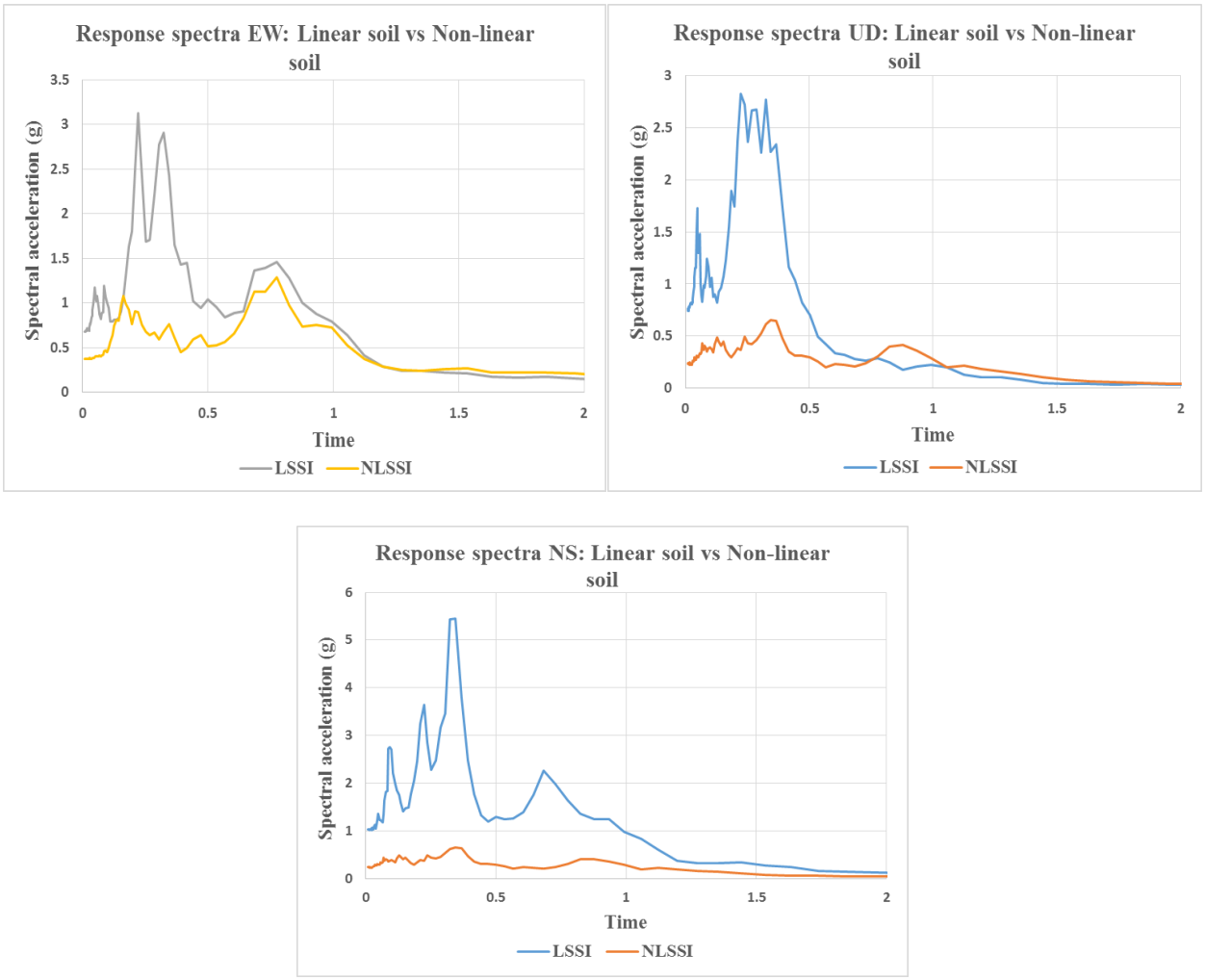

Fig 6.11: Comparison of response spectra for free field motion from LSRA and NLSRA analysis

The spurious amplifications in the free field motions observed in the LSRA is a result of the coincidence of the natural frequencies of the soil deposits with the input ground motion. In the NLSRA, the shear strain, damping characteristics and stiffness of the soil changes over the duration of the ground motion which allows us to efficiently predict the free field response without magnifying the response acceleration amplitude.

6.3.2 Sensitivity study on the basis of material nonlinearity

In Chapter 4, an array of sensitivity studies were performed on the basis of geometrical nonlinearities at the soil-structure interface for LSSI analysis. This section will focus on the variation in structural response at the basemat when material nonlinearities are introduced to the SSI analyses. The study is performed in the three phases during which the foundation is tied to the underlying soil domain, to arrest the effects of gapping and sliding. In the first phase, the linear elastic soil domain is considered for the soil surrounding the foundation as well as the large soil domain, referred to as EL+EL case. During the second phase, the soil in the vicinity of the basemat is modelled with ABQ_HYSTERETIC_SOIL model while the large soil domain is linear elastic, referred to as the NL+EL case. Finally, in phase 3 the entire soil strata is modelled with non-linear hysteretic soil for different reference pressures which is identified as the NL+NL case.

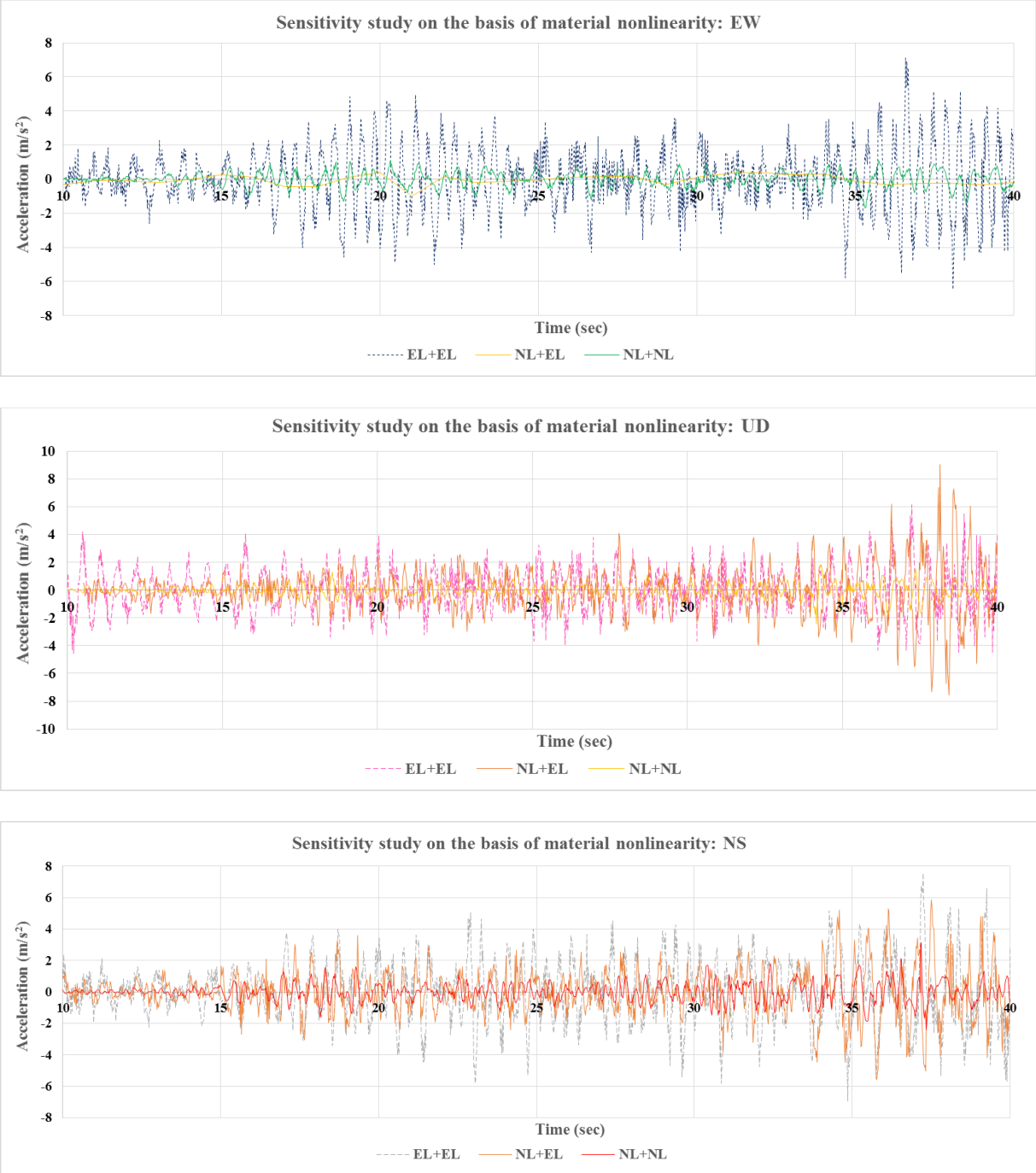

Fig 6.12: Response acceleration time history for comparison between linear, partially nonlinear and nonlinear soil properties

The peak spectral accelerations for the EL+EL case overestimate the structural response and large amplifications are observed for low periods. The PSA in EL+EL case exceeds the NL+EL case by 37% for the EW component and 15% for the NS component. However, the values are quite close for the UD component. This is due to the considerable larger reflections of the vertically propagating shear waves at the NL-soil – EL-soil interface which amplifies the acceleration response. The PSA for the EL-EL and NL-EL are attained abruptly as compared to the NL-NL case, due to artificial resonance induced in the basemat response. The NL-NL case generates values closest to the true response of the basemat, within a 20% to 30% range.

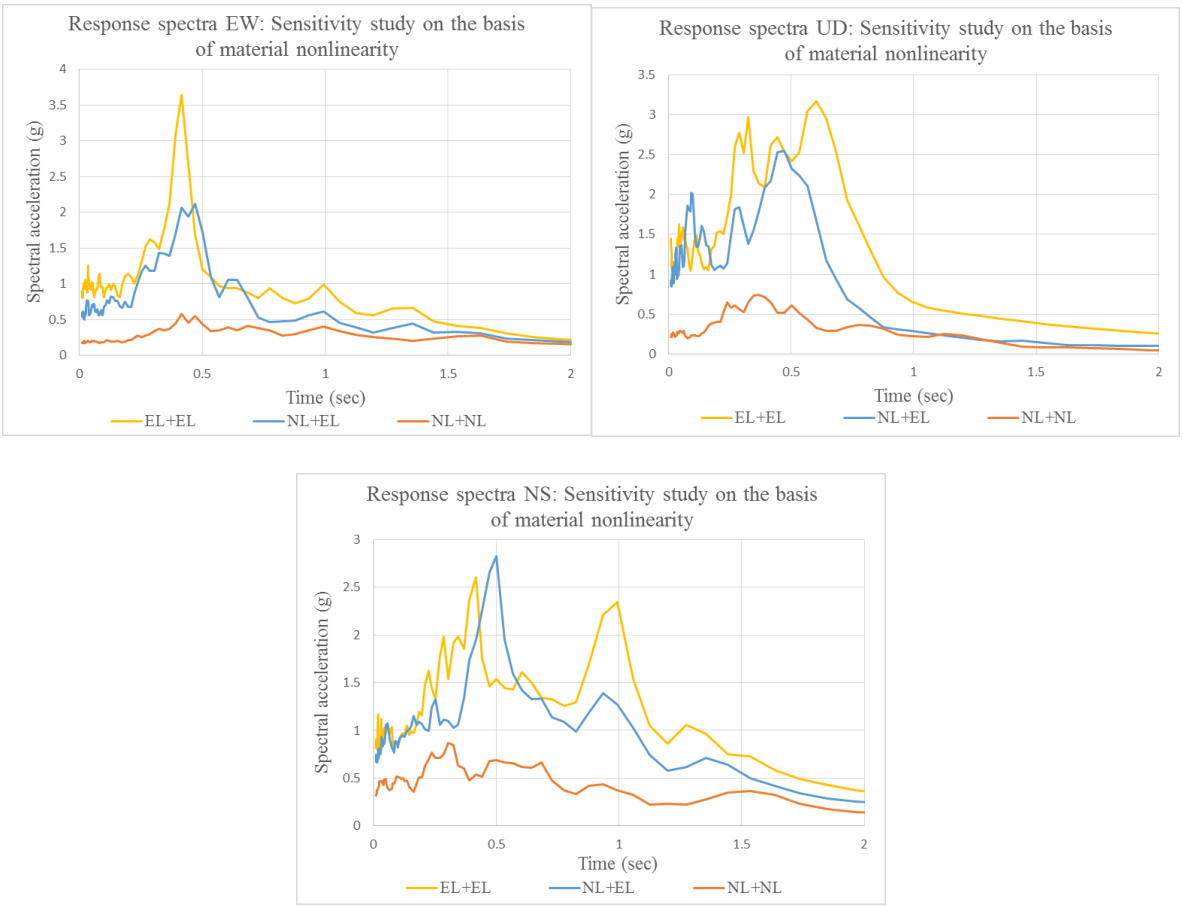

Fig 6.13: Response spectra: Sensitivity study on the basis of material nonlinearity

6.3.3 Sensitivity study on the basis of geometric nonlinearity

This sensitivity study captures the combined influence of material and geometric nonlinearity on the structural response. The analysis is performed in three phases on a completely nonlinear soil domain similar to the previous section. In the first phase, the response acceleration at the basemat is computed for the tied case, referred to as TD. The second phase considers only sliding nonlinearities at the interface (referred as SL), while the third phase considers both gapping and sliding (referred as GP+SL). This study also gives us an idea about the individual contributions of the material and geometric nonlinearities at the soil-structure interface for assessing the structural response.

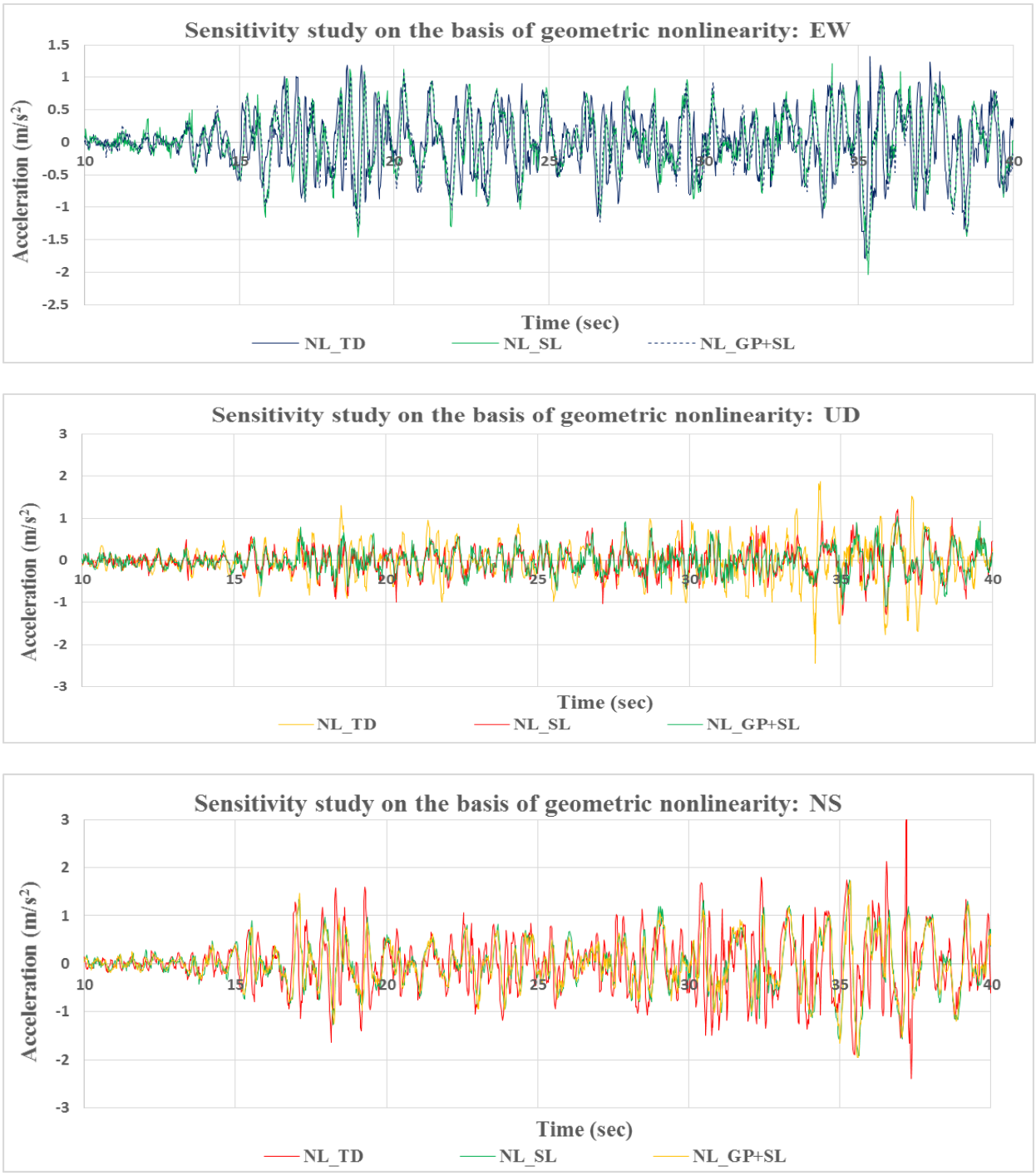

Fig 6.14: Response acceleration time history for comparison between tied, gapping and combined gapping + sliding condition

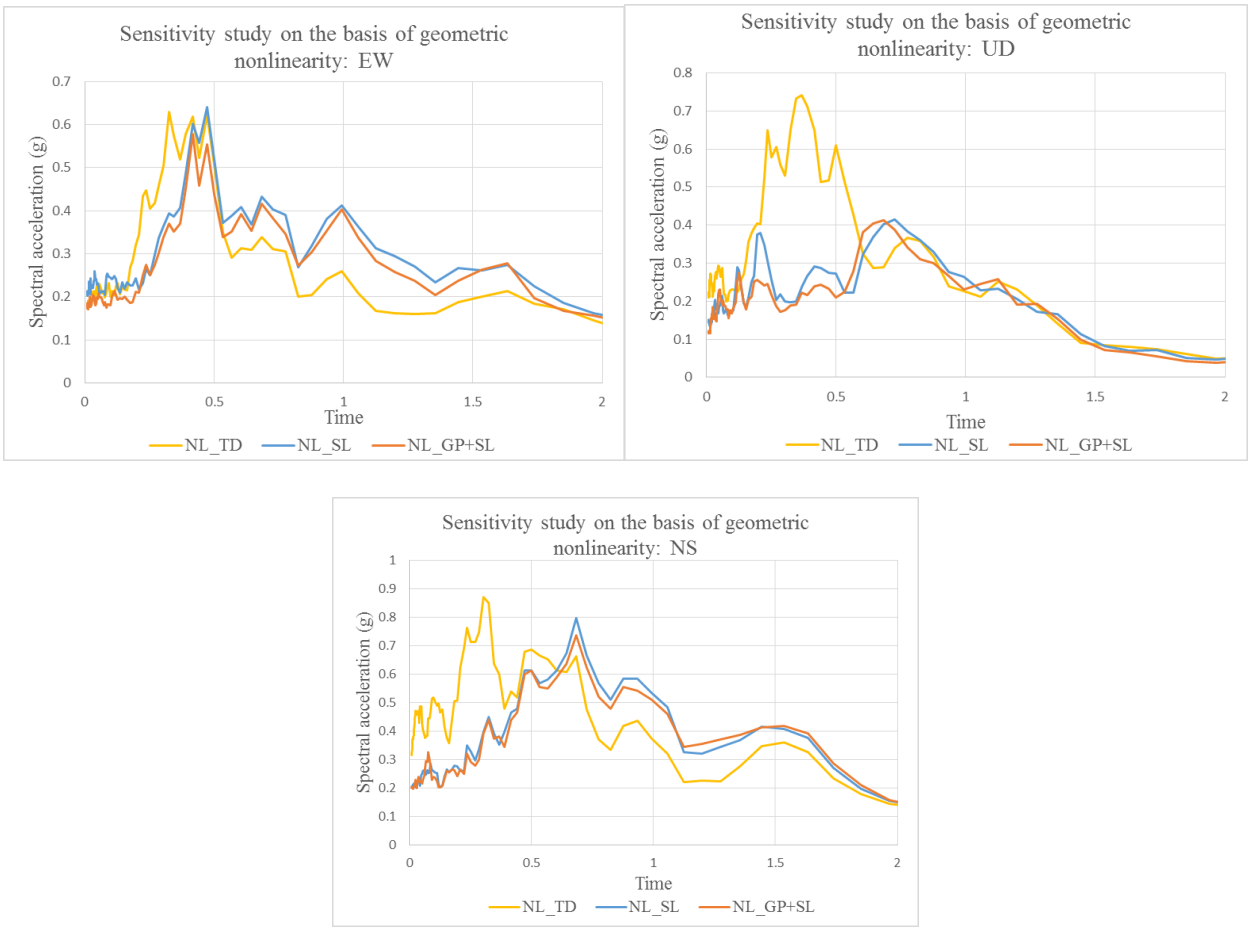

Fig 6.15: Response spectra: Sensitivity study on the basis of geometric nonlinearity

The response spectra revealed that the PSA was highest for the tied case and accounts for large amplifications in the acceleration. As discussed in section 6.1, the NLSSI analysis relies on the properties of the hysteretic soil model in addition to the kinematic contact algorithm to simulate sliding at the soil-structure interface. The NL_SL case considers the structure resting on the nonlinear soil without specifying the pressure overclosure relationship in the normal direction. The PSA for tied contact exceeds the sliding case by 20% in the EW direction, 40% in the UD direction and 35% in the NS direction. The variations in the SL and the GP+SL case is within a range of 10%, which proves that the nonlinear material in the vicinity of the soil accounts for the maximum

attenuation due to geometric nonlinearity. This proves that the hysteretic material model plays a crucial role in simulating sliding behavior.

6.3.4 Full scale NLSSI analysis results

The full scale NLSSI analysis integrates the dynamic equations of motion in small time intervals while accounting for the material nonlinearity. The nodes follow the shear stress vs. shear strain relationship of the backbone curve and the appropriate soil properties are used for each time step. The response of the basemat is a cumulative response of the nodes at each time step. The peak accelerations at the basemat compare well with the site response data obtained from TEPCO [2]. The free field motion obtained from site response analysis vary within a range of 13% to 20% of the actual recorded data. The Fukushima NPP is supported on stiff mudstone deposits, which explains the reduction in the basemat acceleration due to energy dissipation and radiation damping at the interface.

An array of parametric studies were performed to determine the variations in free field motion and basemat acceleration when the material parameters and interaction mechanisms were varied. The free field data obtained from the Fukushima Unit 6 [120] was the reference point of comparison (denoted by FF_TEPCO). The free-field motion obtained from the non-linear site response analysis is denoted by FF_NL. The response acceleration at basemat when the structure is tied to the soil domain is computed for three cases (1) BM_MAT_EL+EL: Linear elastic material properties assigned to the subsoil surrounding the basemat as well the large soil domain, (2) BM_MAT_EL+NL: Subsoil surrounding the basemat modelled with nonlinear hysteretic soil properties and the larger soil domain modelled with linear elastic properties and (3) BM_MAT_NL+NL: The subsoil in the vicinity of the foundation as well as the larger soil modelled with hysteretic soil properties.

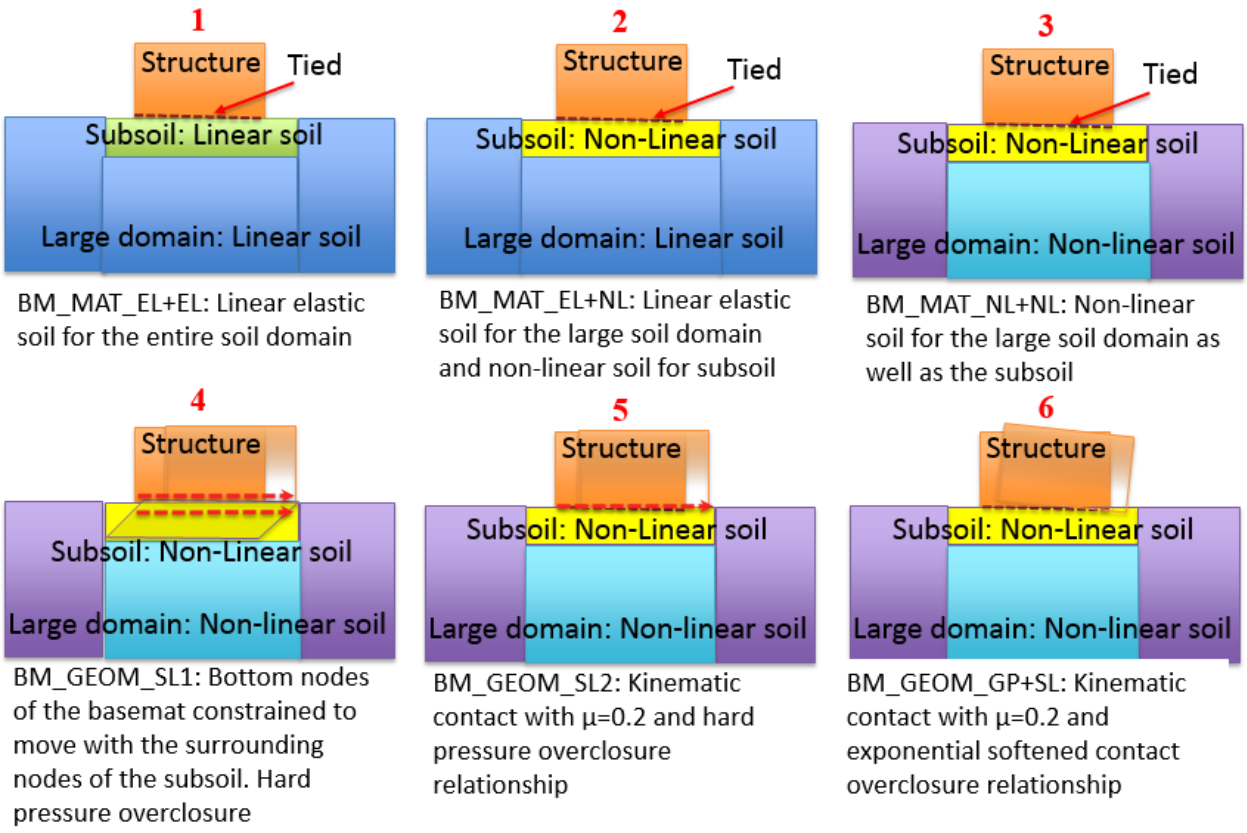

Fig 6.16: The phases of full scale NLSSI analysis for the Fukushima Daichii NPP

After performing sensitivity studies on the basis of material nonlinearity, geometric nonlinearities were added to the system. (4) BM_GEOM_SL1 depicts the scenario where the tied constraint in the BM_MAT_NL+NL case was removed and the nodes at the base of the foundation were constrained to move with the nodes of the surrounding soil in the lateral direction with hard pressure overclosure relationship in the normal direction. In (5) BM_GEOM_SL2 case, the nodal constraint at the interface was replaced with the kinematic friction formulation. Finally, the gapping behavior was incorporated into the NLSSI analysis using the softened pressure overclosure relationship in the (6) BM_GEOM_GP+SL case. The stages of the NLSSI analysis are depicted in Fig 6.16 and the peak basemat response accelerations obtained after multiple stages of sensitivity analysis pertaining to material and geometric nonlinearities is depicted in Fig. 6.17.

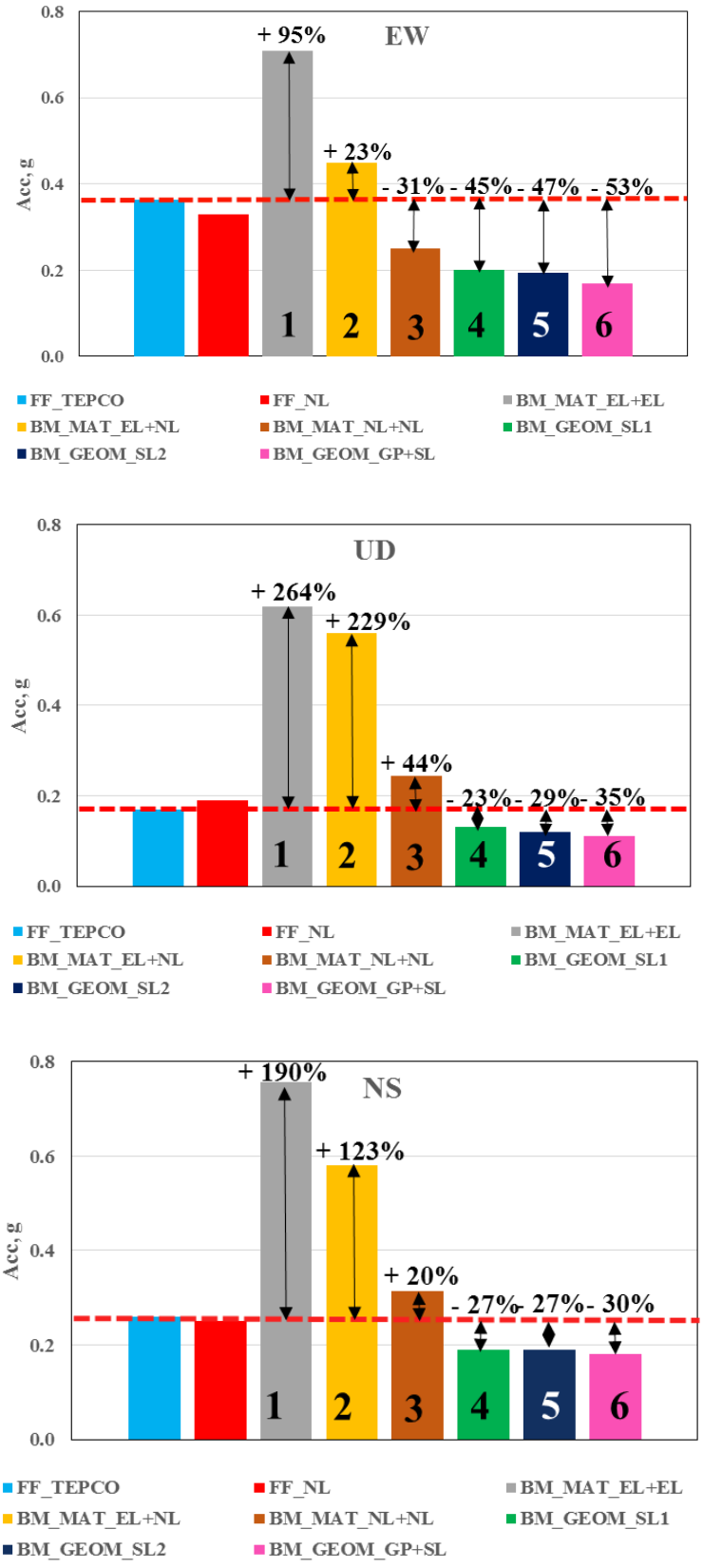

Fig 6.17: Comparison of the peak basemat accelerations during the stages of NLSSI analysis

The step-by-step analysis helps us in identifying some key trends in the acceleration attenuation at the basemat. The first and most evident observation is the significant reduction of the PSA (by an average of 50%) when the linear soil domain in replaced with non-linear soil. It is also observed that there is significant reduction in the PSA for the BM_MAT_NL+NL case when compared with the BM_MAT_EL+NL case, which leads to the inference that the entire soil domain needs to be modelled with the ABQ_HYST_SOIL model in order to generate believable response acceleration-time history at the basemat. When the entire soil domain is modelled with non-linear soil, the basemat acceleration reduces by more than 100% as compared to the LSSI results. There is reduction of 2% in the observed PSA between the BM_GEOM_SL1 and BM_GEOM_SL2 case. This points to the fact that the kinematic contact only contributes to the numerical stability of the analysis procedure and prevents the uncontrolled sliding of the NPP superstructure with respect to the surrounding soil layer. The shearing or sliding behavior of the foundation on the surrounding soil layer is governed by the hysteretic material model (as discussed in Sec 5.6, 6.1 and 6.3.3). When the hard pressure overclosure relationship in the BM_GEOM_SL1 and BM_GEOM_SL2 case is replaced with softened pressure overclosure relationship (BM_GEOM_GP+SL), there is an additional reduction of about 5% in the PSA. Therefore, the BM_GEOM_GP+SL case provided us with the best results for the full scale analysis of the Fukushima Daichii NPP. The detailed acceleration-time history and response spectrum analysis of this case is shown in Fig 6.18-19.

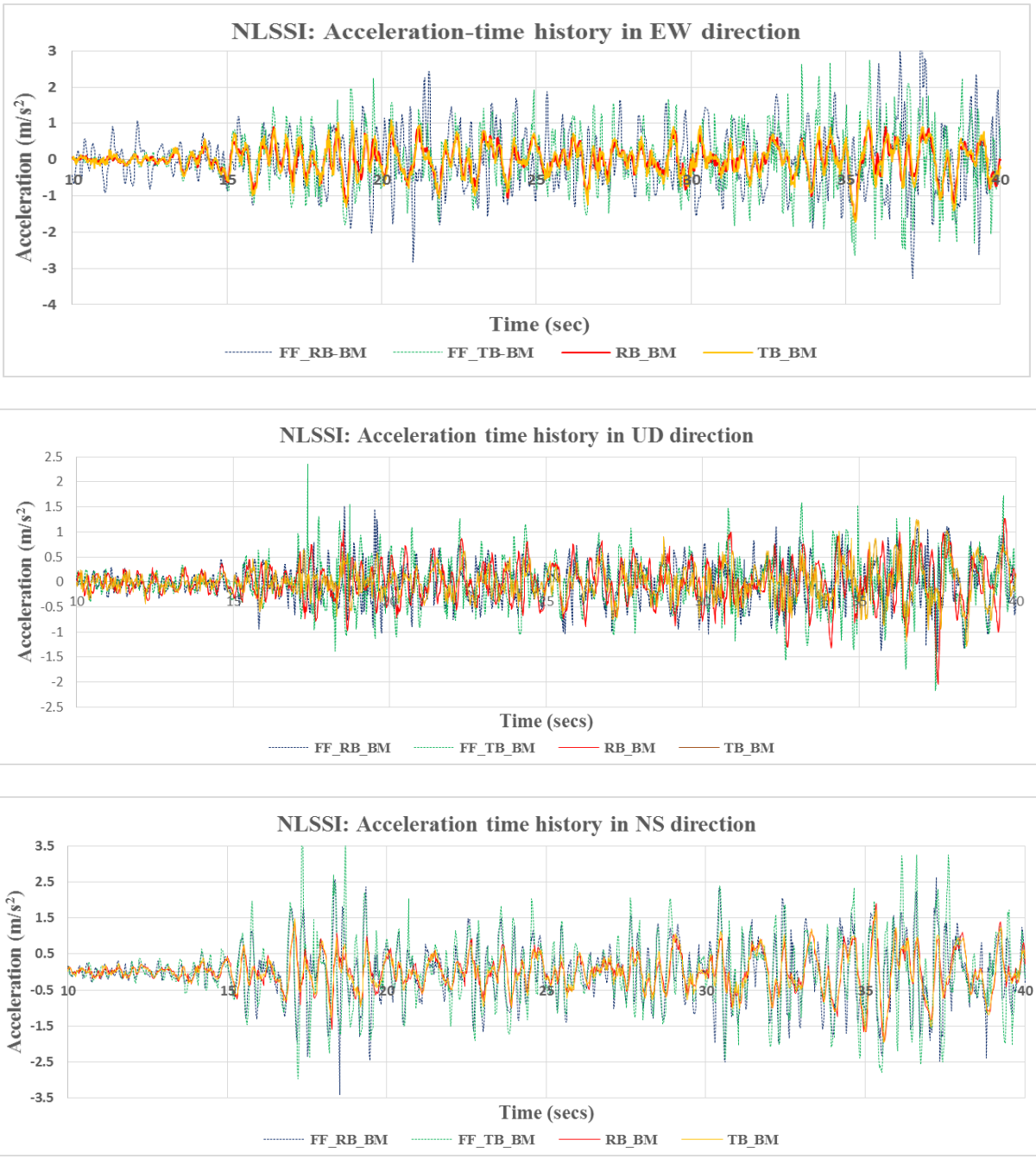

Fig 6.18: Comparison of acceleration time history at basemat and free-field for NLSSI analysis

Table 6.1: Summary of NLSSI results and comparison with free-field data from TEPCO [120]

	Peak acceleration in g.		
Locations	EW	NS	UD
Free field (TEPCO)-P13	0.405	0.252	0.194
Free field (TEPCO)-P4	0.387	0.209	0.189
Free field (TEPCO)-P14	0.302	0.313	0.113
RB-Free field (ABAQUS)	0.35	0.23	0.26
TB-Free field (ABAQUS)	0.32	0.15	0.23
RB-Basemat soil (ABAQUS)	0.20	0.11	0.18
TB-Basemat (ABAQUS)	0.17	0.12	0.16

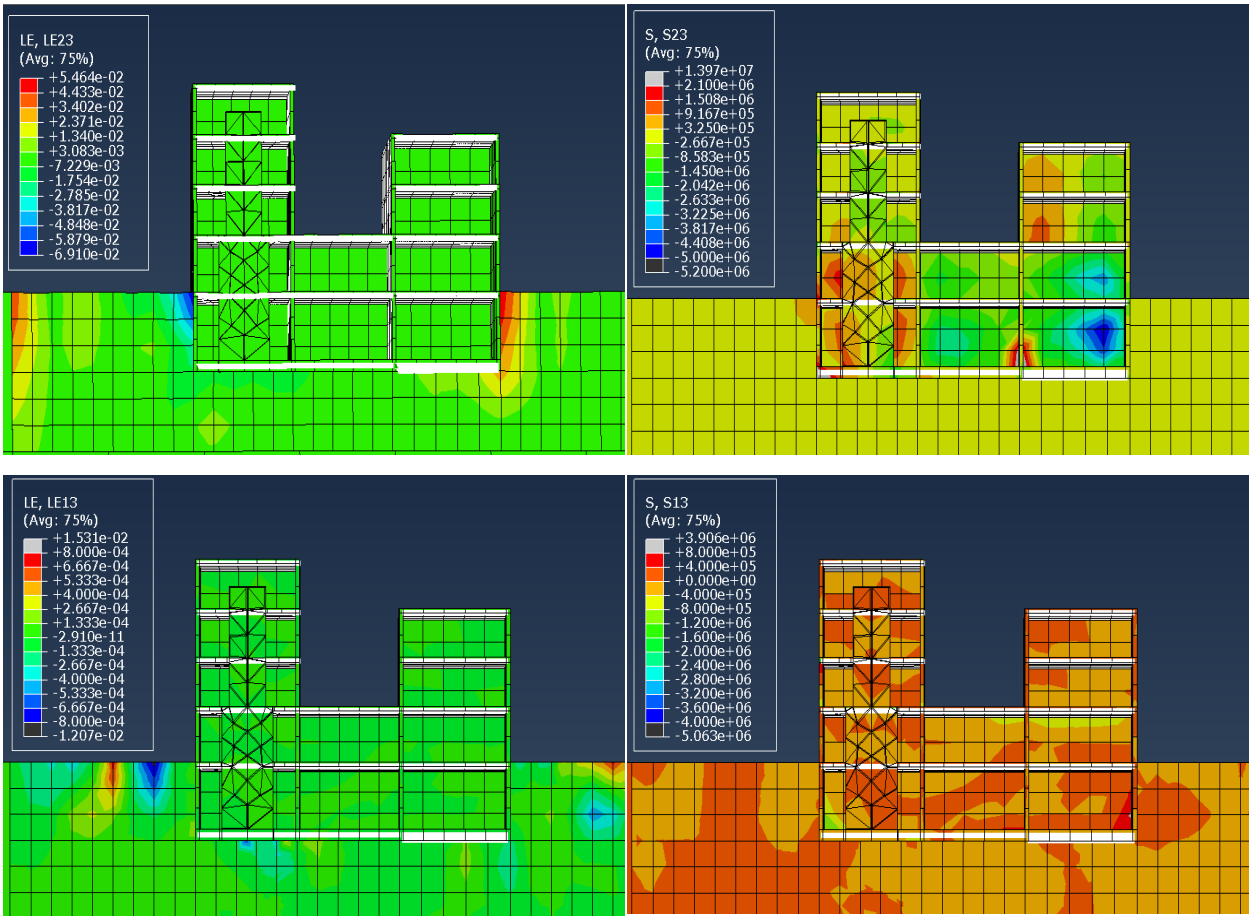

Fig 6.19: Shear stress and shear strain profile for the full-scale NLSSI analysis

The shear stresses in the vicinity of the interface occur within a range of 10^5 - 10^6 Pa which is significantly reduced from the LSSI case. The shear stresses in the vicinity of the interface diminish during the course of the applied ground motion. This is due to dissipation of energy in the vicinity of the interface when some of the elements undergo yielding. The stress concentrations which were observed along the edges of the basemat footprint are not captured by the hysteretic soil model. The lateral shear strains in the vicinity of the interface is in the range of 0.004-0.003, which is similar to those calculated for the site. Higher strains were observed in the subsoil surrounding the basemat in the range of 0.01-0.05, which can be attributed to the activation of gapping nonlinearity.

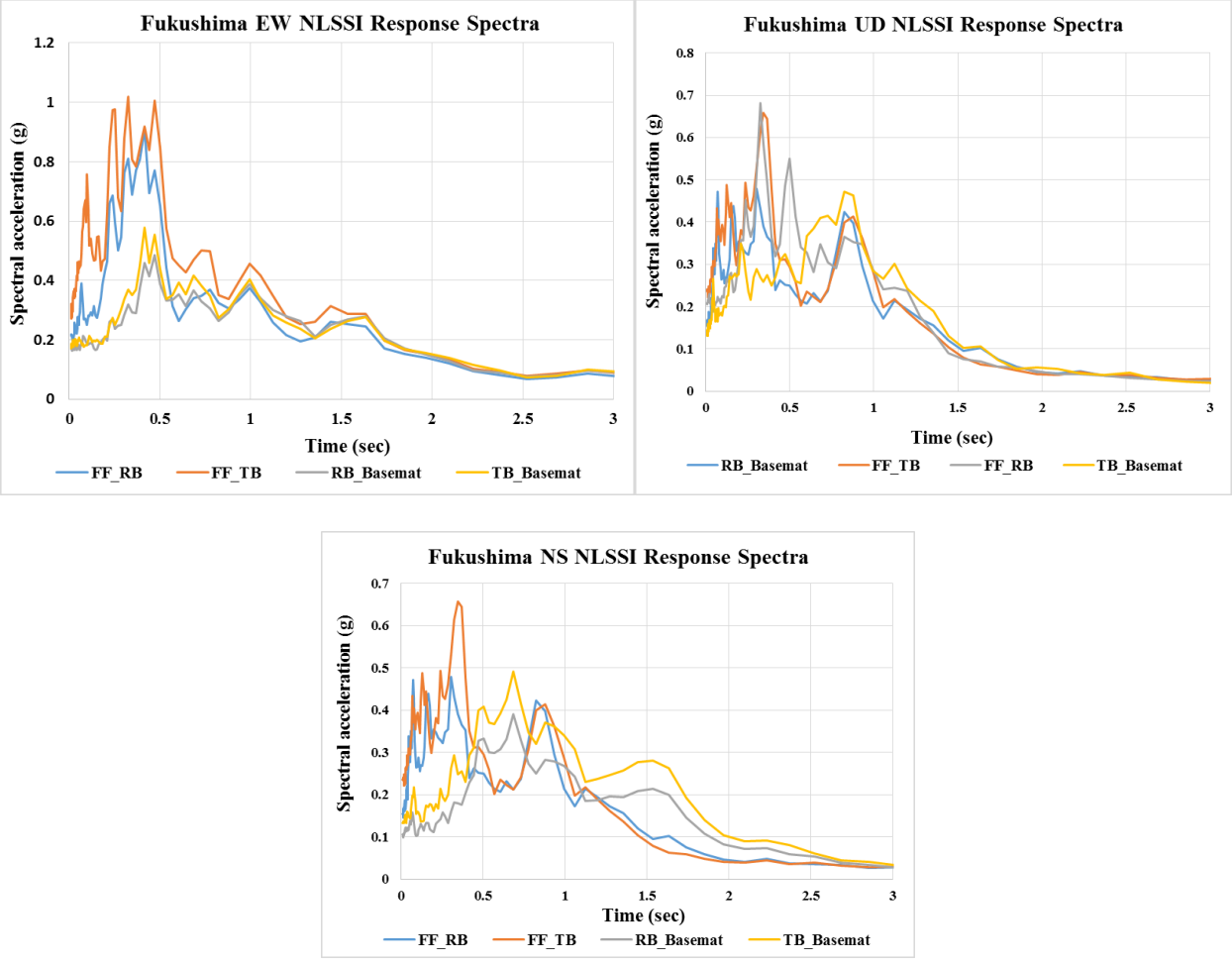

Fig 6.20: Response spectra for full-scale NLSSI analysis

The peak accelerations obtained from the acceleration-time history portrayed a reduction by approximately 40% in the EW direction, 50% in the NS direction and 30% in the UD directions with respect to the TEPCO free field data. This supports our initial hypothesis that the presence of material and geometric nonlinearities can attenuate the basemat response when compared with the free-field data. The response spectra analysis revealed that the peaks of the PSA were between 0s to 0.5s. The spurious amplifications observed in LSSI were reduced and the reduction of PSA with increasing period was gradual. As expected, PSA at reactor and turbine building basemat was less than the free field motion. However, the PSA of the basemat marginally exceeds the free-field acceleration within periods of 0.5s to 1s. This can be attributed to the reduction of foundation stiffness with the progression of the ground motion which causes an amplification in the basemat response due to slipping or gapping. The response acceleration at the topsoil was compared with that of the basemat, and slight amplifications were observed for the PSA of the topsoil at lower input ground motions while the trends were reversed when the amplitude of input motion increased. This is characteristic to the response of most stiff structures resting on medium to course stiff sands [9].

6.4 Chapter Summary

Full-scale nonlinear SSI analysis was performed on the Fukushima Daichii NPP. The hysteretic soil model used for our analysis performs really well for medium to coarse graded sand and sandy clays or mudstones. The sliding behavior at the interface could be best represented by the material model itself. It was an improvement to the previously adopted Coulomb based kinematic contact algorithm, where spurious amplifications in the basemat response was observed. The gapping nonlinearity was simulated using the exponential softened contact.

LSSI analysis largely over predicts the structural response at the basemat and does not provide us with an accurate representation of the interface response. When the soil was modelled with linear elastic material properties, amplifications of more than 100% was observed in the basemat response acceleration. A sensitivity study was performed by introducing material nonlinearity into the subsoil surrounding the basemat followed by modelling the whole soil domain with ABQ_HYSTERETIC_SOIL. It was observed that the basemat response acceleration exceeded the free field motion by more than 200% for the UD component in addition to amplifications of 123% and 23% for the NS and EW component. When the whole soil domain was modelled with non-linear hysteretic soil, the free field motion obtained from the site response analysis compared well with the peak free field acceleration obtained from the Unit 6 site.

The basemat response from the SSI analysis was also in close range of the free field motion when the entire soil domain was modelled with hysteretic soil parameters. After modelling the material nonlinearity, the geometric nonlinearities were gradually introduced into the system by releasing the tie constraint between the basemat and subsoil, and constraining the nodes at the interface to move together (BM_GEOM_SL1). For the first time, the basemat acceleration at the turbine and reactor buildings went below the free field acceleration. In the next stage, friction based kinematic contact was activated (BM_GEOM_SL2). However, no significant changes were observed pointing to the fact that the material model was sufficient to simulate slipping at the interface. In the next stage, gapping was introduced through a soft pressure-overclosure relationship which further attenuated the basemat response by 10%-15% .The BM_GEOM_SL+GP model, which includes both the geometric and material nonlinearities in its analytical formulation performed well, resulting in a reduction of the basemat response acceleration by 30% to 50% as compared to the free field motion, which is characteristic to most

stiff clays and sands [9, 119, 142]. The multilinear hysteretic material was successful in simulating the sliding or slipping nonlinearities at the interface because of its Iwan [38] type formulation. Another advantage of the model is that it scales well with the normal pressure as observed in the MASTODON element tests and the TRISEE experimental simulations. In case of modelling the soils, where damping characteristics are unavailable there is a scope of formulating the backbone curve using Masing hysteresis rules [35] or from empirical formulation [137, 110].

The peak ground accelerations obtained from the full-scale NLSSI analysis agreed well with the basemat acceleration attenuation trends observed at the site. The presence of stiff mudstone in the vicinity of the foundation led to attenuation of basemat response. The sensitivity studies revealed that material nonlinearity is the key contributor towards reduction of basemat acceleration response, with minor contribution from geometric nonlinearities.

7. SUMMARY AND CONCLUSIONS

The dissertation was aimed at determining the role of geometric and material nonlinearities in attenuation or amplification of the basemat response. Varied levels of attenuation were obtained in the acceleration response of the reactor and turbine building basemat of the Fukushima Daichii NPP Unit 6 during the Tohoku Earthquake. The initial hypothesis was that the reduction of response acceleration at the basemat could be attributed to (i) geometric nonlinearities at the interface namely gapping and sliding and (ii) hysteretic behavior or nonlinearity in the soil domain. There have been a multitude of commercially available softwares likes SASSI, CLASSI, etc. which employ the substructure method of analysis to perform SSI analysis, which model the interface through numerical and empirical methods involving transfer functions. The motivation of this dissertation was to develop a comprehensive three-dimensional NLSSI analysis framework in the time domain that would be able to successfully model the material and geometric nonlinearities at the interface and is scalable. The bulk of research performed in the field of NLSSI analyses could be traced back to the nuclear industry which adopted a conservative approach in modelling the structural response. Early research was focused on simulating the structural response using linear lumped mass models using assumptive moment-rotation curves that neglected the soil non-linearity. This focus shifted from spring-dashpot systems to element-based interface models which transmitted forces across the interfaces based on constitutive relationships. However, the early interface element-based models as well as substructure methods in the frequency-domain couldn't capture the inertial and kinematic effects of the structure resting on the soil mass in a single comprehensive model. A series of three-dimensional linear and non-linear SSI analyses were performed on the Fukushima Daichii NPP using the ground motion available from the Tohoku earthquake to capture the localized effects of SSI on the basemat response due to material

and geometric nonlinearities. The development of a comprehensive non-linear SSI analysis methodology was carried out on a step-by-step basis from the identification of appropriate contact algorithms for simulating geometric nonlinearities at the interface, to the establishment of appropriate non-linear material parameters for modelling the soil. The step-by-step analysis helped us in segregating the key contributors of acceleration attenuation at the basemat. An array of sensitivity studies helped us in identifying the changes in the dynamic response of the basemat when material or contact parameters were changed.

7.1 Obtaining the best contact algorithm for simulating gapping and sliding

The first stage in the development of a comprehensive NLSSI analysis methodology was the comparative analysis of pre-existing contact models. The contact models were tested and benchmarked in two independent finite element frameworks, ABAQUS and MASTODON. The contact algorithms that were considered for simulating sliding involved zero-thickness interfacial interaction models like the Kinematic contact method, Lagrange multiplier method and Penalty method and a thin layer element formulation with I-Soil elements (which is similar to the hysteretic soil model in ABAQUS and LS-DYNA). MASTODON is an open source code which allows the user to alter the contact algorithm parameters and understand it's performance in detail while ABAQUS is a black-box. The open source code was used for benchmarking the two-element and full-scale direct shear type tests in ABAQUS. Once the results were verified and the contact algorithm of choice was obtained, the full-scale simulations of the Fukushima NPP were performed in ABAQUS.

The first stage of analysis was performed on two-element models involving a concrete and soil block with linear elastic material properties and subjecting it to displacement-controlled pseudo-static and cyclic loading. The objective was to observe how the individual contact

algorithms performed in simulating the shear stress vs shear strain response at the interface due to Coulomb friction. The analysis was further extended to large-scale direct shear type tests. The novelty of each contact algorithm was judged on the basis of its accuracy, ease of application, convergence and analysis time.

A Dirac-based penalty algorithm was used with normalized stiffness over the nodal area. The selection of penalty parameter involves some trial and error. If the chosen penalty stiffness was too high, it causes ill-conditioning of the stiffness matrix and if the penalty stiffness is too low it results in the penetration of the stiffer element (high elastic modulus) into the softer element (low elastic modulus). The optimal penalty stiffness was found to vary within the range of the bulk modulii of the two elements in contact. For the pseudo static displacement controlled tests, error percentages of 4.77% were observed which increased for the cyclic loading tests. Some convergence issues were also observed when implicit time integration schemes were used for the analysis. The level of accuracy reduced even more for explicit FEA where the penalty contact method tends to alter the stable time increment. For the large-scale models, the error percentages increased upto 25% with oscillations in the shear stress vs shear strain curve at the interface. This could be attributed to the large displacements exceeding the contact tolerance or large value of the penalty parameter which was meant to reduce penetration but causes convergence issues. It could be inferred from the full-scale cyclic direct shear test models that the penalty contact method is not ideal for modelling sliding at the soil-structure interface.

The kinematic contact algorithm is a predictor-corrector algorithm which successfully depicted the shear stress vs. shear strain relationship at the interface for the small and large-scale model with less than 1% error between the theoretical and numerical peak shear strain. When cyclic loading is applied to the concrete block, penetration is caused during the predictive phase

of kinematic contact. However, an acceleration correction is applied to the master nodes during the corrective phase such that the master nodes are in compliance with the slave nodes when the predicted penetration is attained. The hard pressure overclosure relationship is used to simulate the exchange of stresses across the interface. The kinematic contact along with the hard pressure overclosure relationship eliminates any residual penetration at the end of each time increment which is an issue for the penalty method. The time-step size can also be higher than the penalty contact algorithm which helps in speeding up the analysis time. While kinematic contact is not suitable for simulating rigid body contact between two materials, it is suitable for modelling the tangential behavior of the soil-concrete interface due to large variation in the elastic modulii of the two materials.

The thin-layer element formulation was implemented by sandwiching I-Soil element between the soil and the concrete block. The I-Soil material model is similar to the MAT_79 material in LS-DYNA and the ABQ_HYSTERETIC_SOIL model in ABAQUS, which is meant for simulating the hysteretic behavior of soils. The thin layer element is used to initiate the Coulomb friction model by modifying the user defined curve. A single data point which consists of the threshold frictional shear stress and the corresponding shear strain in input into the material model. The slope of the backbone curve is set higher than the shear modulus of the foundation to prevent reduction of the foundation stiffness. The I-soil element based formulation has an added advantage over the kinematic and penalty contact algorithms. It reduces any high frequency response due to the bilinear stress-strain backbone curve which helps in gradual yielding of the interface. Furthermore, the thin layer element accounts for any changes in the normal pressure when cyclic loading is applied. The threshold shear stress values were within a range of 1% and 3% of the actual shear stress.

Although the I-Soil element performed really well, the thin-layer element formulation was not used for the actual NLSSI analysis of the Fukushima Daichii NPP. The hysteretic soil model in ABAQUS was used in Chap 5 and 6 was used to model the entire non-linear soil domain. It was used in conjunction with the kinematic contact model with a friction coefficient of 0.2 to model the tangential behavior of the interface, while the normal behavior was modelled using the softened contact pressure overclosure relationship. The hard pressure overclosure relationship was abandoned as it was not successful in simulating the increase in stiffness of the interface with decreasing overclosure. Hence, the differential settlement during gapping was better captured by the soft pressure overclosure relationship, while the hysteretic soil model helped in simulating the energy dissipation and regaining of stiffness after each cycle.

7.2 Soil structure interaction analysis with an account of geometric nonlinearities

The second chapter was focused on performing SSI analysis on the Fukushima Daichii NPP by modelling the geometric nonlinearities at the interface. However, the entire soil domain and structure was modelled with linear elastic material properties obtained from TEPCO [120]. A detailed model of the NPP assembly was built with fine meshed subsoil surrounding the basemat which was tied to a large soil domain with bigger element size. 2% reinforcement was also embedded in the structure using beam elements. A nominal Rayleigh damping of 5% was incorporated into the soil based on the governing frequency range of the ground motion. Although the mass and stiffness dependent Rayleigh damping parameters were adjusted to obtain a constant damping ratio, it can vary over large frequency ranges. This issue was tackled in the NLSSI analysis where the energy dissipation was taken care of by the hysteretic soil model.

A sensitivity study was performed to obtain the best boundary condition for simulating non-reflecting boundaries. The layers of soil at the boundary of the large soil domain was constrained

to move in pure shear and were surrounded by infinite elements (CIN3D8). The bottom of the soil domain was also surrounded with infinite elements which helped in simulating perfectly transmitting boundaries. The large soil domain was approximately six times the size of the structure footprint to prevent the impinging and reflection of out-of-plane body waves from the boundaries. The simulation was carried out in two steps whereby gravity was applied in the first step followed by an acceleration input from the Tohoku earthquake at the base of the soil strata above the infinite element layer.

In the first stage, a LSSI analysis was performed with linear elastic material properties and the basemat of the NPP was tied to the subsoil. The objective of this step was to observe the acceleration response at the basemat with the absence of geometric and material nonlinearity and compare it with the free field accelerations from the site. The free field acceleration from the linear site response analysis exceeded the free-field acceleration from the site by more than 150%. In the next stage, the numerical free field data was compared to the response acceleration at the reactor and turbine building basemat. The RB basemat had an amplified response in the EW direction by over 26%. The UD component was also amplified due to large inertial effects. The energy dissipation at the interface due to radiation damping, attenuation of basemat response with respect to the free field and reduction of inertial effects were not captured in this step due to lack of tangential and contact definition.

A comparison was also made between the response at the basemat and the 6^{th} floor. The 6^{th} floor peak spectral acceleration exceeded that of the basemat for all components of the ground motion. It should be noted that this was a common trend also observed in the NLSSI analysis. Although, SSI tends to attenuate the response of the basemat for structures resting on stiff soil, there might be re-amplification of the structural response with height. This phenomenon is more

pronounced for structures resting on soft soils or clays where the amplification effects are much higher.

After performing the LSSI analysis, geometric non-linearities were introduced by specifying a contact definition along the tangential and normal direction at the soil-structure interface. The kinematic contact formulation which performed really well in Chap 3 was used to implement the Coulomb friction criterion to simulate sliding across the interface. During the SSI analysis, a node based formulation was adopted to distribute the normal stress across the cross sectional area of the nodes in contact. Gapping was simulated through the hard pressure overclosure relationship for which the penetration of foundation into the soil was arrested. Although not ideal, it effectively simulates stress reversals across loading cycles.

The SSI analysis is carried out by first introducing the tangential interaction formulation for simulating sliding followed by gapping. The basemat peak response accelerations are compared with those obtained from the initial tied case. The reduction in peak spectral acceleration is more pronounced in the lateral direction than in the vertical direction. The interaction model helps in smoothing out the structural response by limiting the transmission of stresses between the soil and basemat through its sliding and pressure overclosure formulation. There is a significant reduction in the basemat response when compared with the linear free field data. A reduction of 31%, 12% and 11% was observed in the peak response accelerations at the RB basemat when sliding was introduced into the system for the EW, UD and NS component respectively. The PRA was further reduced by 3.4%, 28% and 5% respectively for the EW, UD and NS components respectively when gapping was added. It should be noted that sliding nonlinearity has a greater impact on the acceleration attenuation for the EW and NS component while the attenuation in UD direction is governed by the gapping nonlinearity. This is consistent with the fact that the UD component is

responsible for producing overturning effects in the structure and is reduced when the hard pressure overclosure relationship is implemented in the normal direction. Although the trends of acceleration attenuation at the reactor building basemat is improved by introducing geometric nonlinearity at the interface, the EW, UD and NS components still exceed the actual TEPCO free field accelerations by 46%, 157% and 150% respectively. Similar trends were also observed at the turbine building basemat. The results are better than those obtained from LSSI analysis modelled without contact parameters, but still overestimate the basemat response by a large margin due to lack of material nonlinearity. Hence, it is essential to model the soil domain with a nonlinear material model such that the basemat accelerations can reduce more than the actual free field motion.

Following the SSI analysis with geometric nonlinearities, a couple of sensitivity studies were performed to understand the effects of interaction parameters on the basemat response. The first study compared the effects of gapping and sliding separately with the tied case through a response spectrum analysis. . The structure experienced higher spectral acceleration at lower frequencies when the basemat was tied to the soil suggesting a steady growth in the in-structure response. When gapping was introduced, the PSA occurred at higher frequencies owing to loss of contact of the basemat from the soil. The PSA was reduced compared to the tied case, when gapping effects were introduced. When the friction (sliding) component was introduced in addition to gapping, there was further attenuation in the PSA. The highest PSA was observed for the no-gapping (tied) case, as the basemat experienced greater inertia effects and behaved as a single unit with the soil. The second study dealt with the variation of the basemat response with the change in friction coefficient. It was observed that the PSA was higher at lower periods for higher friction coefficients. As the period increased, the PSA increased for lower friction coefficient.

7.3 Validation of hysteretic soil model using cyclic direct shear tests

The LSSI analysis on the Fukushima Daichii NPP revealed that simulating geometric nonlinearities at the interface is not enough to replicate the acceleration attenuation at the basemat. Hence it is very important to model the non-linear behavior of the soil which accounts for the material damping as well as localized dissipation of energy in the vicinity of the interface. The ABQ_HYSTERETIC_SOIL model, which is similar to the I-Soil material in MASTODON and MAT_HYSTERETIC_SOIL model is LS-DYNA, was chosen as the material model for the NLSSI analysis of cyclic direct shear tests. The hysteretic soil model is capable of replicating the low strain stiffness of soil in addition to the post yielding shear stress vs. shear strain behavior. It is also sensitive to variations in pressure during the analysis.

The cyclic shear experiments used for testing the hysteretic soil model were performed at the ELSA facility in Italy under the TRISEE program. The setup consisted of a large concrete sandbox filled with medium to coarse grained Ticino sand. A rigid steel foundation was placed in a trench surrounded by a steel formwork for retaining the surrounding sand which created an overburden pressure of 20 kPa. A constant vertical load was imposed on the sand while slow cyclic displacement-controlled loading was applied through a steel framework.

The hysteretic soil model consists of a multilinear backbone curve where each data point represents an elastic-perfectly plastic layer with varying yield stress-strain values. The material model has an Iwan-type formulation which represents the post-yielding behavior of the soil through differential yielding of layers of the backbone curve based on the strain level at each element. The backbone curve is valid for a single hydrostatic stress and can be made pressure dependent. The reference pressure and the initial hydrostatic stress is specified for the backbone curve by performing a gravity analysis on the undisturbed soil. The data points for the backbone

curve was obtained from a series of resonant column and cyclic torsional shear tests on Ticino sand for a large strain range.

A set of element tests were performed with a non-linear soil element and the foundation element to calibrate the parameters of the hysteretic soil model. The backbone curve for the nonlinear soil was defined for the initial hydrostatic stress. The lateral cyclic displacement was applied on top of the foundation element and the nodes of the foundation were constrained to move in pure shear. The load-displacement history and the hysteretic behavior of the foundation closely resembled the experimental results. A pressure sensitivity study was also performed on the two-element models, and no significant change was observed in the shear stress vs. shear strain response. The interaction definition for the element models included a kinematic friction formulation in the tangential direction and softened pressure overclosure relationship in the normal direction. The presence of the kinematic contact did not alter the force-displacement response of the foundation element. The shear stress vs shear strain behavior of the soil was efficiently replicated by the hysteretic soil model itself, while the kinematic interaction prevented excessive sliding of the foundation block and prevented convergence issues.

A full scale NLSSI analysis was performed on the TRISEE experimental prototype and the soil domain was partitioned on the basis of its initial hydrostatic stresses obtained from gravity analysis. The backbone curve for the soil domain was scaled according to the confining pressure. The analysis was performed in three stages to segregate the effects of geometric nonlinearity from material nonlinearity. In the first stage (GEOM_SL1), the nodes of the basemat were constrained to move with the nodes of the subsoil. The constraint was replaced by kinematic contact in the second stage (GEOM_SL2) and the softened pressure overclosure was activated in the third stage (GEOM_GP+SL). The force vs. displacement response of the foundation was compared with the

experimental results. The initial stiffness of the hysteretic response and its degradation with increasing shear strain was captured with reasonable accuracy. There was no change in the response obtained from the GEOM_SL1 and GEOM_SL2 case, which points to the fact that the nonlinear soil plays the key role in replicating the hysteretic behavior of the soil and the localized nonlinearity in the vicinity of the interface, and is only slightly altered by the introduction of kinematic contact. The introduction of gapping causes a small but noticeable reduction in the force-displacement response.

The force-displacement response was symmetric and reached a maximum displacement of around 6 mm for the high density Ticino sand, which was corroborated by the experiments. Most of the horizontal displacement of the foundation was recovered when the load amplitude was increased. The numerical model captures the gaining of the lateral capacity of the system at an ultimate moment of about 100 kNm. The rotational stiffness of the system gradually decreases with the increase in rotation. The moment-rotation curve obtained from the experiments is S-shaped, signifying an uplift-controlled response. The pinching of the hysteresis loop is not captured efficiently by the numerical model.

The ABQ_HYSTERETIC_SOIL model was successful in replicating the force-displacement response of the TRISEE cyclic shear experiments and was used to model the non-linear soil surrounding the Fukushima Daichii NPP.

7.4 Full-scale NLSSI analysis of the Fukushima Daichii NPP considering material and geometric nonlinearities

The LSSI analysis performed on the NPP failed to capture the attenuation of the basemat response with respect to the free field motion, due to absence of material nonlinearity in the soil. The same finite element model used in the LSSI analysis was used for performing NLSSI analysis with a

few changes. The soil domain was split in terms of the initial hydrostatic stress at the top of each partitioned domain such that the backbone curve could be specified. The entire soil domain was modelled with ABQ_HYSTERETIC_SOIL and the backbone curve was obtained from a series of cyclic shear and triaxial tests on sandy mudstone from Makinohara and Fujeida districts in the vicinity of the Fukushima NPP. The hard pressure overclosure relationship used in the LSSI analysis was replaced with the softened contact relationship. The softened contact relationship was effective in simulating the increasing stiffness of the interface with the increase in penetration of the foundation or decreasing overclosure.

Before proceeding with the NLSSI analysis, the free field motion was obtained from a nonlinear site response analysis and the results were compared with the actual site data and the numerical results obtained from the linear site response analysis. Modelling the entire soil domain with the hysteretic soil model significantly reduced the free field accelerations when compared with the linear site response analysis. The error percentages reduced from more than 150% to an average of 10% for the EW, UD and NS components.

The NLSSI analysis was performed on a step-by-step basis to distinguish between the effects of material and geometric nonlinearity on the basemat response. The first phase of analysis involved the introduction of material nonlinearity where the structure was tied to the soil domain to arrest the effects of gapping and sliding. In the first stage (BM_MAT_EL+EL), the entire soil domain was modelled with linear elastic soil (as in Sec 4.4) which serves as the base case. In the next stage (BM_MAT_EL+NL), the subsoil in the vicinity of the foundation was modelled with ABQ_HYSTERETIC_SOIL while the large soil domain had linear elastic properties and in the final stage (BM_MAT_NL+NL) the entire soil domain was modelled with ABQ_HYSTERETIC_SOIL. For the BM_MAT_EL+EL case, the peak response acceleration at

the basemat exceeded the free field acceleration by 95%, 264% and 190% respectively in the EW, UD and NS direction. When the subsoil was modelled with the hysteretic soil model, there was some attenuation in the basemat response; but it still exceeded the free-field acceleration by 23%, 229% and 123% for the EW, UD and NS components due to lack of material damping in the large soil domain. The linear elastic soil domain remains in the elastic range throughout the entire loading history, and there is no reduction of dynamic shear modulus. Hence, the energy is not dissipated for the linear elastic soil domain resulting in spurious amplification of the basemat response. For the BM_MAT_NL+NL case, the EW component was found to be attenuated by 31% although the UD and NS component still exceeded the free field acceleration by 44% and 20% respectively. Although this was a significant improvement from the BM_MAT_EL+NL case, the existing amplifications in the UD and NS component could be attributed to the fact that the basemat was tied to the soil which results in high inertia effects, since the basemat behaves as a single unit with the soil (see Sec 4.5.2).

In the next phase of analysis, the tied contact was eliminated and geometric nonlinearities were introduced. The stages of analysis were similar to the NLSSI analysis of the TRISEE cyclic direct shear tests. When the nodes of the basemat were constrained to move with the subsoil (BM_GEOM_SL1), the response acceleration at the basemat reduced by 45%, 23% and 27% below the free field acceleration. This was the first case for which acceleration attenuation was observed for all components of ground motion. When kinematic contact was introduced (BM_GEOM_SL2), the change was very minimal. The acceleration attenuation further reduced by 2% and 6% for the EW and UD components and no change was observed for the NS components. This proves the fact that the behavior of the soil in the vicinity of the interface is replicated by the hysteretic soil model while the kinematic contact helps in controlling the sliding

of the structure and prevents numerical convergence issues. In the final stage, gapping is introduced (BM_GEOM_GP+SL) which reduces the basemat response acceleration by 6% in the EW and UD direction and 3% in the NS direction. This is the final stage of NLSSI analysis which portrays the acceleration attenuation of the basemat due to combined material and geometric nonlinearities. From the various stages of the NLSSI analysis of the Fukushima NPP, it can be concluded that material nonlinearity plays the dominant role in the reduction of basemat acceleration when compared with the free field motion.

7.5 Key conclusions

The key findings from the various stages of non-linear soil structure interaction analysis of the Fukushima Daichii NPP and the TRISEE cyclic shear experiments can be listed as:

- The acceleration attenuation at the basemat of the Fukushima Daichii NPP was a result of the hysteresis behavior of the soil and geometric nonlinearities at the interface.
- The material nonlinearities play the dominant role in the attenuation of acceleration response at the basemat relative to the free field motion. The hysteretic behavior of the soil is responsible for approximately 70 to 80 percent of the acceleration attenuation while geometric nonlinearities account for the remaining 20%.
- Linear soil structure interaction analysis over-predict the foundation response by more than 100% and fail to replicate the trends in attenuation of the structural response.
- Non-reflective boundaries play a crucial role in preventing reflection of stress waves from the boundaries and were simulated using infinite elements and pure shear boundary constraints.
- Partially modelling the soil domain in the vicinity of the foundation is not enough to replicate the acceleration attenuation at the basemat.

- The kinematic contact algorithm was useful in modelling the contact along tangential direction. However, the stress profile in the vicinity of the soil-structure interface due to shearing or slip is governed by the hysteretic material model.
- The softened pressure overclosure relationship is ideal for simulating gapping due to its capability of simulating the increase in stiffness of the interface with reduction in overclosure.
- The presence of two structures in close vicinity did not have a significant influence on the acceleration response of each other
- Throughout the NLSSI analysis procedure, the structure was modelled with linear elastic material properties. The acceleration response in the structure was amplified as the height increased. This may reduce if the structure was modelled with nonlinear material properties.
- Rayleigh damping was not effective in modelling the energy dissipation in the soil. The ABQ_HYSTERETIC_SOIL was successful in portraying the dissipation of energy and radiation damping when exposed to cyclic loading.

REFERENCES

[1] P. Negro, Large-scale geotechnical experiments on soil-foundation interaction (TRISEE task 3), 1998.

[2] J. Coleman, "Light Water Reactor Sustainability Program Seismic Data Gathering and Validation," INL/EXT-15-34425, Idaho National Laboratory, Idaho Falls, Idaho, 2015.

[3] R. P. Kennedy, S. A. Short, D. A. Wesley and T. H. Lee, "Effect on Non-linear Soil-structure Interaction Due to Base Slab Uplift on the Seismic Response of a High-temperature Gas-cooled Reactor (HTGR)," *Nuclear Engineering and Design,* vol. 38, no. 2, pp. 323-55, 1976.

[4] F. Richart, "Some Effects of Dynamic Soil Properties on Soil-structure Interaction," *Journal of the Geotechnical Engineering Division, ASCE,* vol. 101(GT12), pp. 1193-1240, 1975.

[5] K. Toki and F. Miura, "Non-linear Seismic Response Analysis of Soil-structure Interaction Systems," *Earthquake Engineering & Structural Dynamics,* vol. 11, no. 1, pp. 77-89, 1983.

[6] K. Toki, T. Sato and F. Miura, "Separation and Sliding between Soil and Structure during Strong Ground Motion," *Earthquake Engineering & Structural Dynamics,* vol. 9, no. 3, pp. 263-277, 1981.

[7] J. Coleman, A. Slaughter, S. Veeraraghavan, C. Bolisetti, R. Spears and W. Hoffman, "MASTODON Theory Manual," Idaho National Laboratory, INL/EXT-17-41930, Idaho Falls, ID, 2017.

[8] "ABAQUS Documentation," Dassault Systemes, Providence, RI. USA, 2017.

[9] S. L. Kramer, Geotechnical Earthquake Engineering, Upper Saddle River, N.J. USA: Prentic Hall, 1996.

[10] "Soil-structure interaction for building structures," NEHRP Consultants Joint Venture, NIST GCR 12-917-21, Gaithersburg, MD. USA, 2012.

[11] D. H. Griffiths and R. F. King, Applied geophysics for engineers and geologists, New York, N.Y. USA: Pergamon Press, 1965.

[12] R. L. Nigbor and T. Imai, "The suspension p-s velocity logging method," in *Geophysical characterization of sites, R.D. Woods, ed.*, Rotterdam, A.A.Balkema, 1994, pp. 57-61.

[13] S. Marchetti, "In situ tests by flat dilatometer," *Journal of Geotechnical Engineering Division, ASCE*, vol. 106, no. GT3, pp. 299-321, 1980.

[14] T. Konno, Y. Suzuki, A. Tatoishi, K. Ishihara, K. Akino and I. Satsuo, "Gravelly soil properties by field and laboratory tests," in *Proceedings, 3rd International Conference on Case Histories in Geotechnical Engineering*, St.Louis, Missouri, 1993.

[15] S. Gajan, B. L. Kutter, J. D. Phalen, T. C. Hutchinson and G. R. Martin, "Centrifuge modeling of load-deformation behavior of rocking shallow foundations," *Soil Dynamics and Earthquake Engineering*, vol. 25, no. 7, pp. 773-783, 2005.

[16] J. Coleman, A. Tessari, J. Colletti and A. Whittaker, "Large-scale geotechnical laminar box experimental tests and seismic site-response benchmarking," in *Proceedings, 24th International Conference on Structural Mechanics in Reactor Technology, SMiRT-24*, Busan, S.Korea, 2017.

[17] R. S. Steedman, "Centrifuge modelling for dynamic geotechnical studies," in *Proceedings, 2nd International Conference on Recent Advances in Geotechnical Earthquake Engineering and Soil Dynamics*, St.Louis, Missouri, 1991.

[18] A. Hettler and G. Gudehus, "A pressure-dependent correction for displacement results from1 g model tests with sand," *Geotechnique,* vol. 35, no. 4, pp. 497-510, 1985.

[19] T. Suzuki, Y. Ogase, T. Honda, S. Akita, N. Yabushita and N. Nakamura, "Centrifuge Testing and Seismic Response Analysis for Uplift Behavior of Spread Foundation Structures on Rock," *Frontiers in Built Environment ,* vol. 2, p. `, 2016.

[20] B. L. Kutter and R. G. James, "Dynamic Centrifuge Model Tests on Clay Embankments," *Geotechnique,* vol. 39, no. 1, pp. 91-106, 1989.

[21] S. Gajan, B. L. Kutter and J. Thomas, "Physical and Numerical Modeling of Cyclic Moment-Rotation Behavior of Shallow Foundations," in *Proceedings, 16th International Conference on Soil Mechanics and Geotechnical Engineering*, Osaka, Japan, 2005.

[22] H. Kishida and M. Uesugi, "Tests of the interface between sand and steel in the simple shear apparatus," *Géotechnique,* vol. 37, no. 1, pp. 45-52, 1987.

[23] J. Tejchman and W. Wu, "Experimental and numerical study of sand–steel interfaces," *International Journal for Numerical and Analytical Methods in Geomechanics,* vol. 19, no. 8, pp. 513-536, 1995.

[24] J. D. Frost, J. T. Dejong and M. Recalde, "Shear failure behavior of granular–continuum interfaces," *Engineering Fracture Mechanics,* vol. 69, no. 17, pp. 2029-2048, 2002.

[25] D. Porcino, V. Fioravante, V. N. Ghionna and S. Pedroni, "Interface Behavior of Sands from Constant Normal Stiffness Direct Shear Tests," *ASTM Geotechnical Testing Journal*, vol. 26, no. 3, pp. 289-301, 2003.

[26] C. S. Desai, E. C. Drumm and M. M. Zaman, "Cyclic Testing and Modeling of Interfaces," *Journal of Geotechnical Engineering*, vol. 111, no. 6, pp. 793-815, 1985.

[27] M. I. Arshad, F. S. Tehrani, M. Prezzi and R. Salgado, "Experimental Study of Cone Penetration in Silica Sand Using Digital Image Correlation," *Geotechnique*, vol. 64, no. 7, pp. 551-569, 2014.

[28] R. D. Tovar-Valencia, A. Galvis-Castro, R. Salgado and M. Prezzi, "Effect of Surface Roughness on the Shaft Resistance of Displacement Model Piles in Sand," *Journal of Geotechnical and Geoenvironmental Engineering*, vol. 144, no. 3, 2017.

[29] F. S. Tehrani, F. Han, R. Salgado, M. Prezzi, R. D. Tovar and A. G. Castro, "Effect of Surface Roughness on the Shaft Resistance of Non-displacement Piles embedded in Sand," *Geotechnique*, vol. 1, no. 15, 2016.

[30] L. Hu and J. Pu, "Testing and Modeling of Soil-Structure Interface," *Journal of Geotechnical and Geoenvironmental Engineering*, vol. 130, no. 8, pp. 851-860, 2004.

[31] B. Hardin and V. Drnevich, "Shear Modulus and Damping in Soils: Design Equations and Curves," *Journal of the Soil Mechanics and Foundations Division, ASCE*, vol. 98, no. SM7, pp. 667-692, 1972.

[32] B. Hardin and V. Drnevich, "Shear Modulus and Damping in Soils: Measurement and Parameter Effects," *Journal of the Soil Mechanics and Foundations Division, ASCE*, vol. 98, no. SM6, pp. 603-624, 1972.

[33] S. Barani, R. De Ferrari and G. Ferretti, "Influence of soil modeling uncertainties on site response," *Earthquake Spectra,* vol. 29, no. 3, pp. 705-732, 2013.

[34] M. Erdik, "Soil structure interaction effects on strong ground motion," *Proc. NATO ASI, Ankara,* pp. 559-580, 1985.

[35] G. Masing, "Eigenspannungen und verfestigung beim messing (self stretching and hardening for brass)," in *Proceedings, 2nd International Congress for Applied Mechanics,* Zurich, Switzerland, 1926.

[36] N. Matasovic, Seismic response of composite horizontally-layered soil deposits, PhD Thesis, University of California, Los Angeles, 1993.

[37] C. Phillips and Y. Hashash, "Damping formulation for nonlinear 1D site response analyses," *Soil Dynamics and Earthquake Engineering,* vol. 29, no. 7, pp. 1143-1158, 2009.

[38] W. D. Iwan, "A distributed-element model for hysteresis and its steady-state dynamic response," *Journal of Applied Mechanics, Transactions ASME,* vol. 33, no. 4, pp. 893-900, 1964.

[39] R. M. Pyke, "Nonlinear soil models for irregular cyclic loading," *Journal of the Geotechnical Engineering Division, ASCE,* vol. 105, no. GT6, pp. 715-726, 1979.

[40] R. M. Pyke, "TESS1: A computer program for nonlinear ground response analysis, User's Manual," TAGA Engineering Software Services, Lafayette, CA USA, 1985.

[41] R. B. Brinkgreve, "Selection of Soil Models and Parameters for Geotechnical Engineering Application," *ASCE Geotechnical Special Publication,* no. 128, pp. 69-98, 2005.

[42] M. Goldscheider and G. Gudehus, "True triaxial tests on dense sand," in *Constitutive Relations for Soils. Workshop Results*, Grenoble, France, 1984, pp. 11-54.

[43] D. C. Drucker and W. Prager, "Soil Mechanics and Plastic Analysis or Limit Design," *Journal of Applied Mathematics,* vol. 10, no. 2, pp. 157-165, 1952.

[44] K. H. Roscoe, A. N. Schoefield and A. Thrairajah, "Yielding of clays in states wetter than critical," *Geotechnique,* vol. 13, no. 3, pp. 211-240, 1963.

[45] K. H. Roscoe and J. B. Burland, "On the generalized stress-strain behaviour of wet clay," in *Engineering Plasticity, ed: J. Heyman and FA Leckie*, London, Cambridge University Press, 1968, pp. 535-609.

[46] Z. Mroz, "On the description of anisotropic work hardening," *Journal of the Mechanics and Physics of Solids,* vol. 15, no. 3, pp. 163-175, 1967.

[47] Y. Dafalias and E. Popov, "Cyclic loading for materials with a vanishing elastic region," *Nuclear Engineering and Design,* vol. 41, no. 2, pp. 293-302, 1977.

[48] R. B. Brinkgreve and P. A. Vermeer, PLAXIS finite element code for soil and rock analysis, Version 7, Rotterdam: A.A. Balkema, 1997.

[49] R. E. Goodman, R. Taylor and T. L. Brekke, "A model for the mechanics of jointed rock," *Journal of Soil Mechanics and Foundation Engineering,* vol. 94, no. 3, pp. 637-659, 1968.

[50] O. C. Zienkiewicz and C. J. Parekh, "Transient field problems: Two-dimensional and three-dimensional analysis by isoparametric finite elements," *International Journal for Numerical Methods in Engineering,* vol. 2, no. 1, pp. 61-71, 1970.

[51] J. Ghaboussi, E. L. Wilson and J. Isenberg, "Finite element for rocks, joints and interfaces," *Journal of Soil Mechanics and Foundation Engineering Division, ASCE,* vol. SM 10, no. 99, pp. 833-848, 1973.

[52] M. G. Katona, "A simple contact–friction interface element with applications to buried culverts," *International Journal for Numerical and Analytical Methods in Geomechanics,* vol. 7, no. 3, pp. 371-384, 1983.

[53] C. Desai, M. Zaman, J. Lightner and H. Siriwardane, "Thin-layer element for interfaces and joints," *International Journal for Numerical and Analytical Methods in Geomechanics,* vol. 8, no. 1, pp. 19-43, 1984.

[54] C. Desai and Y. Ma, "Modelling of joints and interfaces using the disturbed-state concept," *nternational Journal for Numerical and Analytical Methods in Geomechanics,* vol. 16, no. 9, pp. 623-653, 1992.

[55] Z. Chen and H. L. Schreyer, "Simulation of soil-concrete interfaces with nonlocal constitutive models," *Journal of Engineering Mechanics,* vol. 113, no. 11, pp. 1665-1677, 1987.

[56] M. Boulon and R. Nova, "Modelling of soil-structure interface behaviour a comparison between elastoplastic and rate type laws," *Computers and Geotechnics,* vol. 9, no. 1, pp. 21-46, 1990.

[57] H. B. Seed and I. M. Idriss, "Influence of soil conditions on ground motions during earthquakes," *Journal of Soil Mechanics and Foundation Engineering Division, ASCE,* vol. 95, pp. 99-137, 1969.

[58] P. B. Schnabel , J. L. Lysmer and H. B. Seed, SHAKE: A computer program for earthquake response analysis of horizontally layered sites, Berkeley, CA USA: Earthquake Engineering Research Center, 1972.

[59] I. M. Idriss and J. I. Sun, SHAKE 91: A computer program for conducting equivalent linear seismic response analyses of horizontally layered soil deposits, Davis, CA USA: Department of Civil and Environmental Engineering, University of California Davis, 1992.

[60] M. Hudson, I. M. Idriss and M. Beikae, QUAD4M - A computer program to evaluate the seismic response of soil structures using finite element procedures and incorporating a compliant base, Davis, CA USA: Center for Geotechnical Modelling, UC Davis, 1994.

[61] J. Roesset and M. Ettouney, "Transmitting boundaries: A comparison," *International Journal for Numerical and Analytical Methods in Geomechanics,* vol. 1, no. 2, pp. 151-176, 1977.

[62] M. Sugito, H. Goda and T. Msuda, "Frequency dependent equi-linearized technique for seismic response analysis of multi-layered ground," *Proceedings of the Japan Society of Civil Engineers,* vol. 493, no. 3-2, pp. 49-58, 1994.

[63] W. B. Joyner and A. T. Chen, "Calculation of nonlinear ground response in earthquake," *Bulletin of the Seismological Society of America,* vol. 65, pp. 1315-1336, 1975.

[64] N. Matasovic and M. Vucetic, "Cyclic Characterization of Liquefiable Sands," *Journal of Geotechnical and Geoenvironmental Engineering,* vol. 119, no. 11, pp. 1805-1822, 1993.

[65] M. K. Lee and W. D. Finn, "DESRA-2, Dynamic effective stress response analysis of soil deposits with energy transmitting boundary including assessment of liquefaction potential," Soil Mechanics Series, No.36, Department of Civil Engineering, University of British Columbia, Vancouver, CA, 1978.

[66] J. H. Prevost, "DYNA1D: A computer program for nonlinear site response analysis; technical documentation," National Center of Earthquake Engineering Research, SUNY Buffalo, Buffalo, NY, 1989.

[67] J. H. Prevost, "DYNAFLOW: A nonlinear transient finite element analysis program," Department of Civil Engineering, Princeton University, Princeton, NJ USA, 1981.

[68] Y. M. Hashash, "DEEPSOIL V 3.7, Tutorial and User Manual. 2002-2009," University of Illinois at Urban-Champaign, Urbana, Illinois USA, 2009.

[69] X. Li, Z. L. Wang and C. K. Shen, "SUMDES: A nonlinear procedure for response analysis of horizontally layered sites subjected to multi-directional earthquake loading," Department of Civil Engineering, UC Davis, Davis, CA USA, 1997.

[70] F. McKenna and G. L. Fenves, "The OpenSees Command Language Manual: version 1.2," PEER Center, University of California, Berkeley, Berkeley, CA USA, 2001.

[71] GeoMotions LLC, "D-MOD2000: A nonlinear computer program for seismic response analysis of horizontally layered soil deposits, earthfill dams and solid-waste landfills," 2000.

[72] Y. Hashash and D. Park, "Soil damping formulation in nonlinear time domain site response analysis," *Journal of Earthquake Engineering*, vol. 8, no. 2, pp. 249-274, 2004.

[73] BSSC-NIBS, FEMA P750: NEHRP recommended Seismic Provisions for New Buildings and Other Structures, Washington D.C, USA: Building Seismic Safety Council, 2009.

[74] J. P. Wolf, Dynamic soil-structure interaction in time domain, New Jersey: Prentice Hall, Inc, 1988.

[75] N. M. Newmark and W. I. Hall, "Seismic design criteria for nuclear reactor facilities,," in *Report no 46, building practices for disaster mitigation*, National Bureau of Standards, U.S. Department of Commerce, 1973, pp. Vol 209-236.

[76] E. Miranda and V. Bertero, "Evaluation of strength reduction factors of earthquake-resistant design," *Earthquake Spectra,* vol. 10, no. 2, pp. 357-379, 1994.

[77] G. Mylonakis and G. Gazetas, "Seismic soil-structure interaction: beneficial or detrimental?," *Journal of Earthquake Engineering,* vol. 4, no. 3, pp. 277-301, 2000.

[78] ATC (ATC-55 Project), FEMA 440: Improvement of Nonlinear Static Seismic Analysis Procedures, Redwood City, CA USA: FEMA, Department of Homeland Security, 2005.

[79] ASCE, ASCE 41-06: Seismic Rehabilitation of Existing Buildings, 2006.

[80] R. V. Whitman and U. Luscher, "Basic Experiment into Soil-Structure Interaction," *Journal of the Soil Mechanics and Foundations Division,* vol. 88, no. 6, pp. 135-168, 1962.

[81] G. B. Warburton, "Soil-structure interaction for tower structures," *Earthquake Engineering and Structural Dynamics,* vol. 6, no. 6, pp. 535-556, 1978.

[82] G. N. Bycroft, "Forced vibrations of a rigid circular plate on semi-infinite elastic space and on an elastic stratum," *Philosophical Transaction Royal Society London,* vol. 248, pp. 327-368, 1956.

[83] T. H. Lee and D. A. Wesley, "Soil–structure interaction of nuclear reactor structures considering through-soil coupling between adjacent structures," *Nuclear Engineering and Design,* vol. 24, no. 3, pp. 374-387, 1973.

[84] M. Yashinsky, "The Loma Prieta, California, Earthquake of October 17, 1989—Highway Systems," USGS Paper 1552-B, 1998.

[85] P. Badry and N. Satyam, "Seismic soil structure interaction analysis for asymmetrical buildings supported on piled raft for the 2015 Nepal earthquake," *Journal of Asian Earth Sciences,* vol. 133, pp. 102-113, 2017.

[86] M. Ciampoli and P. E. Pinto, "Effects of soil-structure interaction on inelastic seismic response of bridge piers," *Journal of Structural Engineering,* vol. 121, no. 5, pp. 806-814, 1995.

[87] P. Raychowdhury, "Seismic response of low-rise steel moment-resisting frame buildings incorporating nonlinear SSI," *Engineering Structures,* vol. 33, no. 3, p. 958–967, 2011.

[88] T. Akiyoshi, "Compatible viscous boundary for discrete models," *Journal of Engineering Mechanics, ASCE,* vol. 104, pp. 1253-1265, 1978.

[89] E. Saez, F. L. Caballero and A. M. Razavi, "Inelastic dynamic soil-structure interaction effects on moment resisting frame buildings," *Engineering Structures,* vol. 51, pp. 166-177, 2013.

[90] H. R. Tabatabaiefar and B. Fatahi, "Idealisation of soil-structure system to determine inelastic seismic response of mid-rise building frames," *Soil Dynamics and Earthquake Engineering,* vol. 66, pp. 339-351, 2014.

[91] S. Jarernprasert, E. Bazan-Zurita and J. Bielak, "Seismic soil structure interaction response of inelastic structures," *Soil Dynamics and Earthquake Engineering,* vol. 47, pp. 132-143, 2013.

[92] T. Kobori, R. Minai and K. Kusakabe, "Dynamical characteristics of soil–structure cross-interaction system," *Bulletin of Disaster Prevention,* vol. 22, no. 204, pp. 111-151, 1973.

[93] H. L. Wong and M. D. Trifunac, "Two-dimensional, antiplane, building–soil–building interaction for two or more buildings and for incident plane SH waves," *Bulletin of Seismological Society of America,* vol. 65, no. 6, pp. 1863-1885, 1975.

[94] T. Triantafyllidis, "Dynamic stiffness of rigid rectangular foundations on the half-space," *Earthquake Engineering and Structural Dynamics,* vol. 14, no. 3, pp. 391-411, 1986.

[95] T. Triantafyllidis, "Some aspects of dynamic subsoil-coupling between circular and rectangular foundations," *Ground Motion and Engineering Seismology,* pp. 259-275, 1987.

[96] T. Triantafyllidis and B. Prange, "Rigid circular foundation : Dynamic effects of coupling to the half-space," *Soil Dynamics and Earthquake Engineering,* vol. 7, no. 1, pp. 40-52, 1988.

[97] J. S. Mulliken and D. L. Karabalis, "Discrete model for foundation–soil–foundation interaction," *Soil Dynamics and Earthquake Engineering,* vol. 7, pp. 501-508, 1995.

[98] L. Menglin, W. Huaifeng, C. Xi and Z. Yongmei, "Structure–soil–structure interaction: Literature review," *Soil Dynamics and Earthquake Engineering,* vol. 31, pp. 1724-1731, 2011.

[99] A. M. Kaynia and E. Kausel, "Dynamics of piles and pile groups in layered soil media," *Soil Dynamics and Earhquake Engineering,* vol. 10, no. 8, pp. 386-401, 1991.

[100] J. Lysmer and R. L. Kuhlemeyer, "Finite Dynamic Model For Infinite Media," *Journal of the Engineering Mechanics Division, ASCE,* vol. 95, no. 4, pp. 859-878, 1969.

[101] V. C. Laing, Dynamic response of structures in layered soils, Cambridge, MA USA: Department of Civil Engineering, Massachussetts Institute of Technology, 1974.

[102] M. N. Aydinoglu and A. Cakiroglu, "Dynamici nteraction between soil and a group of buildings," in *Proceedings, 6th World Conference on Earthquake Engineering* , New Delhi, India, 1977.

[103] G. W. Clough and J. M. Duncan, "Finite element analysis of retaining wall behavior," *Journal of the Soil Mechanics and Foundations Division, ASCE* , vol. 97, no. 12, pp. 1657-1672, 1971.

[104] A. Zhou and T. Lu, "Elasto-plastic constitutive model of soil-structure interface in consideration of strain softening and dilation," *Acta Mechanica Solida Sinica,* vol. 22, no. 2, pp. 171-179, 2009.

[105] C. Bolisetti, J. Coleman and A. Whittaker, "Time-domain soil-structure interaction analysis of nuclear facilities," *Nuclear Engineering and Design,* vol. 298, pp. 264-270, 2016.

[106] D. Datta, A. H. Varma and J. Coleman, "Investigation of interface nonlinearity on soil-structure interaction analyses," in *Transactions, Structural Mechanics in Reactor Technology, SMiRT-24*, Busan, S.Korea, 2017.

[107] O. Baltaji, O. Numanoglu, S. Veeraraghavan, Y. Hashash and J. Coleman, "Non-linear Time Domain Site Response and Soil Structure Analyses for Nuclear Facilities using MASTODON," in *Transactions, Structural Mechanics in Reactor Technology, SMiRT-24*, Busan, S.Korea, 2017.

[108] D. Gaston, C. Newman, G. Hansen and D. Lebrun-Grandie, "MOOSE: A parallel computational framework for coupled systems of nonlinear equations," *Nuclear Engineering and Design,* vol. 239, no. 10, pp. 1768-1778, 2009.

[109] M. B. Darendeli, Development of a new family of normalized modulus reduction and material damping curves, Austin, TX: University of Texas, Austin, 2001.

[110] D. Groholski, Y. Hashash, B. Kim, M. Musgrove, J. Harmon and J. Stewart, "Simplified model for small-strain nonlinearity and strength in 1d seismic site response analysis," *Journal of Geotechnical and Geoenvironmental Engineering,* vol. 142, no. 9, 2016.

[111] A. H. Varma, J. Seo and J. Coleman, "Application of nonlinear seismic soil-structure interaction analysis for identification of seismic margins at nuclear power plants," Idaho National Laboratory, INL/EXT-15-37382, Idaho Falls, ID, 2015.

[112] C. Desai, H. Phan and J. Perumpral, "Mechanics of Three Dimensional Soil-Structure Interaction," *Journal of Engineering Mechanics,* vol. 5, no. 731-747, p. 108, 1982.

[113] H. Tabatabaiefar, B. Fatahi, K. Ghabraie and W. Zhou, "Evaluation of Numerical Procedures to Determine Seismic Response of Structures under Influence of Soil–Structure Interaction," *Structural Engineering and Mechanics,* vol. 56, no. 1, pp. 27-47, 2015.

[114] A. L. Kwok, J. P. Stewart, Y. M. Hashash, N. Matasovic, R. Pyke, Z. Wang and Z. Yang, "Use of exact solutions of wave propagation problems to guide implementation of nonlinear, time-domain ground response analysis routines," *ASCE Journal of Geotechnical and Geoenvironmental Engineering*, pp. 1385-1398, 2007.

[115] F. Y. Menq, "Dynamic properties of sandy and gravelly soils," PhD dissertation, University of Texas at Austin, 2003.

[116] D. F. Lo Presti, O. Pallara and A. Cavallaro, "Damping ratio of soils from laboratory and in-situ tests," in *Proceedings of the 14th Intl Conference in Soil Mechanics and Foundation Engineering*, Hamburg, Germany, 1997.

[117] S. Shibuya, T. Mitachi, F. Fukuda and T. Degoshi, "Strain rate effects on shear modulus and damping of normally consolidated clay," *ASTM Geotechnical Testing Journal*, vol. 18, no. 3, pp. 365-375, 1995.

[118] L. S. T. C. (LSTC), "LS-DYNA Theory Manual," Lawrence Livermore National Laboratory, Livermore, CA, 2009.

[119] W. Matthees and G. Magiera, "A sensitivity study of seismic structure-soil-structure interaction problems for nuclear power plants," *Nuclear Engineering and Design*, vol. 73, no. 3, pp. 343-363, 1982.

[120] TEPCO-1, "Acceleration Time-History Waveforms of the 2011 Pacific coast of Tohoku Earthquake observed at Fukushima Daiichi and Daini NPP," CD ROM.

[121] ASCE, Seismic Analysis of Safety-Related Nuclear Structures and Commentary, Reston, VA USA, 1998.

[122] R. Belotti, M. Jamiolkowski, D. C. Lo Presti and D. A. O'Neill, "Anisotropy of smallstrain stiffness in Ticino sand," *Géotechnique,* vol. 46, no. 1, pp. 115-131, 1996.

[123] D. C. Lo Presti, "Non-linear stress strain relations of soils for cyclic loading," in *Proceedings of the Eleventh European Conference on Earthquake Engineering*, Paris, France, 1998.

[124] I. Anastasopoulos, F. Gelagoti, R. Kourkoulis and G. Gazetas, "Simplified constitutive model for simulation of cyclic response of shallow foundations: Validation against laboratory tests," *Journal of Geotechnical and Geoenvironmental Engineering,* vol. 137, no. 12, pp. 1154-1168, 2011.

[125] D. C. Lo Presti, O. Pallara, R. Lancelotta, M. Armandi and R. Manisalco, "Monotonic and cyclic loading behavior of two sands at small strains," *Geotechnical Testing Journal,* vol. 16, no. 4, pp. 409-424, 1993.

[126] D. C. Lo Presti, M. Jamiolkowski, O. Pallara, V. Pisciotta and S. Ture, "Stress Dependence of Sand Stiffness," in *Proceedings, 3rd International Conferences on Recent Advances in Geotechnical Earthquake Engineering and Soil Dynamics*, St.Louis, Missouri USA, 1995.

[127] G. Baldi, "Laboratory Validation of In-Situ Tests," in *Proceedings, llth International Conference on Soil Mechanics and Foundation Engineering*, San Francisco, USA, 1985.

[128] G. Baldi, R. Belotti, V. N. Ghionna, M. Jamiolkowski and D. Lo Presti, "Modulus of sands from CPT's and DMT's," in *Proceedings, 12th International Conference on Soil Mechanics*, Rio Di Janeiro, Brazil, 1989.

[129] M. Armandi, Caratteristiche di deformabilita della sabbia del Ticino e di Toyoura da prove di taglio torsionale e colonna risonante, Torino, Italy: M.Sc Thesis, Politecnico di Torino, 1991.

[130] B. Simpson, N. J. O'Riordan and D. D. Croft, "A Computer Model for the Analysis of Ground Movements in London Clay," *Geotechnique,* vol. 29, pp. 149-175, 1979.

[131] R. J. Jardine, M. J. Symes and J. B. Burland, "The Measurement of Soil Stiffness in the Triaxial Apparatus," *Geotechnique,* vol. 34, pp. 323-340, 1984.

[132] S. Shibuya and F. Tatsuoka, "Deformation characteristics of soil and rocks from ®eld and laboratory tests," in *Proceeedings, 11th Asian Regional Conference in Soil Mechanics*, Bangkok, Thailand, 1992.

[133] W. M. Isenhower and K. H. Stokoe, "Strain-Rate Dependent Shear Modulus of San Francisco Bay Mud," in *Proceedings, 1st International Conference on Recent Advances in Geotechnical Earthquake Engineering and Soil Dynamics*, St.Louis, Missouri USA, 1981.

[134] F. Tatsuoka, T. Iwasaki, S. Fukushima and H. Sudo, "Stress conditions and stress histories affecting shear modulus and damping of sand under cyclic loading," *Soils and Foundations,* vol. No.2, 1979.

[135] A. Alarcon-Guzman, Cyclic stress-strain and liquefaction characteristics of sands, West Lafayette, IN USA: Purdue University, 1986.

[136] D. C. Lo Presti, S. Pedroni and R. Crippa, "Maximum Dry Density of Cohesionless Soils by Pluviation and by ASTM D 4253-83: Comparative Study," *Geotechnical Testing Journal*, vol. 15, no. 2, pp. 180-189, 1992.

[137] R. L. Kondner, "Hyperbolic Stress-Strain Response: Cohesive Soils," *Journal of the Soil Mechanics and Foundations Division, ASCE,* vol. 89, no. 1, pp. 115-143, 1963.

[138] S. Yasuda, S. Yokota, H. Nakamura and K. Inou, "Reduction of static and dynamic shear strength due to the weathering of mudstones,," in *Proceedings, 15th World Conference in Earthquake Engineering*, Lisboa, Portugal, 2012.

[139] V. N. Trinh, A. M. Tang and Y. J. Cui, "Mechanical characterisation of the fouled ballast in ancient railway track substructure by large-scale triaxial tests," *Soils and Foundations,* vol. 52, no. 3, pp. 511-523, 2012.

[140] W. Hu and T. Wang, "Shear moduli and damping of cohesive soils under earthquake loads," in *Proceedings, First International Conference on Recent Advances in Geotechnical Earthquake Engineering and Soil Dynamics*, St.Louis, Missouri, USA, 1981.

[141] C. Zhang, G. Jiang, L. Su and W. Liu, "Dynamic behaviour of weathered red mudstone in Sichuan (China) under triaxial cyclic loading," *Journal of Mountain Science,* vol. 15, no. 8, pp. 1789-1806, 2018.

[142] M. A. Sakr and A. Ansal, Special Topics in Earthquake Geotechnical Engineering,, Heidelberg London New York: Springer, 2012.

[143] D. Datta, A. H. Varma and J. Coleman, "Investigation of interface nonlinearity on soil-structure interaction analyses," in *Transactions, Structural Mechanics in Reactor Technology, SMiRT-24*, Busan, S.Korea, 2017.